AN ABSTRACT OF THE THESIS OF

Min-Chih Huang for the degree of Doctor of Philosophy

in Civil Engineering presented on November 23, 1982

Title: FINITE ELEMENT ANALYSIS OF WAVE INTERFERENCE EFFECTS BETWEEN LARGE STRUCTURES

Redacted for Privacy

Abstract approved: Dr. John W. Leonard

A numerical calculation procedure for the hydrodynamic interference effects between large multiple structures interacting with linear ocean waves is presented in this study. Viscous effects are neglected and the hydrodynamic pressure forces are assumed to be inertially dominated. A finite element method which incorporates radiation boundary dampers is adopted to calculate the wave forces and other field variables in the direct interference model. Numerical solutions in the frequency domain are calculated for three categories of the boundary-value variational functional formulations: two-dimensional horizontal plane, two-dimensional vertical plane and three-dimensional problems.

The two-dimensional horizontal plane interference problems are formulated by incorporating explicit integration in the vertical direction, and applied to fixed, surface-piercing structures only.

Two types of radiation dampers, cylindrical and plane, are investigated. The two-dimensional vertical plane interference problems in finite water depth are formulated with flexural waves approximation to treat oblique wave diffraction and radiation. Plane dampers are used to model the radiation condition and permeable boundaries. Both floating-floating and fixed-floating structural systems are investigated. The three-dimensional interference problems have been formulated by incorporating a fictitious bottom boundary in the finite element functionals. Both cylindrical and plane dampers are used in a variety of wave diffraction and radiation problems.

Isoparametric curved elements with quadratic shape functions are used in this study to represent the structural geometries and the inner fluid domain variables. A complex-valued Gauss elimination technique is used to solve the symmetric, banded matrix equations derived from the wave diffraction and radiation functionals. In the three-dimensional algorithm, a blockform Gauss elimination technique is employed to increase the solution capacity in treating complicated system.

The validity of the present finite element algorithms, both in two- and three-dimensional formulations, are studied extensively. The effects of structural permeability, moorings and inter-structural constraints are also investigated. The versatility of the present three-dimensional finite element algorithm is clearly demonstrated in the design analysis of a loading/unloading facilities, where important interference phenomena are identified.

FINITE ELEMENT ANALYSIS OF WAVE INTERFERENCE EFFECTS BETWEEN LARGE STRUCTURES

by

Min-Chih Huang

A THESIS

submitted to

Oregon State University

in partial fulfillment of
the requirements for the
degree of

Doctor of Philosophy

Commencement June 1983

APPROVED:

Redacted for Privacy

Professor of Civil Engineering in Charge of Major

Redacted for Privacy

Head of Department of Civil Engineering

Redacted for Privacy

Dean of Graduate School

Date thesis is presented November 23, 1982

Typed by Min-Chih Huang

ACKNOWLEDGEMENTS

The author wishes to express his sincere appreciation to Dr. John W. Leonard for his guidance, support and assistance in the undertaking of this research. Acknowledgements must be made to other members of the thesis committe; including Dr. Robert T. Hudspeth for his providing the axisymmetric Green's function results and various discussions; Dr. John H. Nath and Dr. Robert W. Thresher for their advice and encouragements.

Financial support provided by the Oregon State University Sea Grant College Program supported by NOAA office of Sea Grant, Department of Commerce, under grant No. NA81AA-D-00086 is greatly acknowledged.

Finally, the author thanks his mother, May, for her continued support and encouragement, her patience throughout all these years.

M.C.H.

TABLE OF CONTENTS

TABLE OF CONTENTS
(Continued)

LIST OF FIGURES

LIST OF FIGURES
(Continued)

LIST OF FIGURES
(Continued)

LIST OF FIGURES
(Continued)

LIST OF FIGURES
(Continued)

LIST OF FIGURES
(Continued)

LIST OF TABLES

FINITE ELEMENT ANALYSIS OF WAVE INTERFERENCE EFFECTS BETWEEN LARGE STRUCTURES

1.0 INTRODUCTION

There are many offshore, coastal, and harbor operations which involve combinations of closely-spaced or interconnected vessels, wharfs, buoys, platforms, caissons and storage tanks. When two or more structures are close to each other in an incident wave field, the phenomena of wave interference always exist, whether the structures are large or small. For small, slender structures, there is generally a significant interaction between them as the wake of one influences the forces on another (58). When large structures adjoin each other, the incident wave train is disturbed by each of the structures. Wave sheltering by, and reflection from, neighboring structures disturb the incident wave field further, and thus affect the wave exciting forces on the structures. Also, for floating structures, the hydrodynamic restoring forces due to the structures' forced motions would be modified when the radiating waves are diffracted and reflected by the neighboring structures. Their hydrodynamic responses will also be affected by such wave interference phenomena.

Examples of systems involving interference between large fixed bodies include caissons, offshore storage tanks, and neighboring columns of gravity platforms (12,13,37,38,39). The most common

interference phenomena for a mixture of fixed and floating bodies occur in cases of vessels moored adjacent to a wall, wharf or off-shore platforms (30). Systems involving floating bodies include one or more vessels moored to a single-point-moor, storage tank or floating platform; supply vessels stationed adjacent to barges, floating causeways or other vessels (17,49,55,70,71); structural components of integrated multi-hull vessels (catamarans) or semi-submersibles (TLP's) (14,17,48,56). Examples of systems involving interference between small structures include jack-type platforms and pile arrays. The interference effects arising from compound structure geometry can be calculated approximately by first applying diffraction theory around the large component alone and then using the diffracted wave kinematics in the Morison's equation (51) for the small components (22,23,32,34).

The use of the finite element method in the analysis of wave interference effects between large structures is the subject of the present study. Ideal flow boundary-value problems will be posed to solve the corresponding linear diffraction and radiation problems where small amplitude waves and small responses are assumed. The diffraction and radiation problems of a single structure will be used to verify the accuracy of the proposed finite element model. The wave interference effects between multiple structures will be calculated using a direct interference method, where the structures involved will be modeled in an inner finite element domain and the wave field variables can be determined using a single generalized

matrix for the system.

1.1 Review of Previous Studies

The calculation of wave forces on large offshore structures of arbitrary shape is often performed using linear wave diffraction theory. Only a few analytical solutions are available and are limited to problems with special structural geometries. To investigate the interference effects between multiple large structures, it is necessary to use numerical finite element or integral equation methods for the calculation of hydrodynamic forces and field variables. The review of these two approaches will be followed by a description of the available finite element solution procedures.

Analytical Approaches Using Linear Diffraction Theory. The scattering of linear waves by a fixed, vertical, circular cylinder has been solved by MacCamy and Fuchs (47) in an analytical form. Studies of groups of circular cylinders and their steady hydrodynamic interference effects have been reported by Spring and Monkmeyer (63, 64) and by Chakrabarti (12,13) using a series expansion of wave potentials. Their solution technique forms an extension of the work by MacCamy and Fuchs (47): separable structural coordinates are required, and a direct system matrix solution is needed, in constrast to the multiple, iterative, scattering method of Twersky (66).

The added mass coefficients of a two-dimensional horizontal cylinder at a free surface have been calculated by Macagno (46) using

conformal mapping techniques. Solutions were obtained for two-parameter Lewis sections, three-parameter ship sections and higher-order-parameter ship sections. Ohkusu (55) applied a two-dimensional strip theory and was, therefore, limited to the study of interference problems between parallel, slender structures in infinite water depth.

Garrett (21) has solved the scattering of linear waves by a floating vertical circular cylinder in an analytical form similar to the fixed cylinder case of MacCamy and Fuchs (47). Ohkusu (56) has applied an extension of Garrett's method and solved iteratively the interference problem between three vertical cylinders equally spaced from each other. Practically, it is difficult to prove the convergence of the infinite series of velocity potentials given by the iterations.

Numerical Approaches Using Linear Diffraction Theory. In general, there are three major classes of numerical methods applied to free-surface flow problems involving structures of arbitrary shape: Integral Equation Method, Finite Element Method and Finite Difference Method (81). Finite difference with respect to time is used inevitably in most methods for unsteady problems, however, in the spatial domain it lacks flexibility in handling irregular grids associated with Neumann or mixed-type boundary conditions (Yeung, 81). Only the integral equation method and finite element method have been applied extensively to the prediction of wave diffraction and radiation by large structures. Both solution procedures have many variants and

each possesses certain merits and limitations. Integral equations of several forms have been reviewed (50,65,74,75,81). Examples of their applications to single structure wave diffraction and radiation problems may be found in Refs. (16,24,25,52). For structural geometries which have separable boundary coordinates, analytical methods have been combined with numerical procedures which avoid the lengthy numerical integrations required for non-separable structural coordinates (20,35,37,38,39,49).

Integral equation solutions of wave diffraction by a circular surface-piercing cylinder have been reported by Isaacson (37,38,39); solutions of wave diffraction by other basic sections have also been reported, such as those of square sections by Hobgen and Standing (34) and by Isaacson (38). The case of interference between two neighboring circular cylinders has been treated by Lebreton and Cormault (43) using a point wave source representation. Solutions for two neighboring circular cylinders and for two square cylinders have been obtained by Isaacson (37,38,39) using a two-dimensional wave source representation of the cylinders' horizontal contours, which significantly reduced the computing effort.

There has been extensive research reported on the diffraction and radiation problems of a two-dimensional horizontal cylinder with zero forward speed. Among these: Sayer and Ursell (60) have reviewed the John's frequencies (40) and have calculated the added mass coefficient in heave using the integral equation method. Kim (41) has applied the multipole method to solve the horizontal cylinder diffrac-

tion and radiation problems in beam seas. Bird and Shepherd (9) have treated the diffraction problem of a submerged cylinder by using the boundary element method (BEM), where the integral equation is applied over the full boundary of the problem. The wave diffraction and radiation problems of a horizontal cylinder in oblique seas have been solved by Garrison (26) using the integral equation method, and by Bolton and Ursell (10) using the wave source method. The wave field is assumed to have a sinusoidal variation along the cylinder axis.

The studies of multiple horizontal cylinders originated from the need to determine the hydrodynamics of catamarans and other multihull vessels. These include Wang and Wahab (73), Ohkusu (56), Maeda (48), and Wang (72). These results have been limited to the case of only beam seas and infinite water depth. The hydrodynamic coefficients of catamarans with circular sections (14,73) and with bulbous sections (48) have been calculated by using Frank's close fit method (19). Sayer and Spencer (59) have applied a modified multipole method of Wang and Wahab (73) to calculate the interference problems between two freely floating cylinders.

Various designs of offshore structures have incorporated a permeable wall to reduce compression shocks and hammer effects from breaking waves. Typical examples are the Ekofisk storage tanks employed in the North Sea which are surrounded by a perforated Jarlan breakwater wall (28), rubble-mound breakwaters, and open quays (11). The interference effects between a fixed, vertical, impermeable wall and large floating structures have been investigated by Ho and Harten

(30) using the boundary element method. To date, the interference between permeable fixed and floating structures has not been studied.

Three-dimensional diffraction and radiation problems have been studied by Garrison (22,24,25) using the Green's function integral equation method. Hudspeth, et al. (35) have extended the axisymmetric Green's function of Fenton (20) to treat the diffraction and radiation problems of axisymmetric floating structures. Matsui and Tamaki (49) have investigated the interference effects between groups of vertical axisymmetric bodies. Solutions were obtained through a distribution of two-dimensional wave sources over the structures' submerged surfaces. Van Oortmerssen (71) has applied an exact three-dimensional Green's function numerical model to calculate the hydrodynamic interference effects between two floating vertical cylinders with simple geometries (one of circular section, one of square section with rounded corners). The formulation of the mean drift forces due to wave interference effects between multiple structures have been reported by Van Oortmerssen (70) and by Løken (45) based on direct integration of second order pressures as given by Pinkster (57).

So far, theoretical approaches to the determination of hydrodynamic interference effects have been based on frequency-domain description of linearly interacting structures. Inter-structural constraints with linear load-excursion characteristics are assumed in the formulation of the structural restoring forces. Often, in offshore operations such as lightering, both rigid mechanical connectors and compliant mooring constraints may be involved. Examples of rigid

type designs include taut mooring, yoke, turret (27,29,87). In most cases, the inter-structural constraints are provided by multiple combinations of compliant steel or fiber moorings (77). The analysis of mooring systems is complicated by the possibility of either material or geometric nonlinearity (27,42,77). A numerical model taking into account all inter-structural nonlinearities in the time-domain solutions would be very expensive and complicated.

The time domain simulation of nonlinear interacting multiple structures can be achieved by means of convolution integrals of the linear hydrodynamic force coefficients based on Cumming's method (15). Koman (42) has applied this solution technique to the design of an open-sea shiploading berth. However, the hydrodynamic interference effects were not considered. Van Oortmerssen (70) has investigated the time-domain simulation of two floating vertical cylinders in which the interference effects were included. Practical restrictions involved are such that the hydrodynamic force coefficients must be known for all frequencies. However, most numerical methods for obtaining these coefficients break down or are impractical at higher frequencies; the convolution integrals have to be carried out over a larger time interval for a system involving multiple structures.

Finite Element Approaches Using Linear Diffraction Theory. Extensive results for wave interference problems have been reported by the integral equation method in the previous section. However, there are three areas where the most common formulations have shown up potential deficiencies: (1) irregular frequencies (2) the lack of flexi-

bility for modeling complex structural geometries and (3) underestimation of structural volume or area and, therefore, hydrodynamic forces. The irregular frequencies, which arise for surface-piercing or floating structures, are associated with non-unique solutions of the integral equations at certain discrete frequencies corresponding to the eigenvalues of the homogeneous boundary-value problem. This phenomenon has been discussed by John (40) and by Ursell (67). Structural irregularities, such as sharp corners, often induce numerical difficulities in the integral equation method. Most formulations use the point collocation approximation in the discretization procedures and, therefore, curved geometries are modeled with flat facets or straight line segments. This results in underestimation of hydrodynamic forces. This limitation can only be compensated for by using more refined facets or segments with increased computing effort. An alternative solution technique based on the finite element approach is therefore of interest.

Adaptations of the finite element method for fluid problems have been reviewed by Shen (61) and applications to wave diffraction and radiation problems by Mei (50) and by Zienkiewicz, et al. (85). A variety of techniques have been adopted in the finite element method to model the radiation condition at infinity in the three-dimensional fluid domain: boundary dampers (2,54,62); matching analytical boundary series solutions (BSM) (26,79,80); matching boundary integral equation solutions (BIM) (17,82); and infinite elements (6,7,8,86). The use of boundary dampers causes errors and a moderate to extensive part of the

fluid domain must be idealized using finite elements. Techniques of matching finite element inner domains with boundary solutions have been developed using a consistent variational principle which results in symmetric equation systems and guarantees convergence properties (50,79). However, such matching procedures involve a broad front linking between the finite element and the radiation boundary domains and often result in an inconveniently large bandwidth for the equations. If a frontal type solution scheme is adopted, then the width of the front will be governed to an even larger extent by the matching and a reduction of boundary solution order may be necessary (82). In general, such formulations are difficult and costly.

The infinite elements are defined such that their domains extend to infinity and the decaying radiation condition is implicitly formulated within the shape function. Newton-Coates type integration formulas are necessary in the infinite direction to achieve computing economy (7). A narrower front linking is achieved in this formulation. The use of infinite elements also causes errors since an exponential decay function is used to approximate the scattered wave variation in the infinite direction. In the two-dimensional fluid domain of vertical plane problem, the radiation condition at infinity can be achieved by boundary dampers or by matching with boundary solutions. No infinite element exists in the two-dimensional vertical plane domain due to a non-decaying radiation condition.

Finite element solutions of a vertical circular cylinder diffraction problem have been reviewed by Zienkiewicz, et al. (85).

Both two-dimensional horizontal plane and three-dimensional formulations have been incorporated with different matching techniques. In the two-dimensional vertical plane approximation, Newton (54) has applied the boundary damper method to calculate the hydrodynamic coefficients of ship sections. Bai (3) has extended the boundary damper method to treat the diffraction and radiation problems of a horizontal cylinder in oblique seas. Eatock-Taylor and Zietsman (18) have matched boundary series and boundary integral equation solutions with finite element solutions to treat horizontal cylinder diffraction and radiation problems in beam seas. Finite element solutions of a floating dock in shallow water have been investigated by Yue, et al. (79,80) using a boundary series method. To date, there has been only one finite element work on the interference problem between multiple structures, reported recently by Eatock-Taylor and Zietsman (17) using a boundary integral equation method (BIM).

1.2 Thesis Objectives and Scopes

The basic objective of this research is to study the feasibility of using the finite element method to numerically predict the wave interference effects between large multiple structures. In order to investigate the hydrodynamic interference behavior of a multiple structures system, a finite element fluid model is developed with which the wave field variables can be calculated using a direct interference method. In this approach, the hydrodynamic exciting and

restoring forces on each structure, and the hydrodynamic coupling forces between the structures induced by interference effects are determined using a single generalized system matrix. The structures involved are modeled in an inner finite element domain. Isoparametric curved elements are used to represent the structural geometries and the inner fluid domain. 1-D line elements, 2-D quadrilaterals, 3-D rectangular prisms of quadratic shape functions (83) are used in this study. Different radiation condition matching techniques are exploited to model the outer fluid domain. However, extensive studies are limited to boundary dampers and infinite elements due to their straight-forward formulations and narrow-banded symmetric matrices. A direct method equivalent to the direct stiffness method used in solid mechanics is employed in formulating the system matrix (4,76).

The diffraction and radiation problems of a single cylinder oriented, alternatively, in a vertical and horizontal plane are used to verify the accuracy of the proposed finite element fluid model. Comparisons are made with existing finite element, integral equation and analytical solutions (3,18,21,24,30,47,73,78,80). The numerical simulation of a single structure is used to establish the necessary modeling criteria, such as mesh size, boundary damper selection, distance of radiation condition, etc., to be used in subsequent studies of multiple structure systems. The direct finite element interference model is validated for multiple bodies by comparison of computer simulation results to existing experimental results and to numerical

results obtained from integral equation methods (37,38,39,59,70,71).

Parametric studies are performed to investigate the relative importance of various diffraction parameters, wave incident angle, spacing, etc. Consideration is also given to the interference effects between permeable structures. Boundary dampers with fictitious permeability parameters are used to model the permeable structures.

A compatible structure response model is also developed in this study. Complex-valued Gauss elimination and Gauss-Seidel iteration algorithms are used to predict the response of interconnected floating structures. Only linearized inter-structural constraints and moorings are considered in this study.

In Chapter 2, the wave interference effects between multiple fixed surface-piercing structures are treated. Analytical methods are combined with the two-dimensional horizontal plane finite element model to reduce the computing effort. The vertical plane finite element approximation of two-dimensional horizontal structures, interacing with obliquely incident waves in finite water depth, is considered in Chapter 3. Interference analysis between three-dimensional structures is treated in Chapter 4. Chapter 5 summarizes the important aspects of the present study. Detail derivations of shape functions and integration schemes for infinite elements are given in APPENDIX.

1.3 Significance of Study

The hydrodynamic interference effects between large structures have been calculated by using the localized finite element method. Both two-dimensional horizontal and vertical plane approximations and their applications have been identified. The effect of permeable structures and linear inter-structural constraints have been calculated. In the three-dimensional interference problems, a fictitious bottom boundary has been incorporated in the finite element formulation. An example has been given for a design application of the loading/unloading operations between two floating vessels adjacent to a semi-impermeable, semi-permeable wharf.

2.0 TWO-DIMENSIONAL HORIZONTAL PLANE PROBLEM

In this chapter, the linear diffraction of waves by multiple surface-piercing structures is considered. A finite element method which incorporates a cylindrical damper as radiation boundary condition is developed with which the wave field variables are calculated for multiple structure systems. Numerical examples are given for a single cylinder and for two cylinders where both circular and square sections are considered. An alternative solution technique using infinite elements to model the radiation condition is also treated. Numerical results are given for a single circular cylinder only.

2.1 Theoretical Formulation

The scattering of a monochromatic linear wave of height, H, and angular frequency, ω ($=2\pi/T$; T is the wave period), in water of constant depth, d, by a group of large surface-piercing cylinders of arbitrary shape is illustrated in Fig. 2.1. A Cartesian coordinate system (x,y,z) with z measured positive upwards from the still water level is adopted. Let t denote time and η the free surface elevation. The direction of incident wave propagation is defined by the angle α with respect to the x axis, as shown in Fig. 2.1. An ideal fluid is assumed; and, thus, the fluid motion may be described by a scalar velocity potential, Φ, which satisfies the Laplace equation

$$\nabla^2 \Phi = \nabla^2 (\Phi_I + \Phi_S) = 0 \tag{2.1}$$

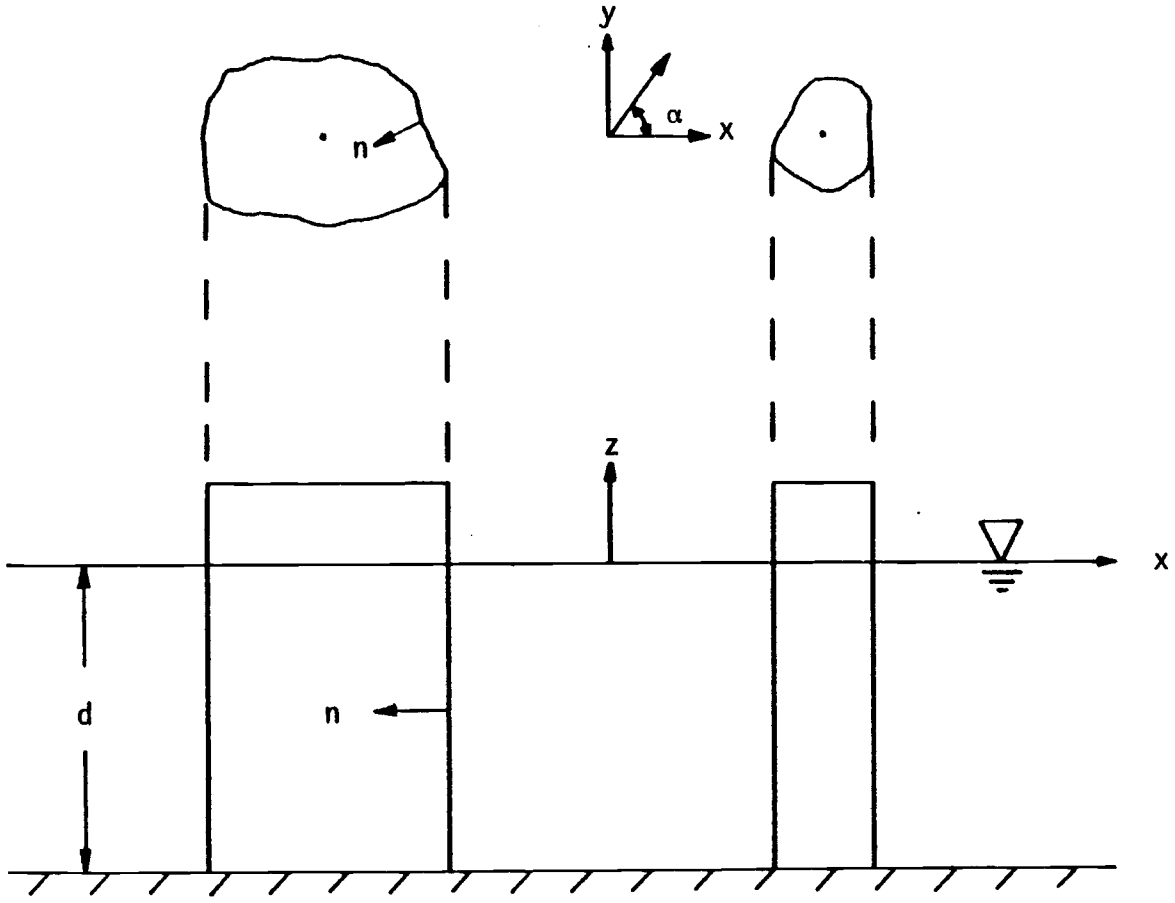

Fig. 2.1. Definition sketch of two-dimensional horizontal plane problem

in which $\nabla^2( ) = \partial^2( )/\partial x^2 + \partial^2( )/\partial y^2 + \partial^2( )/\partial z^2$ and the velocity potential is given by the linear sum of an incident wave potential, Φ_I, and a scattered wave potential, Φ_s. The incident wave potential is specified by the real part of

$$\Phi_I(x,y,z,t) = -\frac{igH}{2\omega}\frac{\cosh K(z+d)}{\cosh Kd}\phi_I(x,y)\exp -i\omega t \tag{2.2}$$

in which g = gravitational acceleration,

$$\phi_I(x,y) = \exp i(Kx\cos\alpha + Ky\sin\alpha) \tag{2.3}$$

$K = 2\pi/L$ (L = wave length) is the wave number, which satisfies the dispersion equation

$$\omega^2 = gK \tanh Kd \tag{2.4}$$

The boundary conditions are given by

$$\frac{\partial\Phi}{\partial z} = 0;\ z = -d \tag{2.5}$$

$$\frac{\partial^2\Phi}{\partial t^2} + g\frac{\partial\Phi}{\partial z} = 0;\ z = 0 \tag{2.6}$$

$$\frac{\partial\Phi}{\partial n} = 0 \text{ on } B_j;\ j = 1,..M_c \tag{2.7}$$

in which n = inward unit normal to the body surface, B_j, and M_c = total number of bodies. The Sommerfeld radiation condition is required for the scattered potential and is given by

$$\lim_{r\to\infty} r^{(m-1)/2} \left[\frac{\partial \Phi_s}{\partial r} - \left(iK - \frac{1}{2r}\right) \Phi_s\right] = 0 \tag{2.8}$$

in which $r = (x^2 + y^2)^{1/2}$ in Fig. 2.1 and m = number of horizontal dimensions.

By separation of variables, the scattered potential is assumed to have a hyperbolic cosine variation with depth of the form of the real part of

$$\Phi_s(x,y,z,t) = \frac{igH}{2\omega} \frac{\cosh K(z+d)}{\cosh Kd} \phi_s(x,y) \exp -i\omega t \tag{2.9}$$

which satisfies exactly the bottom and linearized free surface boundary conditions, Eqs. (2.5) and (2.6). The governing field equation now reduced to the Helmholtz equation

$$\frac{\partial^2 \phi_s}{\partial x^2} + \frac{\partial^2 \phi_s}{\partial y^2} + K^2 \phi_s = 0 \tag{2.10}$$

and the boundary conditions to

$$\frac{\partial \phi_s}{\partial n} + \frac{\partial \phi_I}{\partial n} = 0 \quad \text{on } B_j \tag{2.11}$$

$$\lim_{r\to\infty} \frac{\partial \phi_s}{\partial r} = \left(iK - \frac{1}{2r}\right) \phi_s \tag{2.12}$$

Eq. (2.12) is derived from the Sommerfeld radiation condition which specifies an outgoing scattered wave with radial decay. In

cylindrical coordinates, the scattered potential may be expressed approximately as

$$\phi_s \propto r^{-1/2} \exp i(Kr-\omega t) \tag{2.13}$$

and therefore Eq. (2.12) follows (vide Ref. 84). The plane wave case, i.e., m = 1 without radial decay, may be obtained from Eq. (2.8) as

$$\frac{\partial \phi_s}{\partial r} = iK\phi_s \tag{2.14}$$

As $r \to \infty$, both radiation boundary conditions given by Eqs. (2.12) and (2.14) give the same result in the context of finite element discretizations. However, if the radiation boundary is applied at a small or moderate distance from the origin of the coordinate system, the adoption of Eq. (2.12) should give improvement of numerical results over the use of Eq. (2.14). This will be illustrated in a subsequent section.

2.2 Finite Element Formulation

Solutions for Eqs. (2.10-2.12) are now formulated using the standard finite element method where a cylindrical boundary damper employing Eq. (2.12) is applied at a moderate distance r_D from the origin. The use of plane wave boundary dampers causes errors unless an extensive part of the fluid domain is idealized by finite elements.

The development of finite element solutions in the two-dimensional horizontal plane for the boundary-value problem described by Eqs.

(2.10-2.12) may conveniently be based on a variational functional formulation in which a functional, Π, is defined as

$$\Pi(\phi_s) = \iint_D \frac{1}{2}\{(\frac{\partial \phi_s}{\partial x})^2 + (\frac{\partial \phi_s}{\partial y})^2 - K^2 \phi_s^2\} dD$$

$$- \int_S \frac{1}{2}(iK - \frac{1}{2r_D}) \phi_s^2 \, dS + \sum_{j=1}^{M_C} \int_{B_j} \frac{\partial \phi_I}{\partial n} \phi_s \, dS \qquad (2.15)$$

in which D = finite element fluid domain, S = radiation boundary damper domain enclosing all the bodies, dD = differential area on the finite element fluid domain; and dS denotes a differential line element on the damper or body surface. It can be shown that if $\Pi(\phi_s)$ is minimized with respect to ϕ_s then the governing equations, Eqs. (2.10 -2.12), of the previous section obtain.

To discretize the problem in the standard finite element manner, it is necessary to describe the unknown potential ϕ_s in terms of nodal parameters ϕ_k^e and prescribed shape functions, N_k^e ; in which $k = 1, N_E$, and N_E = the number of nodal points for each element. A superscript e is used hereafter to denote parameters or functions within a single typical finite element. The functional in Eq. (2.15) is now minimized with respect to the nodal unknowns ϕ_k^e. This is performed in the element stage as follows:

$$\Pi = \Pi_1 + \Pi_2 + \Pi_3 = \sum_{e=1}^{M_D} \Pi_1^e + \sum_{e=1}^{M_S} \Pi_2^e + \sum_{e=1}^{M_C} \sum_{j=1}^{M_{B_j}} \Pi_3^e \qquad (2.16)$$

in which M_D = number of surface elements in D, M_S = number of damper

elements in S, M_{B_j} = number of line elements on body surface, B_j, and

$$\left[\frac{\partial \Pi_1^e}{\partial \phi_k^e}\right]ij = \iint_{D^e} \left(\frac{\partial N_i^e}{\partial x}\frac{\partial N_j^e}{\partial x} + \frac{\partial N_i^e}{\partial y}\frac{\partial N_j^e}{\partial y} - K^2 N_i^e N_j^e\right)\phi_k^e \; dx\, dy \tag{2.17}$$

$$\left[\frac{\partial \Pi_2^e}{\partial \phi_k^e}\right]ij = -\int_{S^e} \left(iK - \frac{1}{2r_D}\right) N_i^e N_j^e \, \phi_k^e \, dS \tag{2.18}$$

$$\left\{\frac{\partial \Pi_3^e}{\partial \phi_k^e}\right\}i = \int_{B_j^e} \frac{\partial \phi_I}{\partial n} N_i^e \, dS \tag{2.19}$$

The assemblage of the functional derivatives, Eqs. (2.17-2.19), may be performed in the usual manner, as described in standard finite element texts (vide Ref. 83). This may be arranged in matrix form as

$$([A_1] + [A_2])\{\phi_s\} = \{P\} \tag{2.20}$$

in which $[A_1]$ is a real symmetric, N x N matrix assembled from the integral Eq. (2.17), $[A_2]$ is a complex symmetric N x N matrix from the integral Eq. (2.18), $\{P\}$ is a complex N x 1 column vector form the integral Eq. (2.19), and $\{\phi_s\}$ is the complex N x 1 column vector for the unknown scattered potentials at the N total nodal points. The whole matrix is a symmetric, banded matrix which can be solved, for example, by a Gauss elimination technique.

Before presenting numerical results, it is necessary to point out that the functional in Eq. (2.15) may easily be extended to that

corresponding to slowly varying water depth as given by Berkhoff (5) and by Bettess and Zienkiewicz (7) in the context of harbor resonance and wave shoaling problems. Such a functional will be given in the form of

$$\Pi = \iint_D \frac{1}{2}\{C\,C_g[(\frac{\partial\phi_s}{\partial x})^2 + (\frac{\partial\phi_s}{\partial y})^2 - \frac{\omega^2 C_g}{C}\,\phi_s^2]\}\,dD$$

$$- \int_S \frac{1}{2} C\,C_g\,(iK - \frac{1}{2r_D})\,\phi_s^2\,dS + \sum_{j=1}^{M_C} \int_{B_j} C\,C_g \frac{\partial\phi_I}{\partial n}\,\phi_s\,dS \qquad (2.21)$$

in which $C = \omega/K$ = wave celerity, $C_g = \frac{1}{2} C\{1+2Kd/\sinh(2Kd)\}$ = group velocity. Both C and C_g are now functions of local water depth, d. The discretization of the boundary-value problem in Eqs. (2.10-2.12) may also be accomplished by the Galerkin weighted residual process in which the shape functions are chosen as weight functions and application of the divergence theorem follows.

Two isoparametric finite elements with quadratic shape functions will be used; these are the 8-noded quadrilateral and 3-noded line elements. Gauss quadrature is used in the integrations of Eqs. (2.17 -2.19). Once the solutions for ϕ_s are known, other field variables in this two-dimensional horizontal plane problem may be derived from the following analytical expressions:

$$\eta = \mathrm{Re}\{-\frac{1}{g}\frac{\partial\Phi}{\partial t}\} = \mathrm{Re}\{\frac{H}{2}\,\phi(x,y)\,\exp -i\omega t\} \qquad (2.22)$$

$$R = \frac{H}{2}\,|\phi| \qquad \text{on } B_j \qquad (2.23)$$

$$p = -\rho g z + \frac{1}{2}\rho g H \frac{\cosh K(z+d)}{\cosh Kd} \mathrm{Re}\{\phi(x,y) \exp -i\omega t\} \tag{2.24}$$

$$F_j = \frac{\rho g H d}{2} \frac{\tanh Kd}{Kd} \mathrm{Re}\{\int_{B_j} \phi\, n\, dS \exp -i\omega t\} \tag{2.25}$$

$$M_j = \frac{\rho g H d^2}{2} \{\frac{Kd \sinh(Kd)+1-\cosh(Kd)}{(Kd)^2 \cosh(Kd)}\} \mathrm{Re}\{\int_{B_j} \phi\, n\, dS \exp -i\omega t\} \tag{2.26}$$

in which $\phi = \phi_I + \phi_s$, R = wave runup on body B_j, ρ = fluid density, p = pressure, F_j, M_j = horizontal wave force and overturning moment about seafloor on the j^{th} structure, respectively.

2.3 Numerical Results

The finite element computer algorithm based on the methodology described in the previous section has been developed and applied to various geometries and arrangements of multiple surface-piercing structures. Numerical results are here compared with available results obtained from the integral equation method. The diffraction problems of a single cylinder, both of circular and of square section, are used to verify the accuracy of the present finite element model.

2.3.a Single Circular Cylinder

Finite element solutions for a single circular cylinder interacting with linear water waves have been calculated for various values

of diffraction parameter, Ka (in which a = cylinder radius), and compared with the analytical solutions of MacCamy and Fuchs (47). As would be expected, the accuracy of the finite element solution depends not only on the extent of fluid domain discretization but also on a suitable choice of boundary dampers. This is shown in Table 2.1. Here the horizontal diffraction force coefficient, C_h, which is the ratio of the maximum horizontal force to the Froude-Krylov force, is tabulated for Ka = 0.5, 1 and 2 and a/d = 1 using either plane dampers (which employs Eq. 2.14) or cylindrical dampers. The improvement of solution accuracy using the cylindrical damper is clearly indicated. Subsequent numerical calculations in this section are based on the cylindrical damper approach.

Table 2.1 EFFECTS OF BOUNDARY DAMPER SELECTIONS FOR a/d = 1

Ka	Analytical C_h	Plane Damper		Cylindrical Damper	
		C_h	$\frac{(2)-(3)}{(2)} \times 100\%$	C_h	$\frac{(2)-(5)}{(2)} \times 100\%$
(1)	(2)	(3)	(4)	(5)	(6)
0.5	2.070	1.951	5.7	2.001	3.3
1.0	1.557	1.349	13.4	1.497	3.8
2.0	0.9725	0.9647	0.8	0.9688	0.38

Prediction of the horizontal diffraction force coefficient, C_h, over a range of Ka from 0 to 3 is illustrated in Fig. 2.2. Good agreement between the finite element solutions and analytical

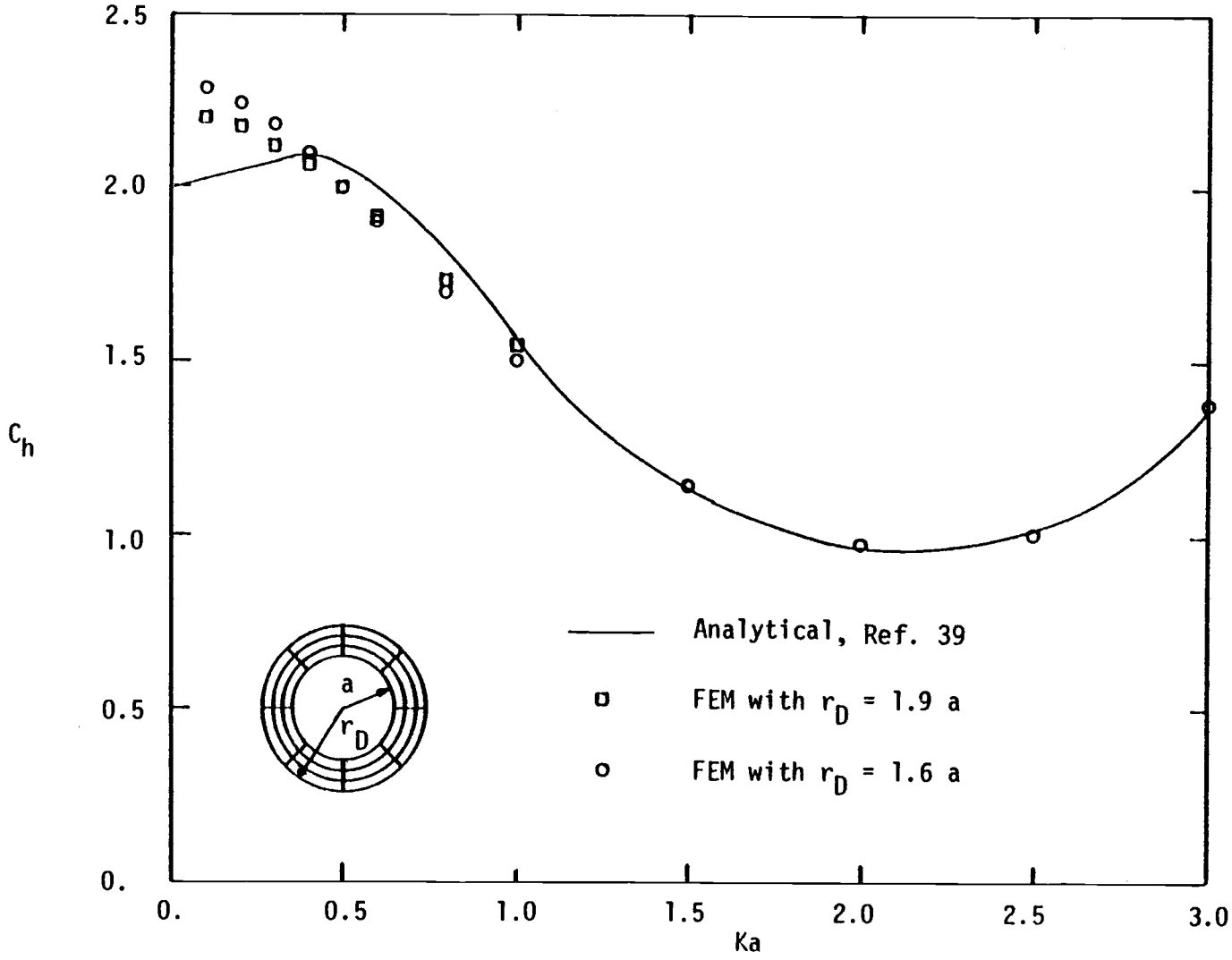

Fig. 2.2. Horizontal diffraction force coefficient, C_h, for a single circular cylinder (a/d = 1)

solutions is obtained by using a coarse 3-ring, 8-segment finite element model except for smaller values of Ka. It should be expected that such a coarse fluid model would not predict the true variation of the diffraction force coefficient for smaller values of Ka, in that small Ka values imply longer waves and requires a more extensive fluid domain discretization. Smaller values of Ka also imply that the diffraction effects become relatively less important compared to viscous drag effects.

The size of element selected directly affects the extent of fluid domain discretization and solution accuracy. The selection of element size can be determined by experience. It is pointed out by Smith (62) that the size of element should be less than about 1/4 of the incident wave length in the two-dimensional vertical plane problems. Such criterion is also valid in the context of the two-dimensional horizontal plane problems studied here. Another requirement in the discretization procedure is that successive elements should change size gradually. Similar requirements are also required in the discretization procedure of the integral equation method where element size should be less than 1/8 of the incident wave length.

Another important variable in offshore design is the wave runup around the cylinder, $R(\theta)$ in which θ = azimuthal coordinate. Fig. 2.3 presents the dimensionless runup profile, $R(\theta)/H$, around the cylinder for the case of Ka = 1. Good agreement between the finite element solutions and the analytical form is shown. The analytical solution for the runup profile depends on higher order terms of a Fourier series expansion and a more refined element discretization is

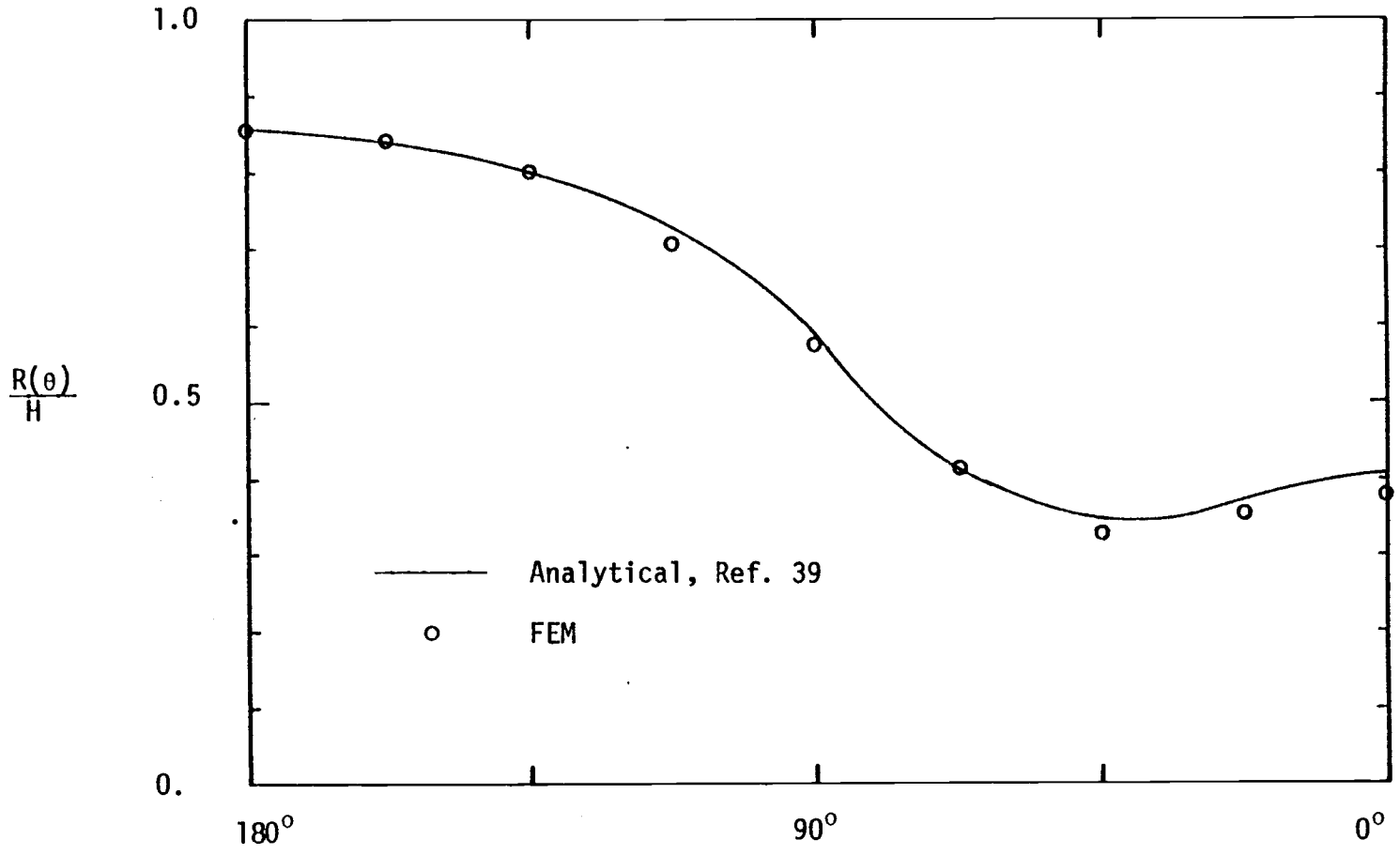

Fig. 2.3. Runup profile for a single surface-piercing cylinder for Ka = 1 and Kd = 1 {____ = analytical solution, o = FEM solution}

necessary to predict the variation more accurately. This is essentially the same if the integral equation method is employed where the evaluation of runup requires at least 32 line segments to obtain an estimate within 15% of the complete solution (vide Ref. 39)

2.3.b Single Square Cylinder

Numerical predictions for the case of linear wave diffraction of a square cylinder are shown in Figs. 2.4-2.5 in terms of the diffraction force coefficient, C_h, and the dimensionless force coefficient, $F'_{max} = F_{max}/\rho gHbd\{\tanh(Kd)/Kd\}$, versus the diffraction parameter, Kb (in which b = cylinder width). F_{max} is the maximum horizontal force predicted by the finite element solution. A coarse finite element model of 3-rings, 8-segments per ring with cylindrical dampers applied at a radius of 1.1b was used in all the calculations. Although analytical solutions for a square cylinder are not available, numerical results of the integral equation method exist and are used here for comparison. The variation of the horizontal diffraction force coefficient, C_h, over a range of Kb from 0 to 5 and b/d = 2 are shown in Fig. 2.4 for two orientations of the incident wave angle, $\alpha = 0^o$ and 45^o. The two curves computed from the present finite element method almost coincide with those calculated by Isaacson (39) in which a 48-segment discretization was used for the integral equation. This essentially confirms the validity of the finite element method in the modeling of structure geometry with sharp variations.

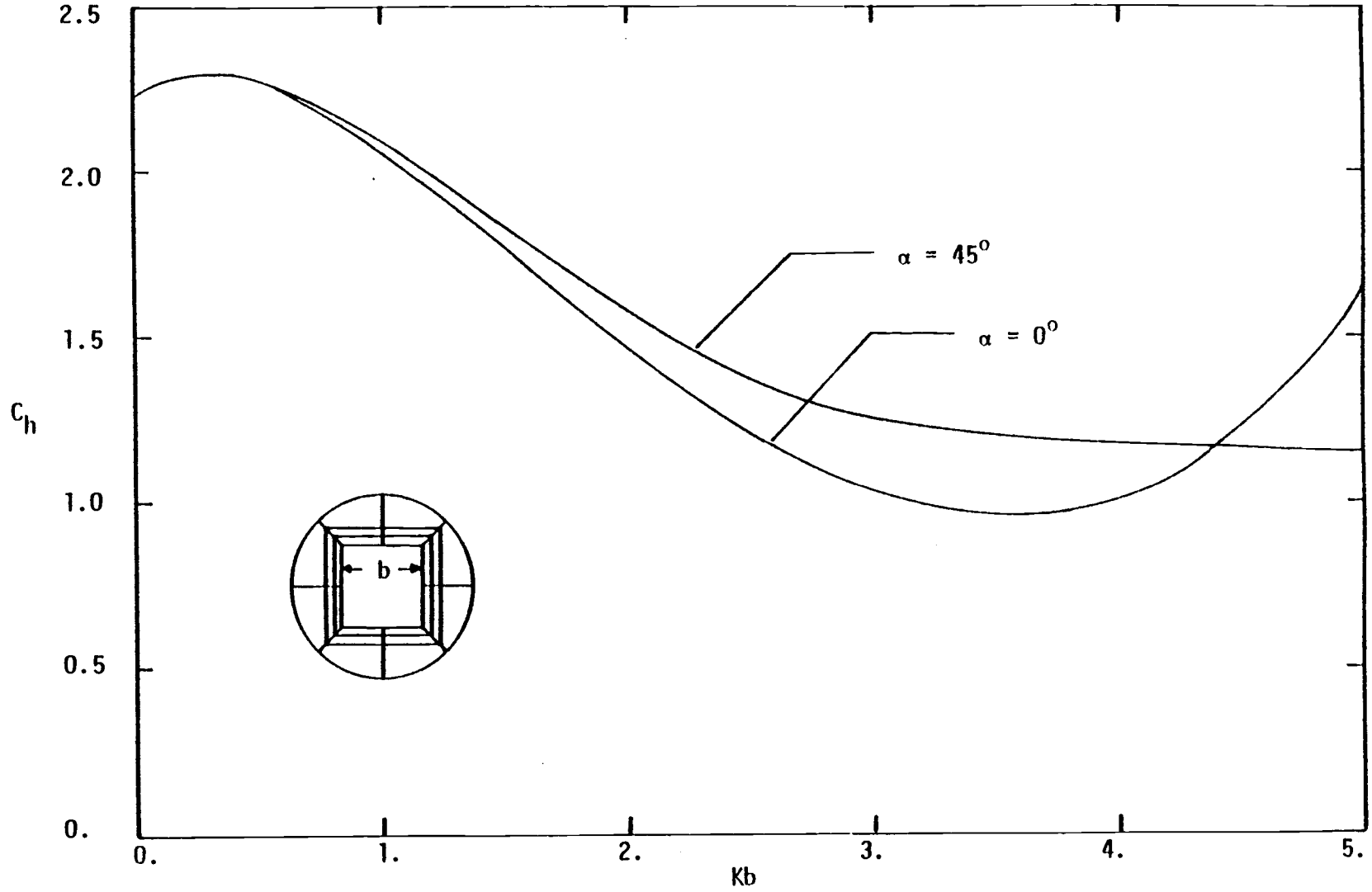

Fig. 2.4. Horizontal diffraction force coefficient, C_h, for a single square cylinder for b/d = 2

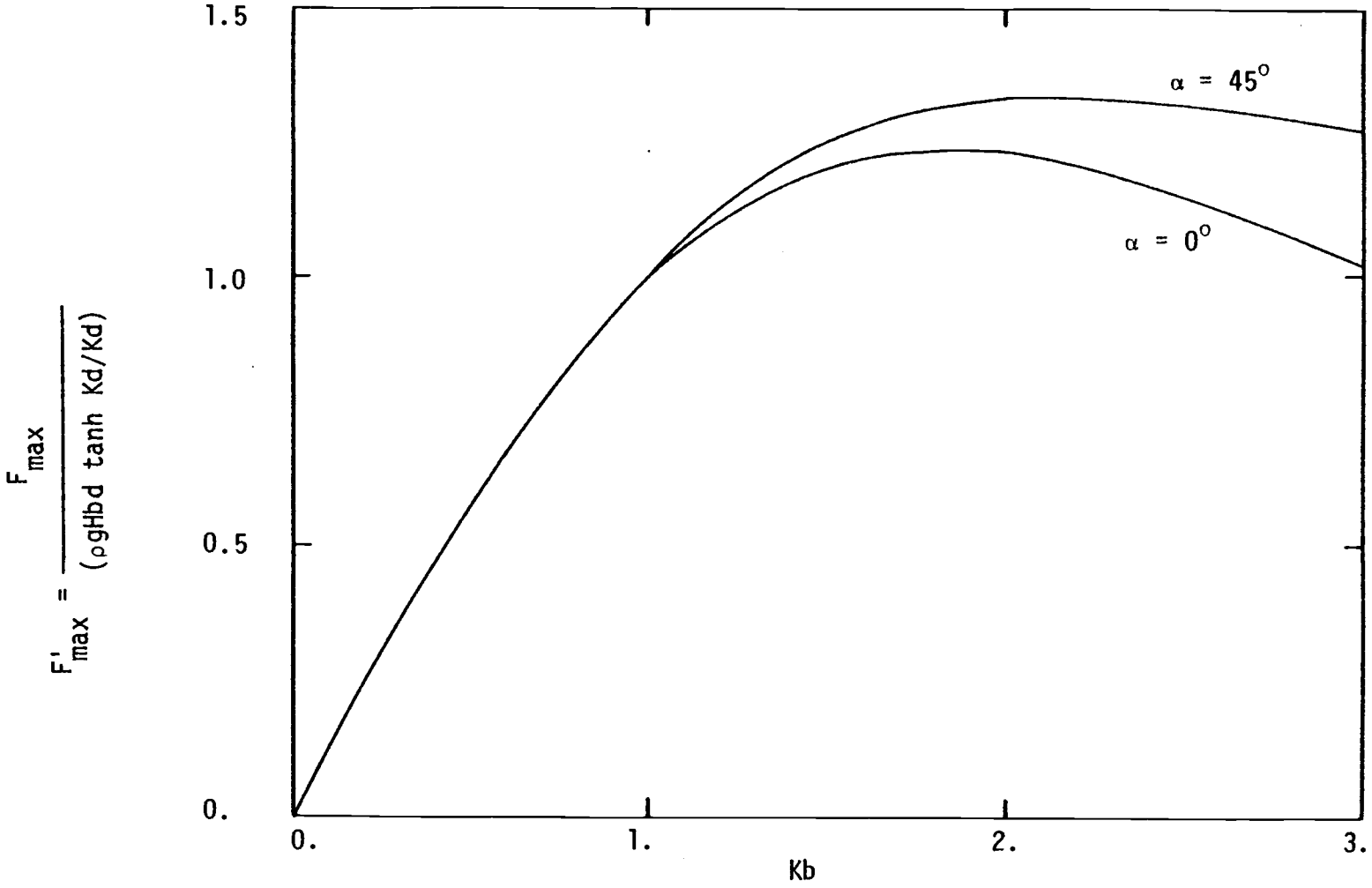

Fig. 2.5. Dimensionless horizontal force coefficient, F'_{max}, for a single square cylinder for b/d = 2

2.3.c Two Circular Cylinders

Lebreton and Cormault (43) have investigated the wave interference effects between two circular cylinders close to each other in a wave field. Significant increases in the wave forces have been calculated by using a point wave source diffraction program, especially when the cylinders were aligned in the direction of incident wave propagation, $\alpha = 0^{\circ}$, where standing waves occurred between the two cylinders. Numerical solutions for different spacings and alignment between the two cylinders have been reported by Isaacson (37) using a two-dimensional wave source integral equation method. The numerical solutions obtained using the finite element algorithm are presented for the case of $\ell/a = 3$ in which ℓ = the horizontal distance between the cylinder centers. The finite element fluid model used in the calculations is shown in Fig. 2.6. Fig. 2.7 presents the variation of C_h'/C_h with Ka for various values of incident wave angle of $\alpha = 0^{\circ}$, 45°, 90°, 135° and 180° where α and C_h' are referenced to cylinder 1 as shown in Fig. 2.6. C_h'/C_h represents the ratio of the horizontal diffraction force coefficient calculated for the cylinder 1, C_h', to that predicted for a single cylinder, C_h. The results from Ref. (37) are also presented in Fig. 2.7, where good agreement between the finite element solutions and the integral equation solutions are clearly shown for the values of incident angle, $\alpha = 0^{\circ}$ and 45°. Smaller variations of C_h'/C_h are predicted by the present finite element solutions for the case of $\alpha = 90^{\circ}$, 135° and

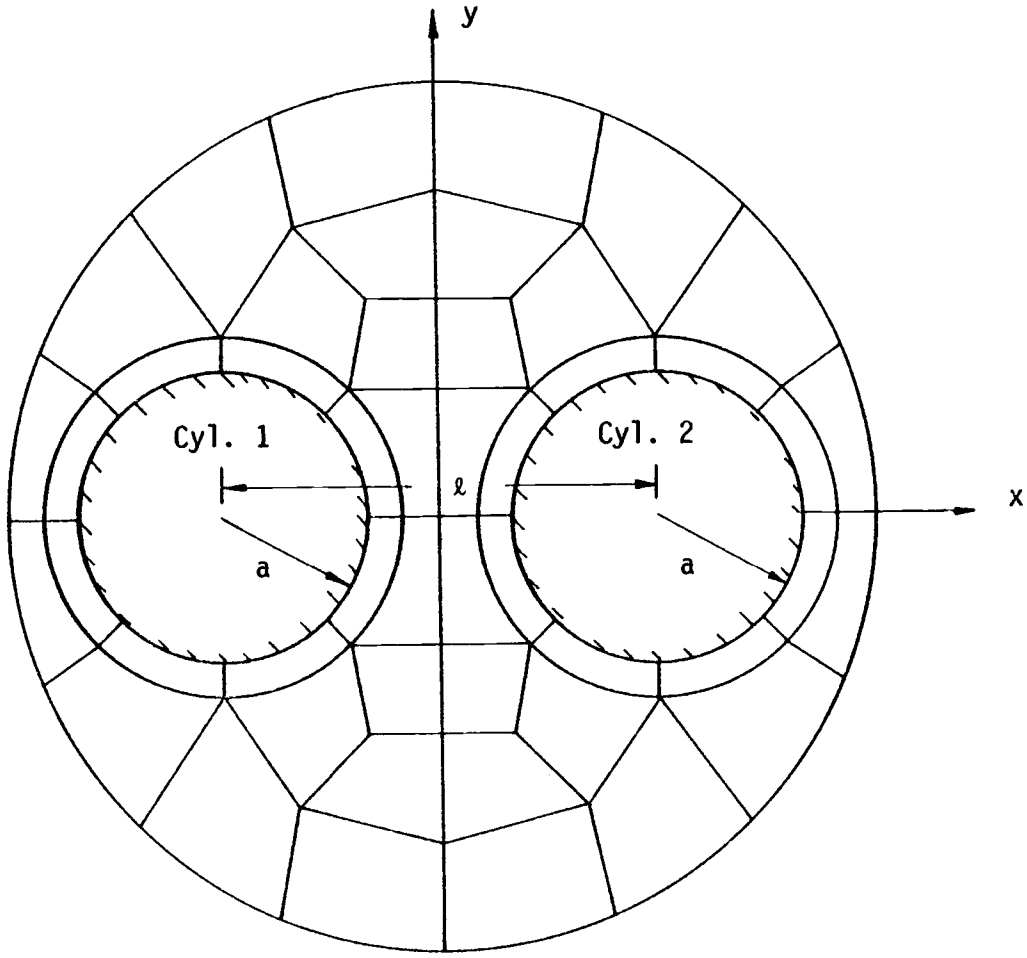

Fig. 2.6. Finite element model for two circular cylinders with $\ell/a = 3$

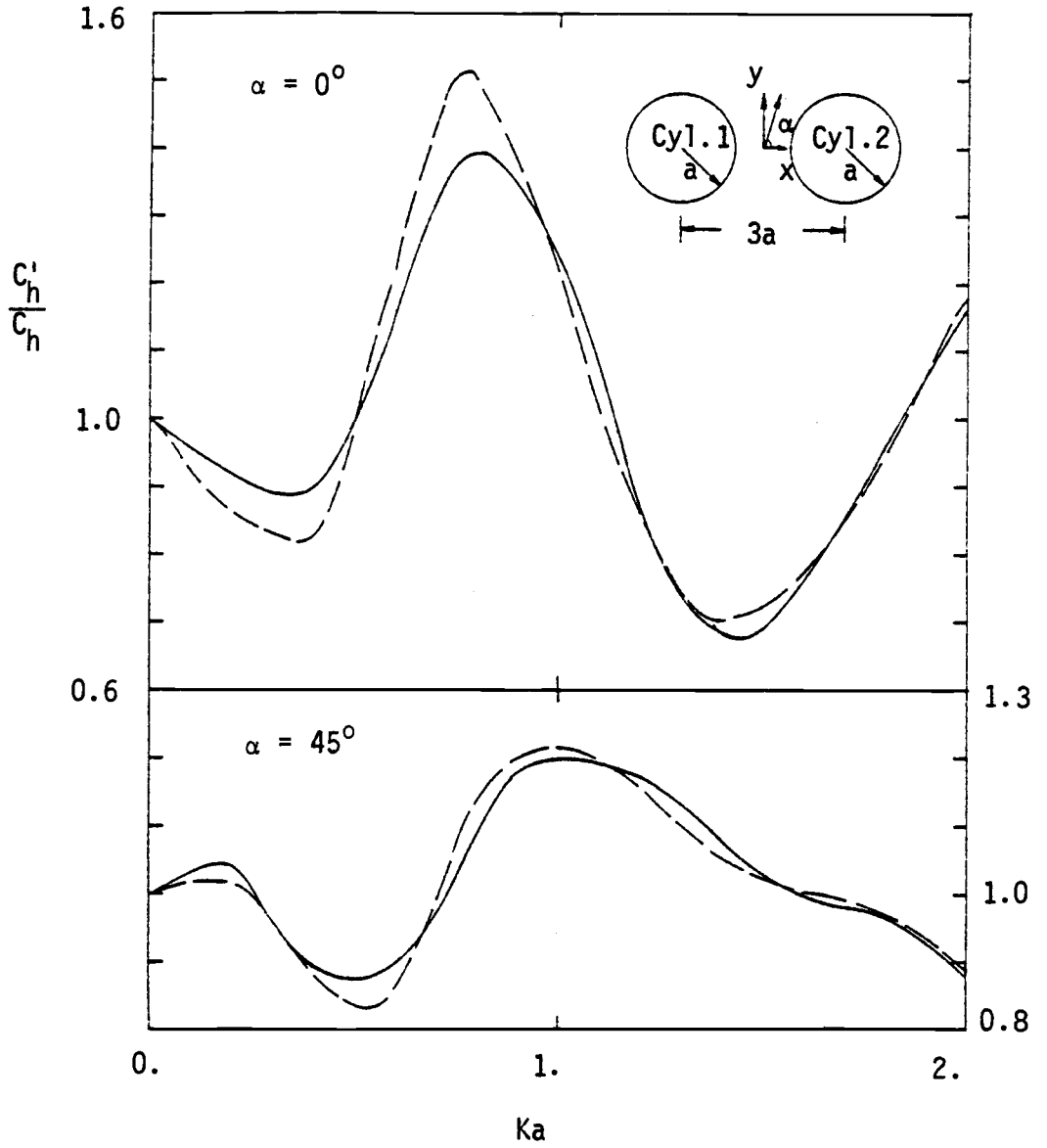

Fig. 2.7. Interference effects on circular cylinder 1 due to cylinder 2 with centers 3a apart for a/d = 1 {____ = FEM results, ---- = Ref. 37}

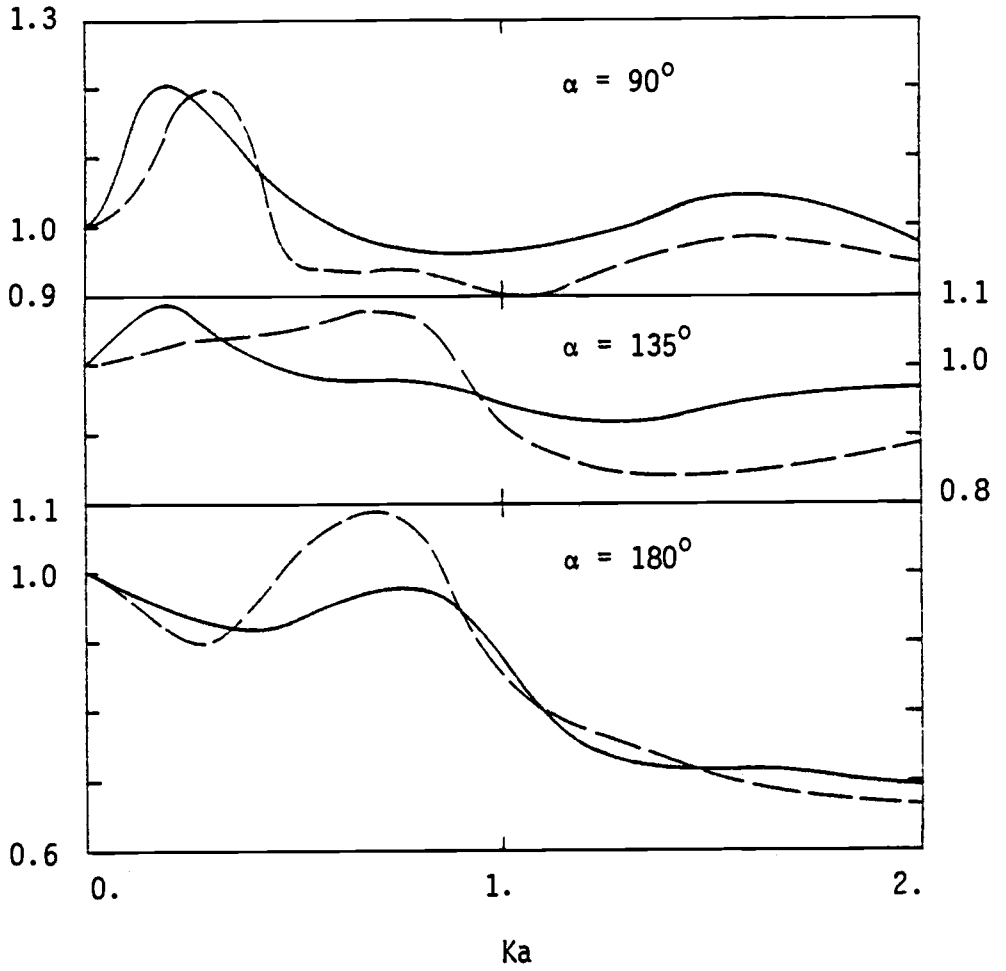

Fig. 2.7. (Continued)

180°.

The wave interference effects are shown to be most severe for $\alpha = 0^{\circ}$ where the wave reflection from the downstream cylinder significantly increases the wave loads on the upstream cylinder. Oblique incident waves of $\alpha = 45^{\circ}$ and 135° have less severe interference effects on the cylinders due to partial wave reflection and partial wave sheltering effects.

2.3.d Two Square Cylinders

The numerical solutions for the wave interference problem between two square cylinders are presented for the case of $\ell/b = 2$ over a range of Kb from 0 to 3 and $b/d = 2$. The finite element model used in the calculations is shown in Fig. 2.8. Results are represented by the variation of C_h'/C_h with Kb for values of $\alpha = 0^{\circ}$, 45°, 90°, 135° and 180°, as shown in Fig. 2.9. The numerical solutions of Isaacson (38) are also presented in Fig. 2.9. It is also seen that both numerical predictions agree very well for the case of $\alpha = 0^{\circ}$. Smaller variations of C_h'/C_h are predicted by the present finite element solutions for the case of $\alpha = 45^{\circ}$, 90°, 135° and 180°. The interference effects between two square cylinders are similar to those between two circular cylinders.

2.4 Summary of Boundary Damper Formulation

In the present finite element method, the fluid domain adjacent

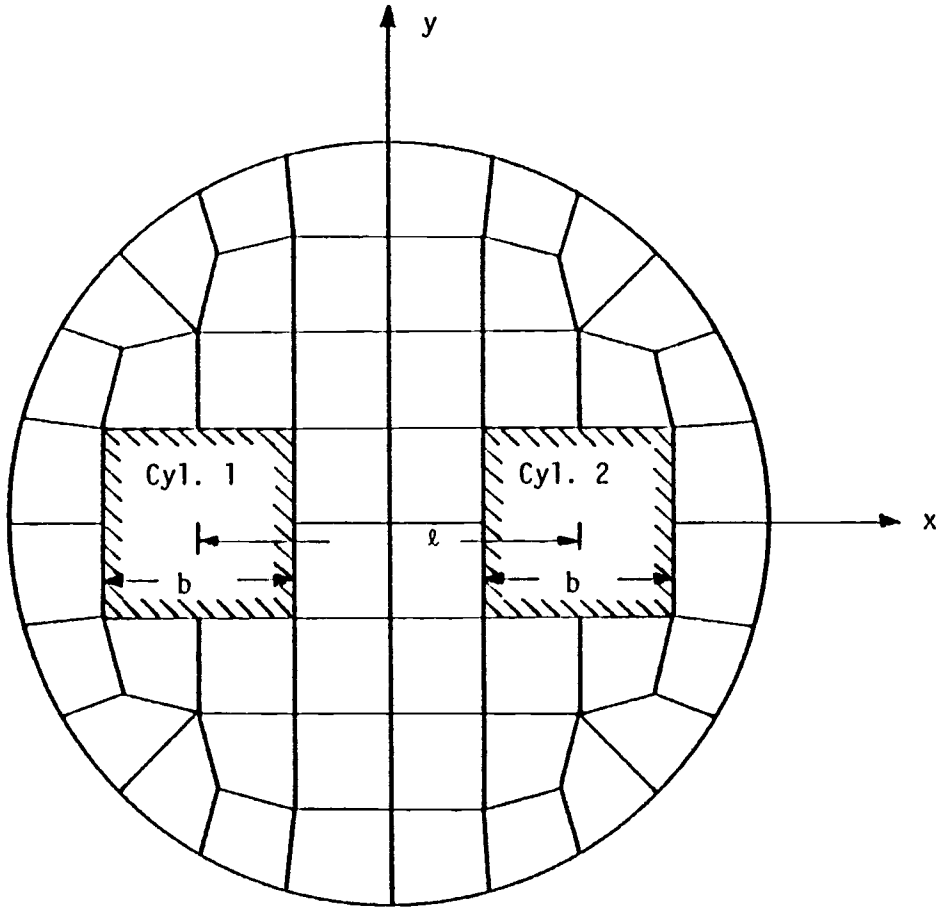

Fig. 2.8. Finite element model for two square cylinder with $\ell/b = 2$

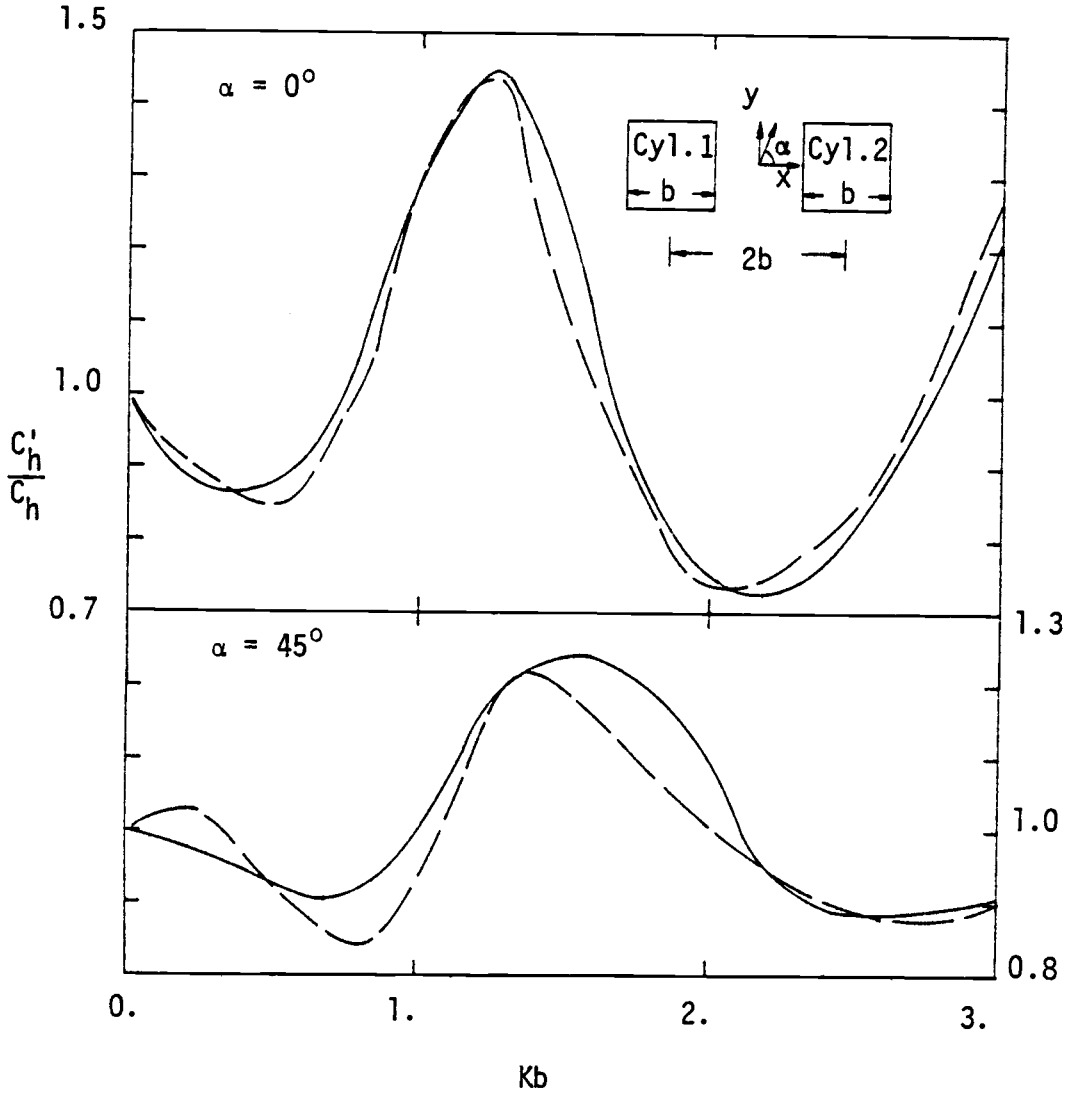

Fig. 2.9. Interference effects on square cylinder 1 due to cylinder 2 with centers 2b apart for b/d = 2 {____ = FEM results; ---- = Ref. (38)}

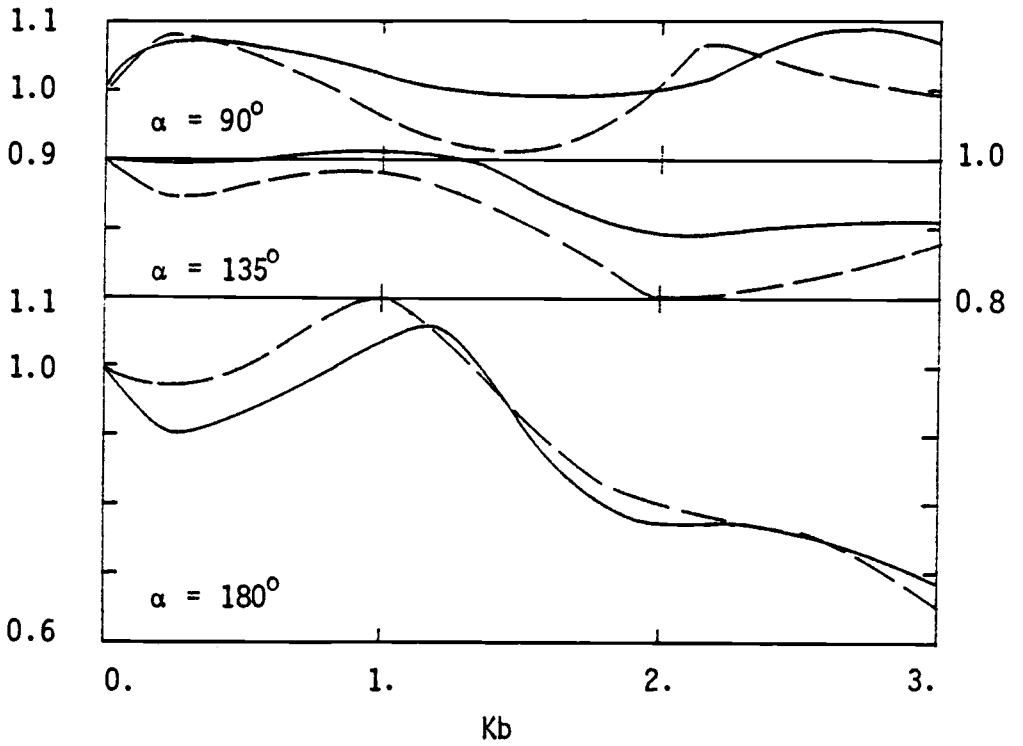

Fig. 2.9. (Continued)

to the structures is divided into a finite number of surface and line elements. Only a small or moderate fluid domain is required to accurately predict the interference effects between multiple structures. This is demonstrated in Figs. 2.7 and 2.9 where comparisons between the present solutions using coarse models and the integral equation solutions are very good in general. The CPU time log for the finite element algorithm indicates a large percentage of time was required for the calculation of the element matrix from Eqs. (2.17-2.19). Computer times are therefore reduced by using regular (i.e., same size) finite elements whenever possible and replicating the element matrices.

The alternative method of using the integral equation requires a similar computing effort in which a full system matrix corresponding to the discretization of the body surface rather than the fluid domain is solved. In the integral equation method, the computer time and storage are proportional to at least the square of the number of unknowns. Thus, if N segments are used to describe a cylinder contour, the number of segments required to describe an M-cylinder system is about MxN and the computing effort would be roughly of order $(MxN)^2$. However, employing the present finite element algorithm, the computer storage would remain roughly the same and the computer time be roughly of order (MxN). This is due to the fact that the number of unknowns (or the size of fluid domain discretized) is approximately proportional to the number of cylinders, if they are close to each other in a wave field. As the distance between the cylinders increases, the wave

interference effects become less important; the diffraction problems of the cylinders can be treated either separately or by using coarse finite elements in between the cylinders in a direct interference model.

The present finite element interference model would be most useful in the analysis of closely spaced multiple cylinders, such as three-legged or four-legged offshore platforms as shown in Ref. (13).

2.5 Infinite Element Formulation

Solutions for Eqs. (2.10-2.12) can also be formulated by using infinite elements to model the radiation boundary condition. The development of finite element solutions adjacent to, and infinite element solutions away from, the structures may also be based on a variational functional formulation. The fluid domain is separated into finite and infinite domains. A finite element functional, Π_f, is defined as

$$\Pi_f(\phi_s) = \iint_D \frac{1}{2}\left\{\left(\frac{\partial \phi_s}{\partial x}\right)^2 + \left(\frac{\partial \phi_s}{\partial y}\right)^2 - K^2\phi_s^2\right\} dD$$

$$+ \sum_{j=1}^{M_c} \int_{B_j} \frac{\partial \phi_s}{\partial n}\phi_s \, dS \qquad (2.27)$$

in which the unknown potential ϕ_s is described in terms of nodal parameters and prescribed finite element shape functions. An infinite

element functional, Π_i, is defined as

$$\Pi_i(\phi_s) = \iint_{D_i} \frac{1}{2} \{(\frac{\partial \phi}{\partial x})^2 + (\frac{\partial \phi}{\partial y})^2 - K^2 \phi_s^2\} \, dD_i \tag{2.28}$$

in which D_i = infinite element fluid domain, dD_i = differential area on the infinite element domain. The unknown potential in this domain is described by nodal parameters and infinite element shape functions which do not satisfy a priori the governing field equation. The constraint of continuity is automatically satisfied across the two domains, therefore, the functional required for discretization is simply of the form

$$\Pi(\phi_s) = \Pi_f(\phi_s) + \Pi_i(\phi_s) \tag{2.29}$$

For a typical infinite element, the special shape function chosen in the infinite direction, s, is in general of the form $p(s) \exp(-s/L_D) \exp(iKs)$; in which $p(s)$ is a polynomial in s, L_D is a decay length and K is the wave number (vide Ref. 7). The first term allows a change of shape for smaller s, the second term approximates the radial scattered wave variation and the last term represents the basic propagating wave form. The shape functions chosen in other directions are conventional Lagrangian polynomials as used in the finite elements. A special integration scheme in the infinite direction is necessary to calculate the functional integral. Detail discussions of the shape functions and Newton-Coates integration scheme

are described in APPENDIX II.

Numerical solutions for a single circular cylinder diffraction problem have been calculated over a range of Ka from 0 to 3, and compared with the analytical solutions of MacCamy and Fuchs (47). Fig. 2.10 illustrates the prediction of the horizontal diffraction force coefficient, C_h, by using a single 8-segment ring of inner domain finite elements matched with 8 infinite elements. The size of finite and infinite elements chosen were 0.2a and 10a, respectively. The length of decay was chosen to be a wave length, $L_D = L$, and 3- to 6 Newton-Coates integration points at (2n-1)L/8 were used.

Good agreement between the 3- and 6-point formulations and the analytical solutions is obtained over the whole range studied. However, numerical instabilities occur for solutions of 4- and 5-point integration schemes. Such numerical instabilities are due to the fact that the integration points chosen at (2n-1)L/8 coincide with the zeros of the real and imaginary parts of exp(i2Ks) in the functional.

Different solution characteristics have been obtained when the integration points were chosen at (2n-1)L/16. The prediction of the horizontal diffraction force coefficient, C_h, is shown in Fig. 2.11. For the diffraction range Ka > 1, there is essentially no difference among the analytical and the 3- to 6-point numerical solutions. The differences are in general less than 1% in this range. For Ka < 1, the 5-point integration formula gives slightly better prediction of C_h. No numerical instabilities are experienced by using these

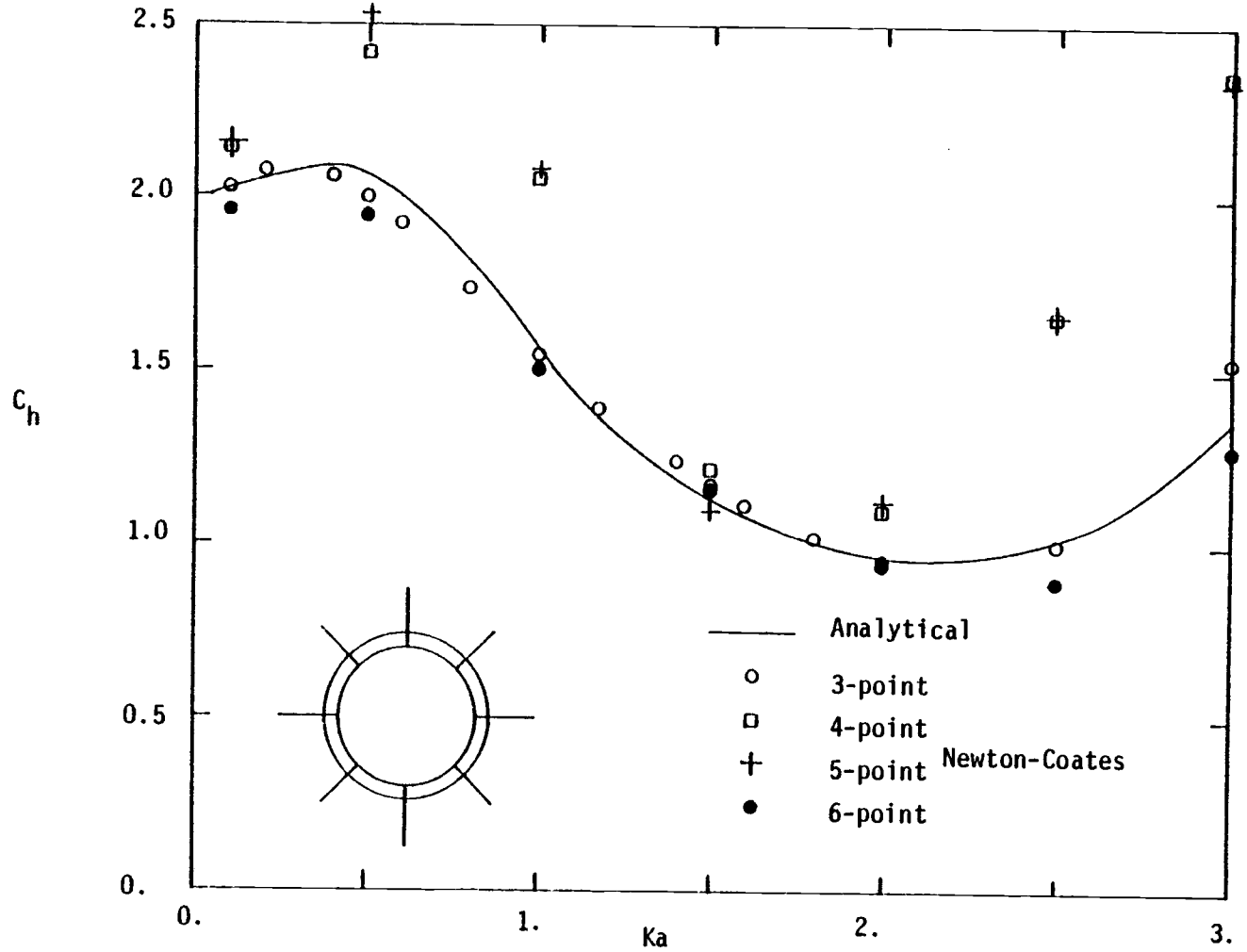

Fig. 2.10. Horizontal diffraction force coefficient, C_h, for a single circular cylinder (d/a = 1) using finite and infinite elements with Newton-Coates integration points at (2n-1)L/8

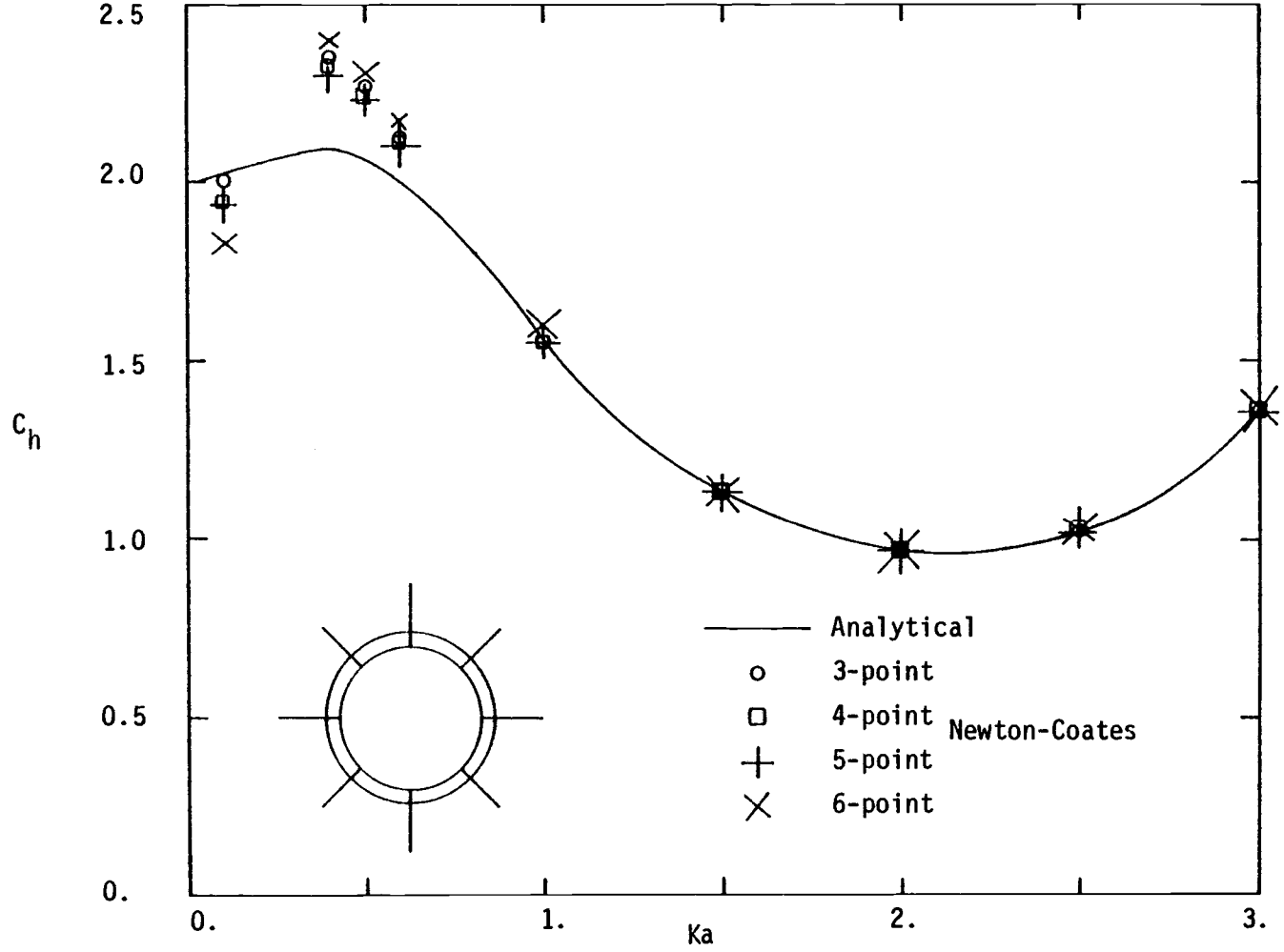

Fig. 2.11. Horizontal diffraction force coefficient, C_h, for a single circular cylinder (d/a =1) using finite and infinite elements with Newton-Coates integration points at (2n-1)L/16

integration points.

Although the infinite element formulation provides good numerical predictions of wave diffraction problems in general, the Newton-Coates integration scheme does not exhibit a well-behaved monotonic converging property in approximation of the harmonic term in the shape function. Other numerical integration schemes, such as the Gauss-Laguerre formula, have been attempted by Bettess and Zienkiewicz (7). However, up to 32 integration points were needed to approximate the harmonic term as a polynomial in order to achieve reasonable accuracy . The infinite element formulation is, therefore, not extended further to calculate the interference effects between multiple structures.

3.0 TWO-DIMENSIONAL VERTICAL PLANE PROBLEM

In this chapter the hydrodynamic interference phenomena arising from multiple two-dimensional horizontal cylinders interacting with obliquely incident linear monochromatic waves are treated. A finite element method incorporating radiation boundary dampers is employed to solve the corresponding diffraction and radiation boundary-value problems. Both extreme cases of a rigidly connected catamaran and freely floating cylinders are studied in detail. Numerical results of both cases are compared with those obtained by the method of multipoles. Numerical prediction of interference effects between a floating structure and a vertical wall are given and compared with those obtained by the boundary element method. The effects of moorings and inter-structural constraints on the structural response are also calculated.

3.1 Theoretical Formulation

Consider the diffraction and radiation of monochromatic linear waves by two-dimensional multiple horizontal cylinders parallel to each other as shown in Fig. 3.1. A Cartesian coordinate system (x,y, z) is employed in which the z coordinate is measured positive upwards from the still water level and the y axis is directed parallel to the horizontal cylinder axes. We assume that the fluid is inviscid, incompressible, and the motion irrotational. Furthermore, the fluid motion is assumed to be sinusoidal in time, t, as well as along the

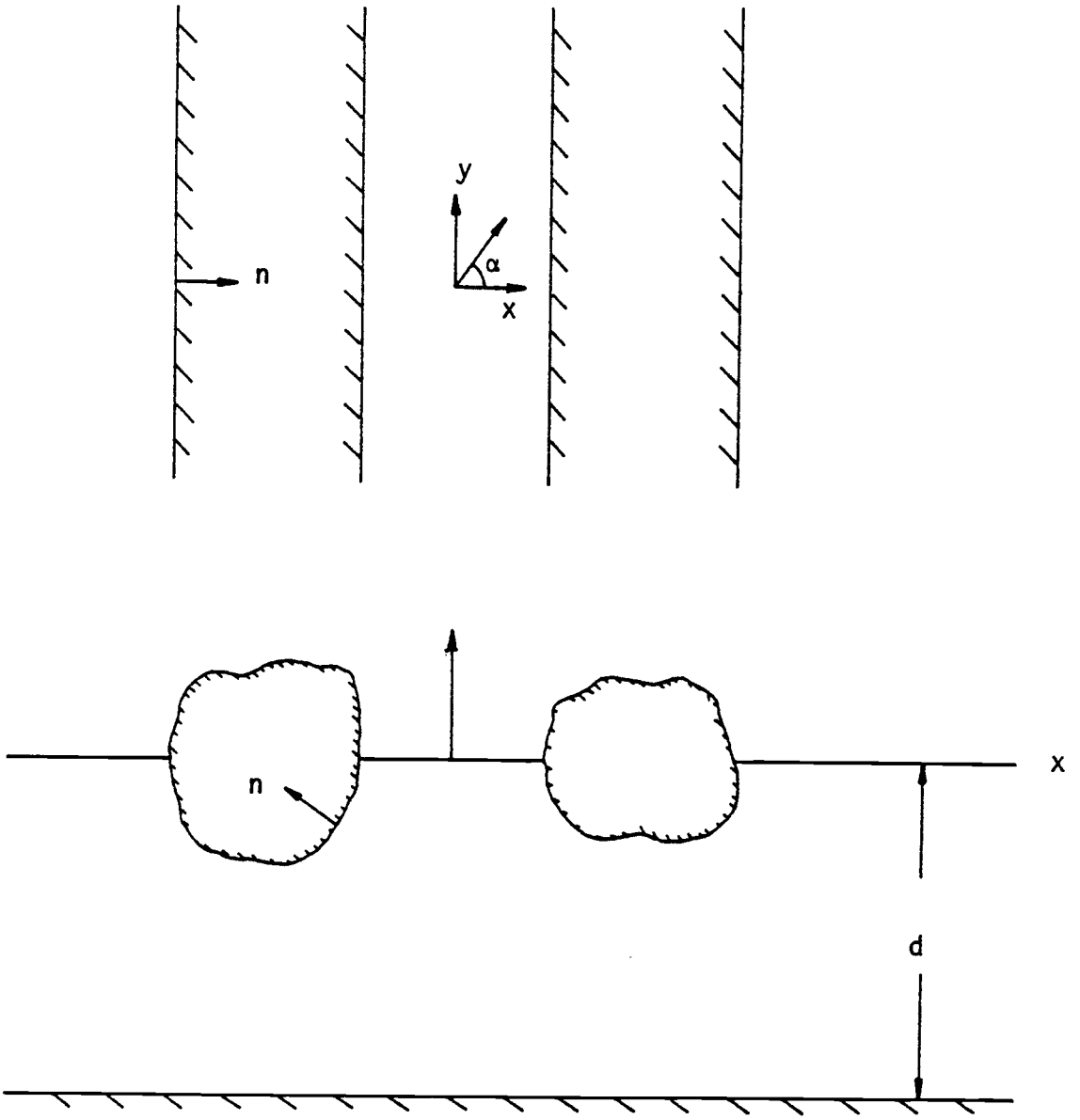

Fig. 3.1. Definition sketch of two-dimensional vertical plane problem

y axis.

A monochromatic linear wave of height, H, and angular frequency, $\omega = 2\pi/T$ (T = the wave period), propagates in water of constant finite depth, d, and is obliquely incident upon the horizontal cylinders. The direction of the wave propagation makes an angle α with the x axis, as shown in Fig. 3.1. The cylinders move in response with the same frequency as the incident waves with three degrees of freedom in the sway, heave and roll modes. The response are also assumed to vary sinusoidally in space along the cylinder axes.

Small body responses are assumed so that the body boundary conditions are satisfied very close to the equilibrium positions of the cylinders, which leads to the separation of the linear wave diffraction and radiation problems. Ideal flow boundary-value problems may therefore be posed corresponding to: 1) the scattering of waves incident at an oblique angle upon fixed cylinders and 2) the wave radiations caused by the forced sway, heave and roll oscillations of the cylinders, respectively, in otherwise still water. The oscillations are assumed to vary sinusoidally in both time and space along the cylinder axes. For clarity, the wave diffraction, radiation boundary-value problems and the body response problem are formulated separately in the following.

•

3.1.a Wave Diffraction Problem

An incident wave which propagates at an oblique angle of α with respect to the x axis may be represented by a velocity potential

given by

$$\Phi_I(x,y,z,t) = \mathrm{Re}\{-\frac{igH}{2\omega}\frac{\cosh K(z+d)}{\cosh Kd}\exp i(Kx\cos\alpha + Ky\sin\alpha - \omega t)\}$$

$$= \mathrm{Re}\{-i\omega\frac{H}{2}\phi_I(x,z)\exp i(Ky\sin\alpha - \omega t)\} \qquad (3.1)$$

in which $i = \sqrt{-1}$, g = gravitational acceleration and $K = 2\pi/L$ (L = wave length) is the wave number, which satisfies the dispersion equation, Eq. (2.4). The linear wave diffraction problem is described by a scattered velocity potential which is assumed to vary sinusoidally in both time and space along the y axis according to

$$\Phi_S(x,y,z,t) = \mathrm{Re}\{-i\omega\frac{H}{2}\phi_S(x,z)\exp i(Ky\sin\alpha - \omega t)\} \qquad (3.2)$$

Both the incident and scattered potentials satisfy the Laplace equation given by

$$\nabla^2(\Phi_I + \Phi_S) = (\frac{\partial^2}{\partial x^2} + \frac{\partial^2}{\partial y^2} + \frac{\partial^2}{\partial z^2})(\Phi_I + \Phi_S) = 0 \qquad (3.3)$$

Substitution of Eqs. (3.1) and (3.2) into Eq. (3.3), reduces Eq. (3.3) to the Helmholtz equation. The linear boundary-value problem posed on the scattered velocity potential is therefore described by the following equations:

$$\frac{\partial^2\phi_S}{\partial x^2} + \frac{\partial^2\phi_S}{\partial z^2} - (K\sin\alpha)^2\phi_S = 0 \qquad (3.4)$$

$$\frac{\partial \phi_s}{\partial z} - \nu \phi_s = 0 \; ; \quad z = 0 \tag{3.5}$$

$$\frac{\partial \phi_s}{\partial z} = 0 \; ; \quad z = -d \tag{3.6}$$

$$\frac{\partial \phi_s}{\partial n_j} + \frac{\partial \phi_I}{\partial n_j} = 0 \; ; \quad \text{on } B_j, \quad j = 1 \ldots M_c \tag{3.7}$$

and

$$\frac{\partial \phi_s}{\partial x} - \text{sgn}(x)\, iK \cos\alpha \, \phi_s \; ; \quad x \to \pm\infty \tag{3.8}$$

in which $\nu = \omega^2/g$, n_j = unit inward normal on cylinder surface, B_j, which lies on the x-z plane, and M_c = number of cylinders.

3.1.b Wave Radiation Problem

Assume the response of the j^{th} cylinder in the k^{th} mode is given by

$$\Xi_{kj}(x,y,z,t) = \text{Re}\{\xi_{kj}(x,z) \exp i(Ky \sin\alpha - \omega t)\} \tag{3.9}$$

in which k = 1,2,3 corresponds to the sway, heave and roll modes, respectively. Hereafter, the subscript j will be used to denote the j^{th} cylinder and subscript k the radiation mode. Each wave radiation problem may now be described by a scalar radiation velocity potential as

$$\Phi_{kj}(x,y,z,t) = \mathrm{Re}\{-i\omega\, \xi_{kj}\ \phi_{kj}(x,z)\, \exp\, i(Ky\sin\alpha - \omega t)\} \quad (3.10)$$

The linear radiation boundary-value problem is defined by the following equations

$$\frac{\partial^2 \phi_{kj}}{\partial x^2} + \frac{\partial^2 \phi_{kj}}{\partial z^2} - (K\sin\alpha)^2\, \phi_{kj} = 0 \quad (3.11)$$

$$\frac{\partial \phi_{kj}}{\partial z} - \nu\, \phi_{kj} = 0 \ ; \quad z = 0 \quad (3.12)$$

$$\frac{\partial \phi_{kj}}{\partial z} = 0 \ ; \quad z = -d \quad (3.13)$$

$$\frac{\partial \phi_{kj}}{\partial n_j} - n_{kj} = 0 \ ; \quad \text{on } B_j$$

$$\frac{\partial \phi_{kj}}{\partial n_m} = 0 \qquad ; \quad \text{on } B_m, \ m \neq j \qquad m,j = 1 \ldots M_c \quad (3.14)$$

and

$$\frac{\partial \phi_{kj}}{\partial x} - \mathrm{sgn}(x)\, iK\cos\alpha\, \phi_{kj} = 0; \quad x \to \pm\infty \quad (3.15)$$

in which n_{kj} = the x and z component of the unit inward normal on the j^{th} cylinder for k = 1,2, respectively, and

$$n_{3j} = (x_j - x_{cj})n_{2j} - (z_j - z_{cj})n_{1j} \quad (3.16)$$

where x_{cj} and z_{cj} are the coordinates of the center of rotation. The generalized radiation problem statement in Eqs. (3.9-3.16) describes a flexural wave which travels along the surface of the cylinder and generates an oblique wave in the water.

If $\alpha = 0^{\circ}$, which corresponds to the special case of beam seas, the generalized radiation problem reduces to the ordinary two-dimensional radiation problem in the vertical x-z plane. For the special case of head seas, $\alpha = 90^{\circ}$, the radiation boundary condition, Eq. (3.15), reduces to that of a rigid wall boundary. This special case has no immediate physical application, as described by Bolton and Ursell (10). The assumption that the direction of incident wave propagation remains parallel to the cylinder axes, corresponding to the diffraction problem in the head seas situation, also breaks down as shown by Ursell (68,69). Such waves cannot travel along a long cylinder without refraction. This shortcoming can only be corrected by using a three-dimensional wave diffraction and radiation theory, as considered in Chapter 4, where the end effects are taken into account.

3.1.c Body Response Problem

If the incident wave is assumed small in amplitude and the cylinders are stable in the equilibrium positions, the resulting responses will be proportionally small. The velocity potential for the wave field may then be expressed by linear superposition of the

incident, scattered and radiation potentials as

$$\Phi(x,y,z,t) = \mathrm{Re}\{-i\omega[(\phi_I+\phi_s)\frac{H}{2} + \sum_{j=1}^{M_c}\sum_{k=1}^{3}\phi_{kj}\xi_{kj}]\exp i(Ky\sin\alpha-\omega t)\} \tag{3.17}$$

The pressure at any point in the fluid follows from

$$p(x,y,z,t) = -\rho(\frac{\partial\Phi}{\partial t} + gz) = \mathrm{Re}\{\rho\omega^2[(\phi_I+\phi_s)\frac{H}{2} + \sum_{j=1}^{M_c}\sum_{k=1}^{3}\phi_{kj}\xi_{kj}]\exp i(Ky\sin\alpha-\omega t)\} - \rho gz \tag{3.18}$$

in which ρ = fluid density. The hydrodynamic forces on the j^{th} cylinder can be determined by integrating the pressure over the wetted surface B_j. These hydrodynamic forces are usually separated into the exciting forces associated with the diffraction problem, and the hydrodynamic and hydrostatic restoring forces associated with the radiation problem. Only the hydrostatic forces are not affected by the interference phenomena from the presence of neighboring cylinders. These physical quantities are discussed below.

The exciting force in the k^{th} mode on j^{th} body is expressed as

$$F_{kj}(x,y,z,t) = \mathrm{Re}\{\rho\omega^2\frac{H}{2}\int_{B_j}(\phi_I+\phi_s)n_{kj}\,dS\exp i(Ky\sin\alpha-\omega t)\}$$

$$= \mathrm{Re}\{f_{kj}\exp i(Ky\sin\alpha-\omega t)\} \tag{3.19}$$

in which dS = differential line segment on a body surface. The

hydrodynamic restoring force in the k^{th} mode on the j^{th} body is given by

$$R_{kj}(x,y,z,t) = \mathrm{Re}\{\rho\omega^2 \sum_{m=1}^{M_c} \sum_{\ell=1}^{3} \xi_{\ell m} \int_{B_j} n_{kj}\, \phi_{\ell m} dS \exp i(Ky\sin\alpha-\omega t)\}$$

$$= \mathrm{Re}\{ \sum_{m=1}^{M_c} \sum_{\ell=1}^{3} \xi_{\ell m} P_{kj\ell m} \exp i(Ky\sin\alpha-\omega t)\} \qquad (3.20)$$

in which $P_{kj\ell m}$ is the hydrodynamic restoring force coefficient in the k^{th} mode on the j^{th} body due to the motion in the ℓ^{th} mode of the m^{th} body. It is common practice to separate $P_{kj\ell m}$ into real and imaginary parts according to the following

$$P_{kj\ell m} = \rho\omega^2 \int_{B_j} n_{kj}\, \phi_{\ell m}\, dS = \omega^2 \mu_{kj\ell m} + i\omega \lambda_{kj\ell m} \qquad (3.21)$$

in which $\mu_{kj\ell m}$ and $\lambda_{kj\ell m}$ are the added mass and hydrodynamic radiation damping coefficients of the j^{th} body in the k^{th} mode due to the motion of the m^{th} body in the ℓ^{th} mode. If $j \neq m$ these coefficients are called the in-phase and out-of-phase interaction coefficients, respectively {cf. Van Oortmerssen (71)}.

Certain symmetric relations between the hydrodynamic coefficients may be obtained by applying Green's theorem to the radiation velocity potentials. A closed contour, S, can be constructed which includes the free surface, $z = 0$, the horizontal sea bottom, $z = -d$, vertical lines at both infinites, $x \to \pm\infty$, and the wetted surfaces of the

cylinders, B_j. From Green's theorem

$$\int_S \left(\frac{\partial \phi_{kj}}{\partial n} \phi_{\ell m} - \frac{\partial \phi_{\ell m}}{\partial n} \phi_{kj} \right) dS = 0 \tag{3.22}$$

A relation between ϕ_{kj} and $\phi_{\ell m}$ may be obtained by applying the boundary conditions given by Eqs. (3.11-3.16), as

$$\int_{B_j} n_{kj} \phi_{\ell m} \, dS = \int_{B_m} n_{\ell m} \phi_{kj} \, dS \tag{3.23}$$

In terms of the hydrodynamic coefficients, Eq. (3.23) implies that

$$P_{kj\ell m} = P_{\ell mkj}$$

or

$$\mu_{kj\ell m} = \mu_{\ell mkj} \quad , \quad \lambda_{kj\ell m} = \lambda_{\ell mkj} \quad , \qquad \begin{matrix} j,m = 1 \ldots M_c \\ \ell,k = 1 \ldots 3 \end{matrix} \tag{3.24}$$

which means that the hydrodynamic restoring force on the j^{th} body in the k^{th} mode due to motion of the m^{th} body in the ℓ^{th} mode equals the force experienced by the m^{th} body in the ℓ^{th} mode due to motion of the j^{th} body in the k^{th} mode. The simpler and more well-known expression of the symmetry relations for a single isolated body may be deduced from Eq. (3.24).

The response of the cylinders in waves, with their amplitudes varying sinusoidally in time as well as along the cylinders, may now be calculated by the following equations

$$\sum_{\ell=1}^{3} \{ [-\omega^2 (M_{kj\ell j} + \mu_{kj\ell j}) - i\omega \lambda_{kj\ell j} + C_{kj\ell j} + Q_{kj\ell j}] \xi_{\ell j}$$

$$+ \sum_{\substack{m=1 \\ m\neq j}}^{M_c} [-\omega^2 \mu_{kj\ell m} - i\omega \lambda_{kj\ell m} + Q_{kj\ell m}] \xi_{\ell m} \} = f_{kj}$$

$$j = 1,\ldots M_c,\ k = 1,..3 \qquad (3.25)$$

in which $M_{kj\ell j}$ and $C_{kj\ell j}$ are the mass and hydrostatic restoring coefficients of the j^{th} body in the k^{th} mode due to motion in the ℓ^{th} mode. These coefficients may be found in standard texts of naval architecture, such as Newman (53). $Q_{kj\ell j}$ is the linear structural restoring force of the jth body, $Q_{kj\ell m}$ is the linear inter-structural restoring force between the j^{th} and the m^{th} body. These structural restoring forces may be caused by mooring, anchoring or other type of inter-structural constraints. In Eq. (3.25), it is understood that a repeated index does not represent summation.

3.2 Finite Element Formulation

Solutions for the diffraction and radiation boundary-value problems are now formulated using the standard finite element method where plane boundary dampers are applied at moderate distances, $x = \pm x_R$, from the cylinders. The use of plane dampers to model the radiation boundary conditions, Eq. (3.9) and Eq. (3.16), causes errors unless an moderate extent of the fluid domain is idealized by finite

elements. Alternative techniques of adopting the boundary series element method (BSM) or the boundary integral element method (BIM) may also be used to model the radiation condition in these vertical plane problems.

Development of finite element solutions for the diffraction and radiation boundary-value problems in the two-dimensional vertical plane, Eqs. (3.4-3.8) and Eqs. (3.11-3.16), may conveniently be based on a variational functional formulation in which a functional, Π, is expressed as

$$\Pi(\phi_s) = \iint_D \frac{1}{2}\left\{\left(\frac{\partial \phi_s}{\partial x}\right)^2 + \left(\frac{\partial \phi_s}{\partial z}\right)^2 + (K\sin\alpha)^2 \phi_s^2\right\} dD$$

$$- \int_{z=0} \frac{1}{2} \nu \phi_s^2 \, dS - \int_{x=\pm x_R} \mathrm{sgn}(x) \frac{1}{2} iK\cos\alpha \, \phi_s^2 \, dS$$

$$+ \sum_{j=1}^{M_c} \int_{B_j} \frac{\partial \phi_I}{\partial n_j} \phi_s \, dS \qquad (3.26)$$

for the diffraction problem, and

$$\Pi(\phi_{kj}) = \iint_D \frac{1}{2}\left\{\left(\frac{\partial \phi_{kj}}{\partial x}\right)^2 + \left(\frac{\partial \phi_{kj}}{\partial z}\right)^2 + (K\sin\alpha)^2 \phi_{kj}^2\right\} dD$$

$$- \int_{z=0} \frac{1}{2} \nu \phi_{kj}^2 \, dS - \int_{x=x_R} \mathrm{sgn}(x) \frac{1}{2} iK\cos\alpha \, \phi_{kj}^2 \, dS$$

$$- \int_{B_j} n_{kj} \phi_{kj} \, dS \qquad j=1,\ldots M_c,\ k=1,2,3 \qquad (3.27)$$

for the radiation problem. D = finite element fluid domain, dD = differential area on the fluid domain; and dS denotes a differential line element on the plane boundary dampers, $x = \pm x_R$, free surface, $z = 0$, or body surface, B_j.

The fluid domain is now discretized into 2-D area and 1-D line elements. The minimization and assemblage of the functional derivatives may be performed in the usual manner as described in Section 2.2. This may be arranged in matrix form as

$$[A] \{\phi_s\} = \{P_s\}$$
$$[A] \{\phi_{kj}\} = \{P_{kj}\} \qquad (3.28)$$

for the diffraction and radiation velocity potentials, respectively. The system matrix A, which is symmetric and banded, is identical for the diffraction and radiation problems. Therefore, it need be formulated only once in a computer program and can then be solved, for example, by the Gauss elimination technique for different system vectors, P_s and P_{kj}. Two isoparametric finite elements with quadratic shape functions are used in this study to formulate the system matrix and vectors: these are the 8-noded quadrilateral and 3-noded line elements. Numerical results based on the above formulations have been calculated for several single cylinder and multiple cylinder systems. These results are discussed in the next section.

3.3 Numerical Results

3.3.a Single Cylinder

In order to compare the accuracy of the present finite element method with various solution techniques, numerical results were obtained for several single cylinder test cases. The hydrodynamic coefficients for a semi-submerged rectangular cylinder (d/a = 2, a is the half beam) using the meshes in Fig. 3.2 were calculated for the case of beam seas ($\alpha = 0^{\circ}$). Numerical results for both the added mass and damping coefficients in the sway mode (μ_{11}, λ_{11}) and in the heave mode (μ_{22}, λ_{22}) are given in Fig. 3.3, where the added mass and damping coefficients are nondimensionalized by ρA_x and $\omega\rho A_x$, respectively, A_x being the submerged area. These results may be compared to those obtained by Eatock-Taylor and Zietsman (18) using the more complicated techniques of boundary series element method (BSM) and boundary integral element method (BIM). The differences between the present results and BIM, BSM results are less than 1.5% over the frequency range of $\nu a = 0.1$ to 4.

The added mass coefficient for heave of a semi-submerged circular cylinder (d/a = 2) was calculated for the case of beam seas using the meshes shown in Fig. 3.4. Numerical results from this study, together with those obtained by Eatock-Taylor and Zietsman (18), are presented in Table 3.1. Good agreement over the whole frequency range was obtained. The differences are in general less than 0.3%, except at $\nu a = 1$ and 5 where a 1% difference exists.

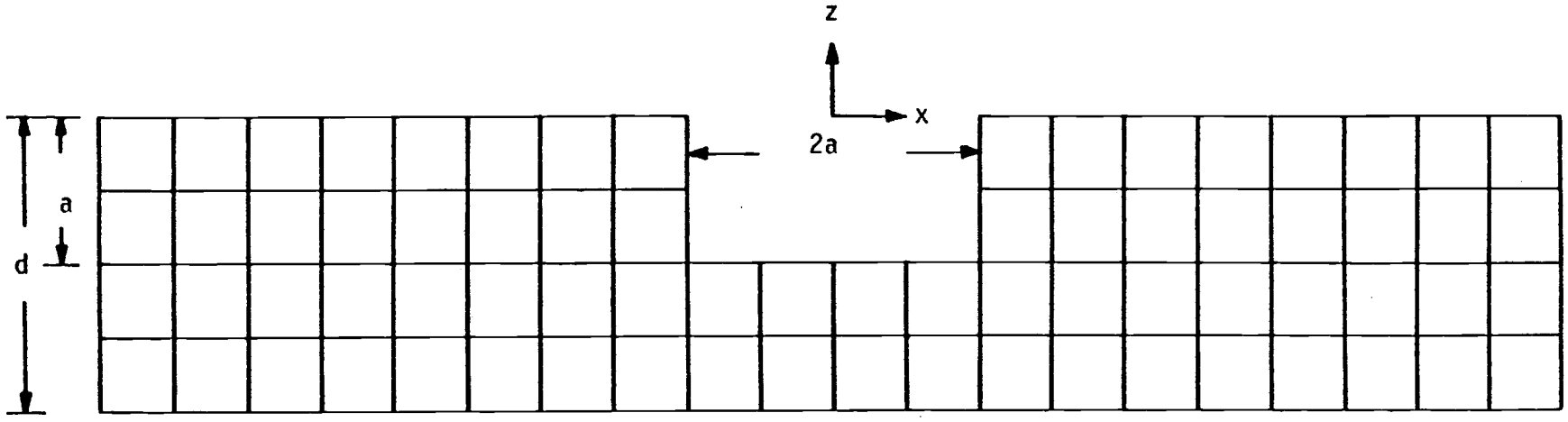

Fig. 3.2. Mesh for semi-submerged rectangular cylinder (d/a = 2)

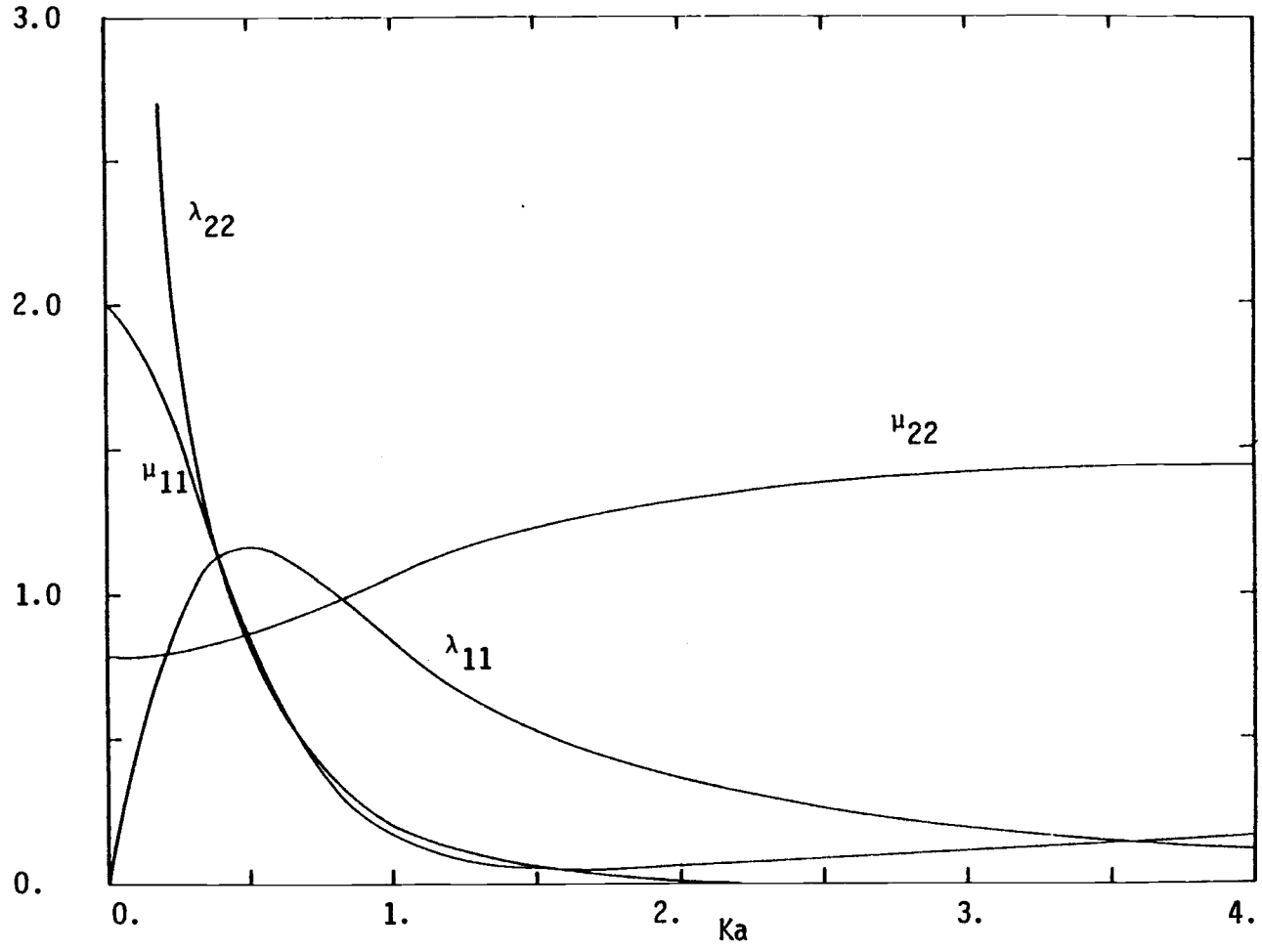

Fig. 3.3. Added mass and damping coefficients for semi-submerged rectangular cylinder (d/a = 2)

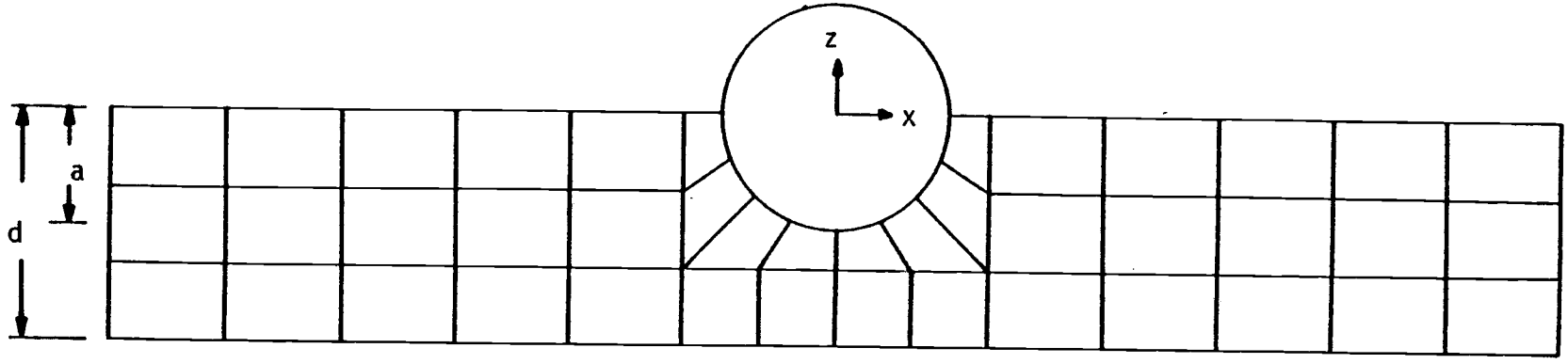

Fig. 3.4. Mesh for semi-submerged circular cylinder (d/a = 2)

TABLE 3.1 COMPARISONS OF HEAVE ADDED MASS OF A SEMI-SUBMERGED CIRCULAR CYLINDER (d/a = 2) OBTAINED IN THIS STUDY WITH THE RESULTS OF EATOCK-TAYLOR AND ZIETSMAN (18)

	Eatock-Taylor and Zietsman		
νa	BIM	BSM	Present Results
(1)	(2)	(3)	(4)
0.01	0.49894	0.49869	0.49736
0.05	0.50164	0.50139	0.50004
0.1	0.50523	0.50499	0.50362
0.2	0.51327	0.51302	0.51164
0.3	0.52255	0.52230	0.52091
0.4	0.53325	0.53300	0.53158
0.5	0.54548	0.54523	0.54374
0.6	0.55936	0.55911	0.55748
0.7	0.57491	0.57466	0.57296
0.8	0.59206	0.59183	0.59014
0.9	0.61607	0.61047	0.60905
1.0	0.63048	0.63035	0.62905
1.822	0.80058	0.80053	0.80009
2.5	0.90670	0.90522	0.90678
5.0	1.0767	1.0764	1.0642

The hydrodynamic coefficients for a semi-submerged circular cylinder in deep water (d/a = 10) were calculated for Ka = 0.25, 1.25 and 2.25, and for the angle of oblique waves generated by oscillating the cylinder in flexural modes of $\alpha = 5^{\circ}$, 45°, and 85°, respectively. The present results of heave added mass and damping coefficients were calculated using the meshes similar to those shown in Fig. 3.5, and are compared with the results of Bai (3) in Table 3.2. Agreement is in general good, except for the damping coefficient at Ka = 2.25 and $\alpha = 85^{\circ}$. The added mass and damping coefficients shown in Table 3.2 are nondimensionalized by $2\rho a^2$ and $2\omega\rho a^2$, respectively, in order to be consistent with the results presented by Bai (3), and by Bolton and Ursell (10)where infinite water depth was assumed. For large values of Ka (i.e., small values of wave length), finer meshes are necessary to calculate the hydrodynamic coefficients accurately: such a modification is discussed by Bai (3). The hydrodynamic coefficients and the cylinder responses over a range of νa = 0.1 to 2 are indicated in a subsequent section together with the results of two free floating cylinders.

3.3.b Single Cylinder With Moorings

Various kinds of moored floating structures, such as floating bridges and breakwaters, have been employed in the coastal and harbor waters. The analyses of motions, wave attenuation and moorings have been investigated by Adee, et al. (1) and by Yamamoto, et al. (78)

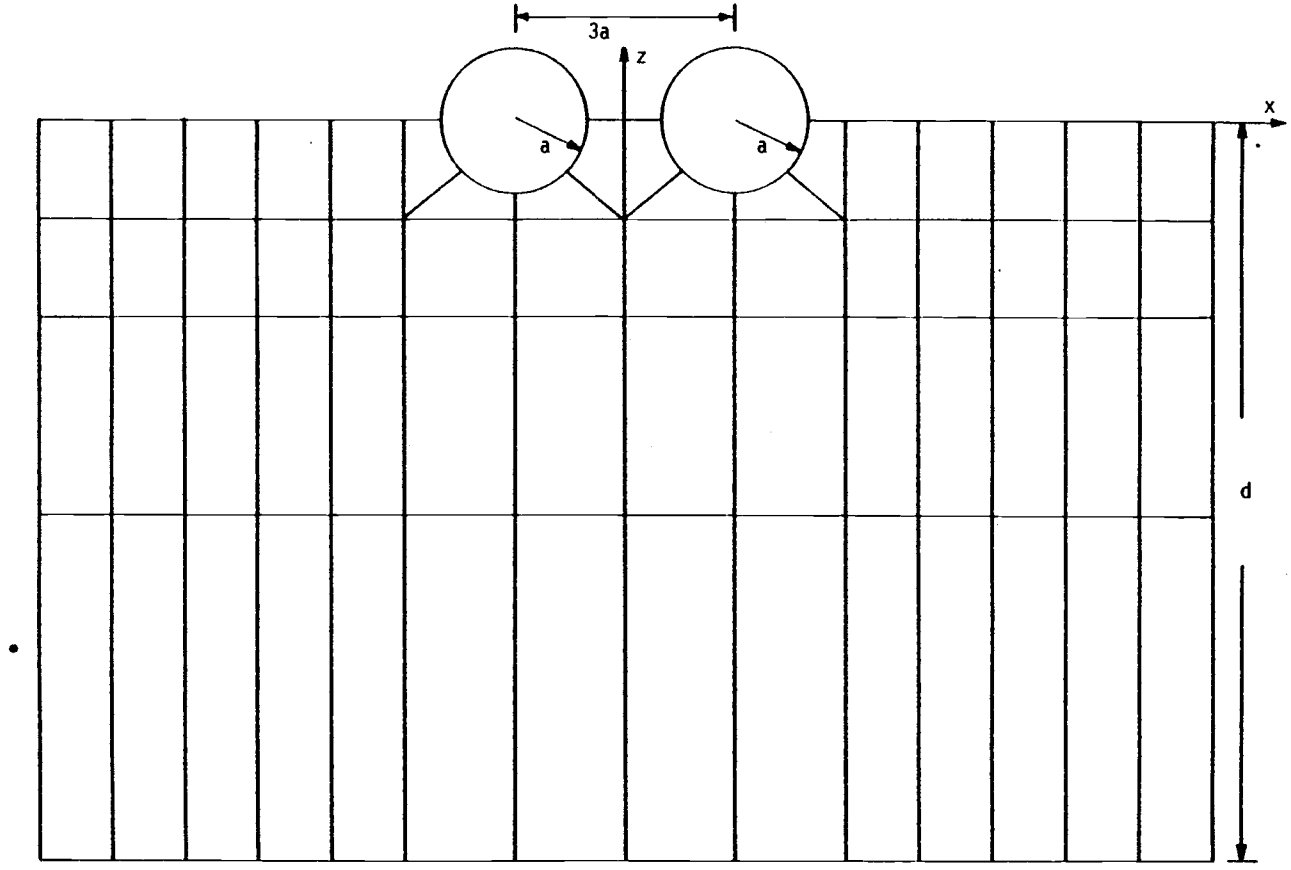

Fig. 3.5. Mesh for semi-submerged circular cylinders (d/a = 10)

TABLE 3.2 COMPARISONS OF HEAVE ADDED MASS AND DAMPING COEFFICIENTS OF A SEMI-SUBMERGED CIRCULAR CYLINDER (d/a = 10) IN OBLIQUE WAVES OBTAINED IN THIS STUDY WITH THE RESULTS OF BAI (3)

		Added Mass		Damping	
Ka	α^{o}	Bai	Present Results	Bai	Present Results
(1)	(2)	(3)	(4)	(5)	(6)
0.25	5	0.6912	0.6960	1.012	0.9498
	45	0.9307	0.9026	1.3423	1.2816
	85	3.7331	3.7629	0.9425	1.0164
1.25	5	0.4864	0.4838	0.2272	0.2241
	45	0.4390	0.4375	0.2055	0.2036
	85	0.7249	0.6874	0.1028	0.0651
2.25	5	0.5605	0.5556	0.0720	0.0725
	45	0.3225	0.3202	0.0488	0.0503
	85	0.3728	0.3141	0.0520	0.0003

using the two-dimensional integral equation methods.

Finite element solutions were obtained for a semi-submerged rectangular cylinder cross-spring moored to the seafloor in the case of beam seas. The geometry of the structure, arrangement of moorings and the meshes used in the finite element solutions are shown in Fig. 3.6, where the moorings are characterized by dimensionless spring constant of $Q/\rho gd = 0.018$ and initial tension of $f/\rho gd = 0.0037$. Numerical results of sway and heave responses from the present study are compared with the experimental and numerical results of Yamamoto, et al. (78) in Figs. 3.7-3.8. The numerical technique used by Yamamoto, et al. (78) is implemented by using Green's second identity and a fundamental solution to form a boundary integral equation (BEM) which is then discretized numerically over the full boundaries of the problem. Numerical results from Yamamoto, et al. (78) are based on using imaginary radiation boundaries taken one wave length from the structure, and using a segment size of L/15 to L/20. Good agreement over a range of diffraction parameter, Ka, from 0 to π was obtained between the finite element and BEM solutions.

3.3.c Single Cylinder Close To A Wall

The standing wave effects between a fixed, vertical, impermeable wall and large floating structures have been investigated by Ho and Harten (30) using the BEM technique. Their technique also incorporated the fitting of bi-cubic splines for the discretization of the

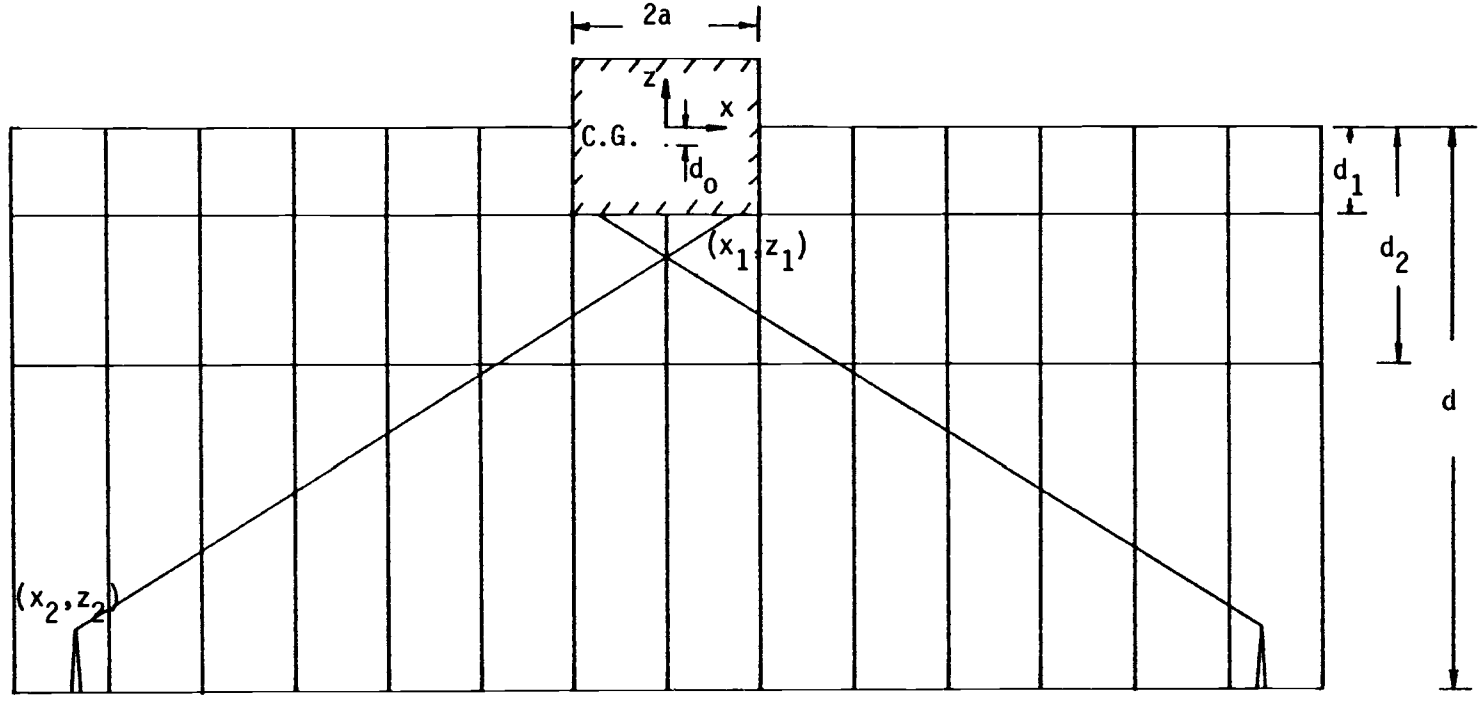

Fig. 3.6. Mesh for a cross-spring moored rectangular cylinder ($a/d = 0.167$, $x_1/d = 0.125$, $z_1/d = -0.156$, $x_2/d = -1.056$, $z_2/d = -0.889$, $d_o/d = 0.015$, $d_1/d = 0.156$, $d_2/d = 0.422$)

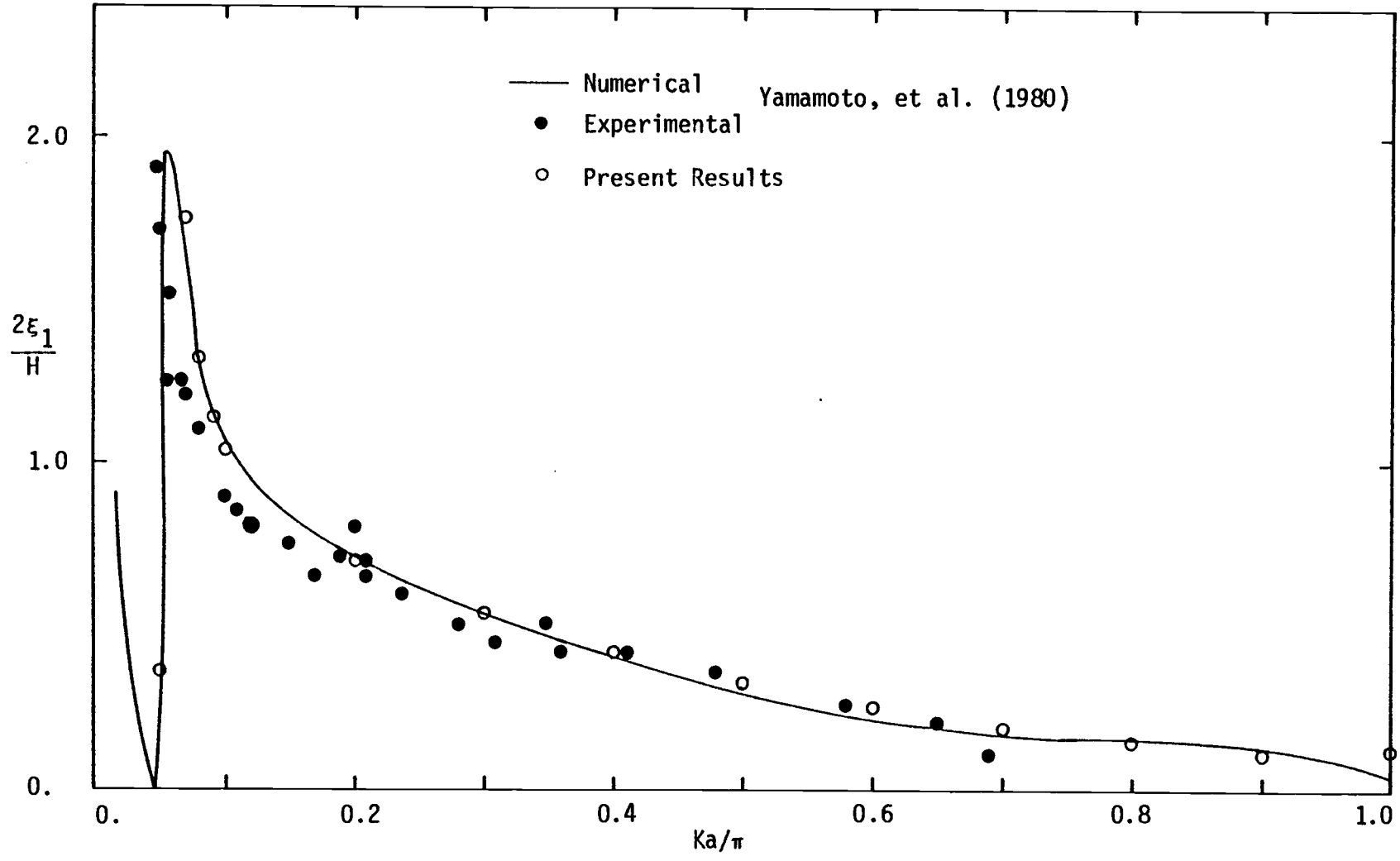

Fig. 3.7. Sway response of a cross-spring moored rectangular cylinder

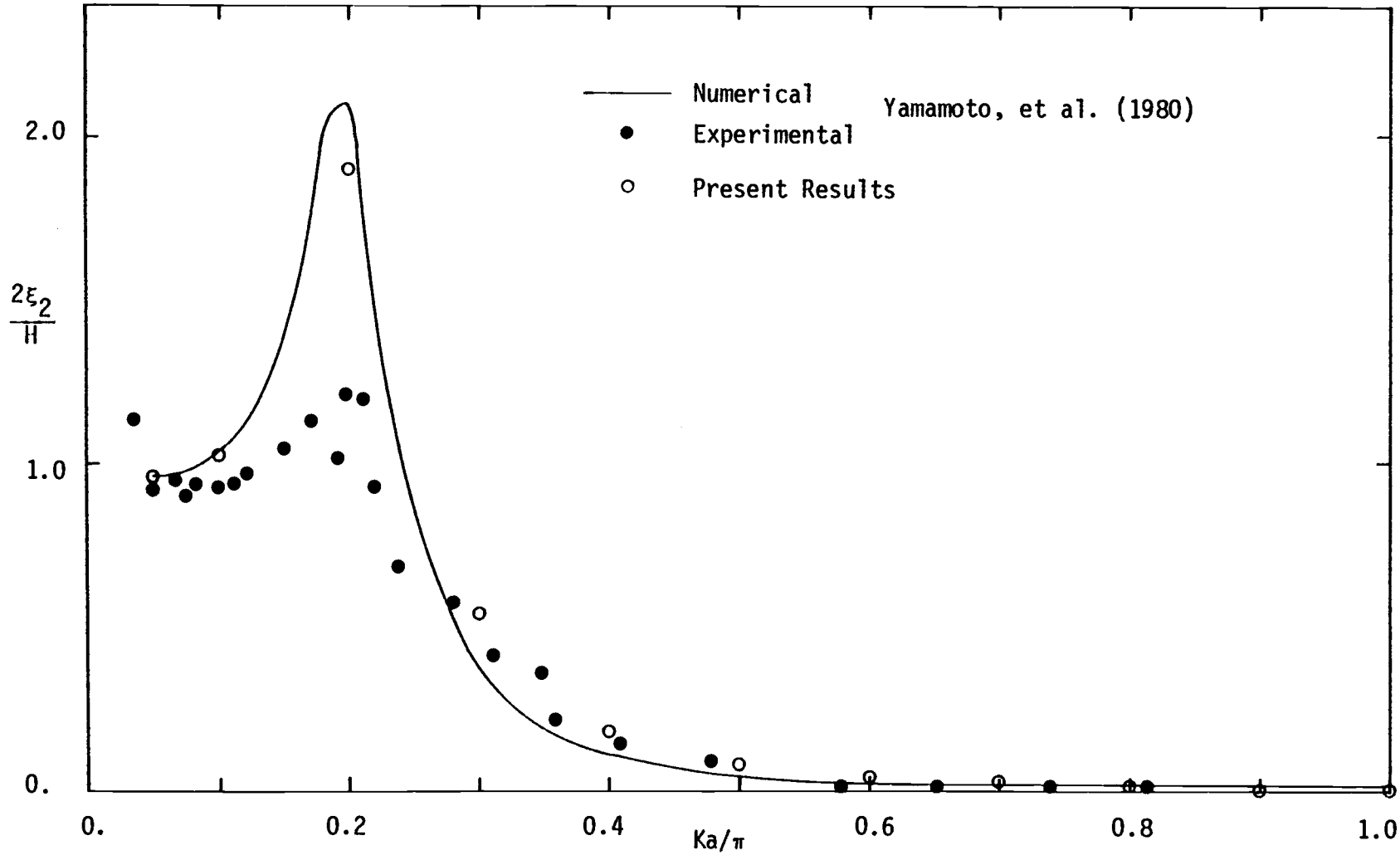

Fig. 3.8. Heave response of a cross-spring moored rectangular cylinder

integral equation. The hydrodynamic coefficients for a semi-submerged rectangular barge oscillating adjacent to a vertical wall with varying permeability were also calculated by using the present finite element method, where the functional integral due to boundary dampers at the wall were multiplied by a fictitious permeability parameter, β.

Numerical results of the heave added mass and damping coefficients (nondimensionalized by ρA_x and $\omega\rho A_x$, respectively) from this study with β = 0, 0.05, 0.25, 0.5 and 0.75; together with those obtained by Ho and Harten (30), are shown in Figs. 3.9-3.10 for the case of beam seas. These results are shown over a wave period range of T from 5 sec to 40 sec (or Ka from 9.82 to 0.66), in order to be consistent with the results presented by Ho and Harten (30). Close agreement over the whole wave range was obtained between the present results and BEM solutions for the case of an impermeable wall (β = 0). Heave resonance corresponding to T = 27.5 sec was predicted, as shown in Figs. 3.9-3.10. Large negative values of added mass coefficient are predicted near the resonance period by both solution methods. Numerical results of the sway added mass and damping coefficients are also seen to have resonance near T = 27.5 sec for the case of impermeable wall; as shown in Figs. 3.11-3.12.

As would be expected, the resonance phenomena become less severe with increasing permeability of the wall. It is shown in Figs. 3.9-3.12 that permeability of the wall has a strong effect on the standing waves system. Numerical results for the case of β = 0.1 and 0.15 are

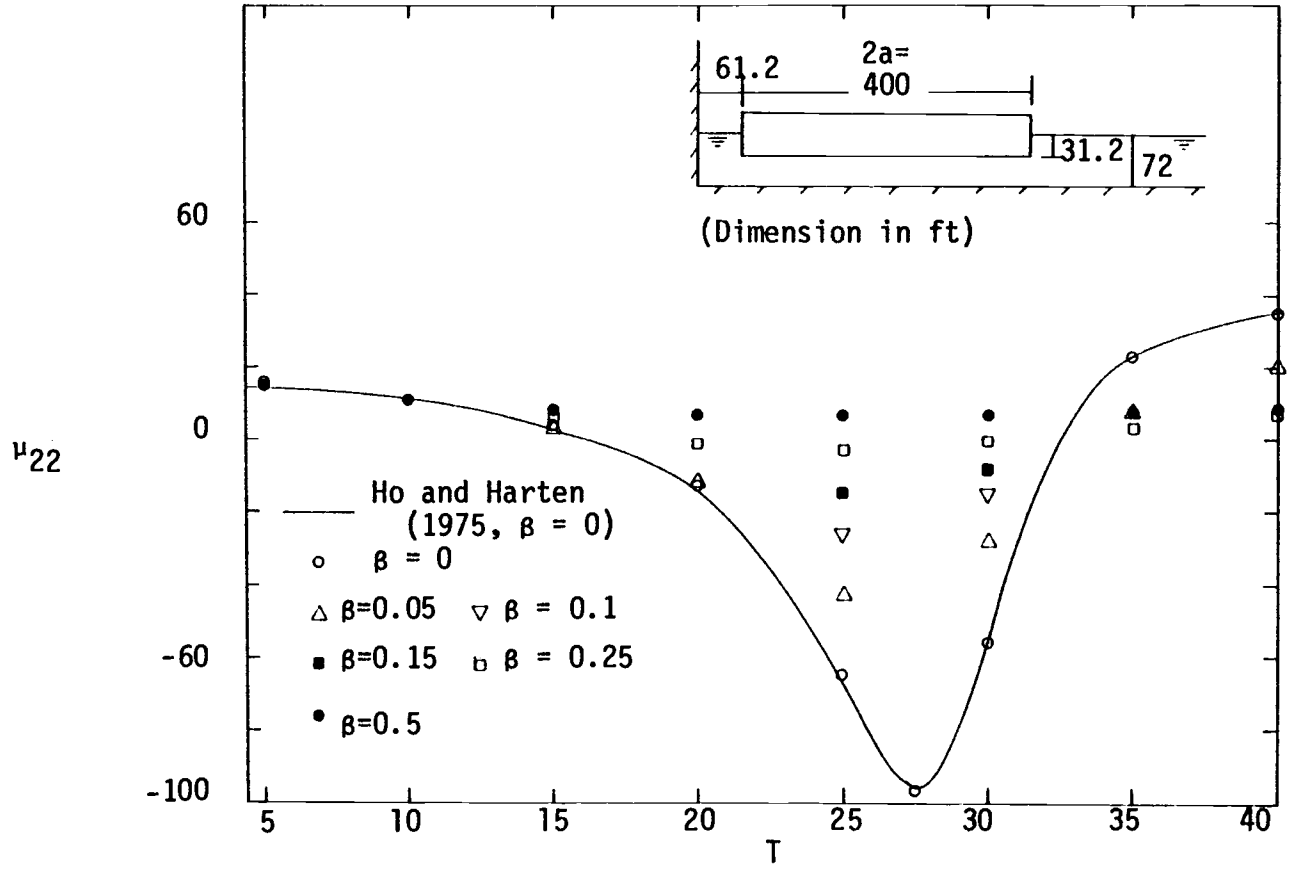

Fig. 3.9. Heave added mass coefficient of a rectangular barge adjacent to a vertical wall with permeability β

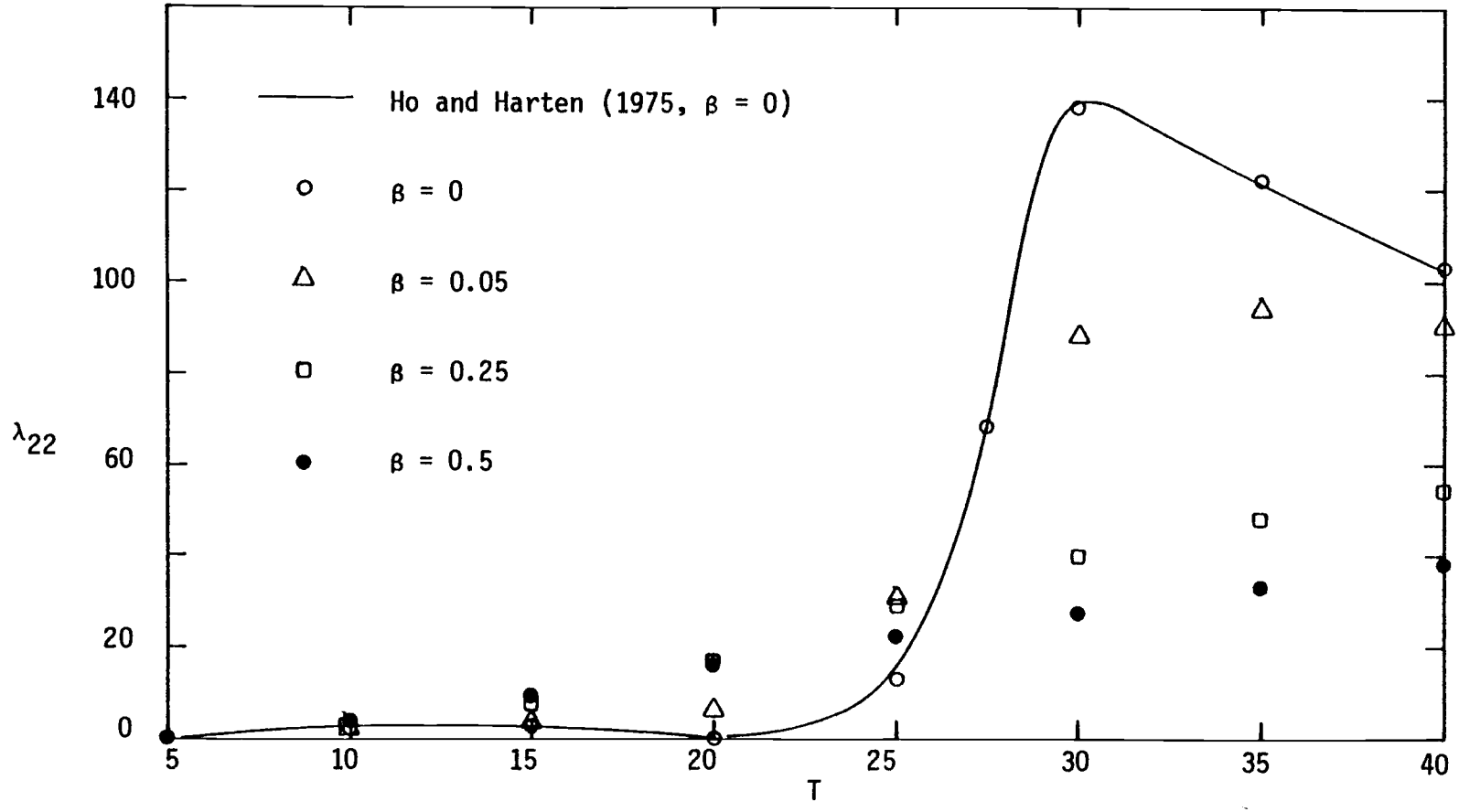

Fig. 3.10. Heave damping coefficient of a rectangular barge adjacent to a vertical wall with permeability β

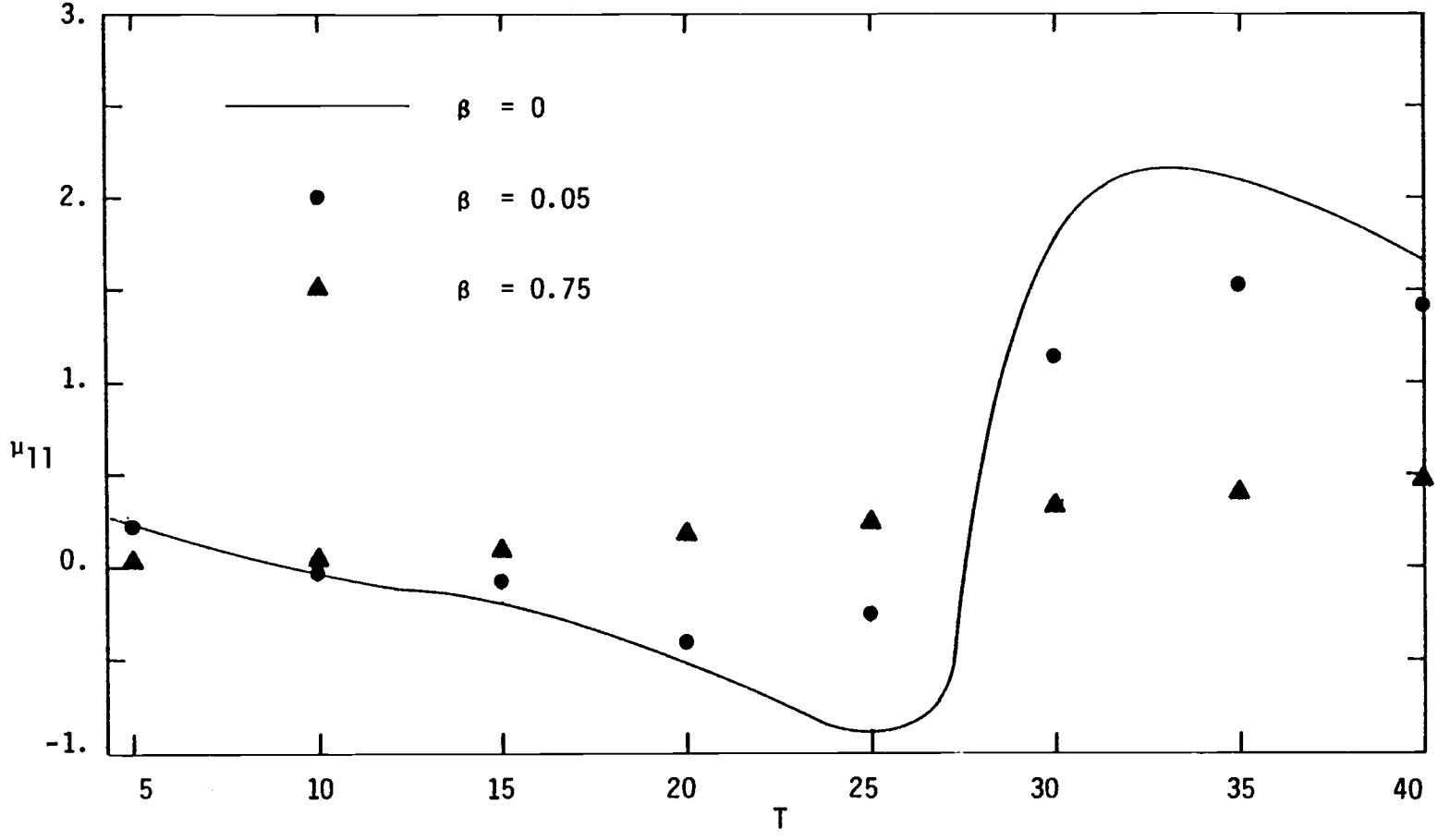

Fig. 3.11. Sway added mass coefficient of a rectangular barge adjacent to a vertical wall with permeability β

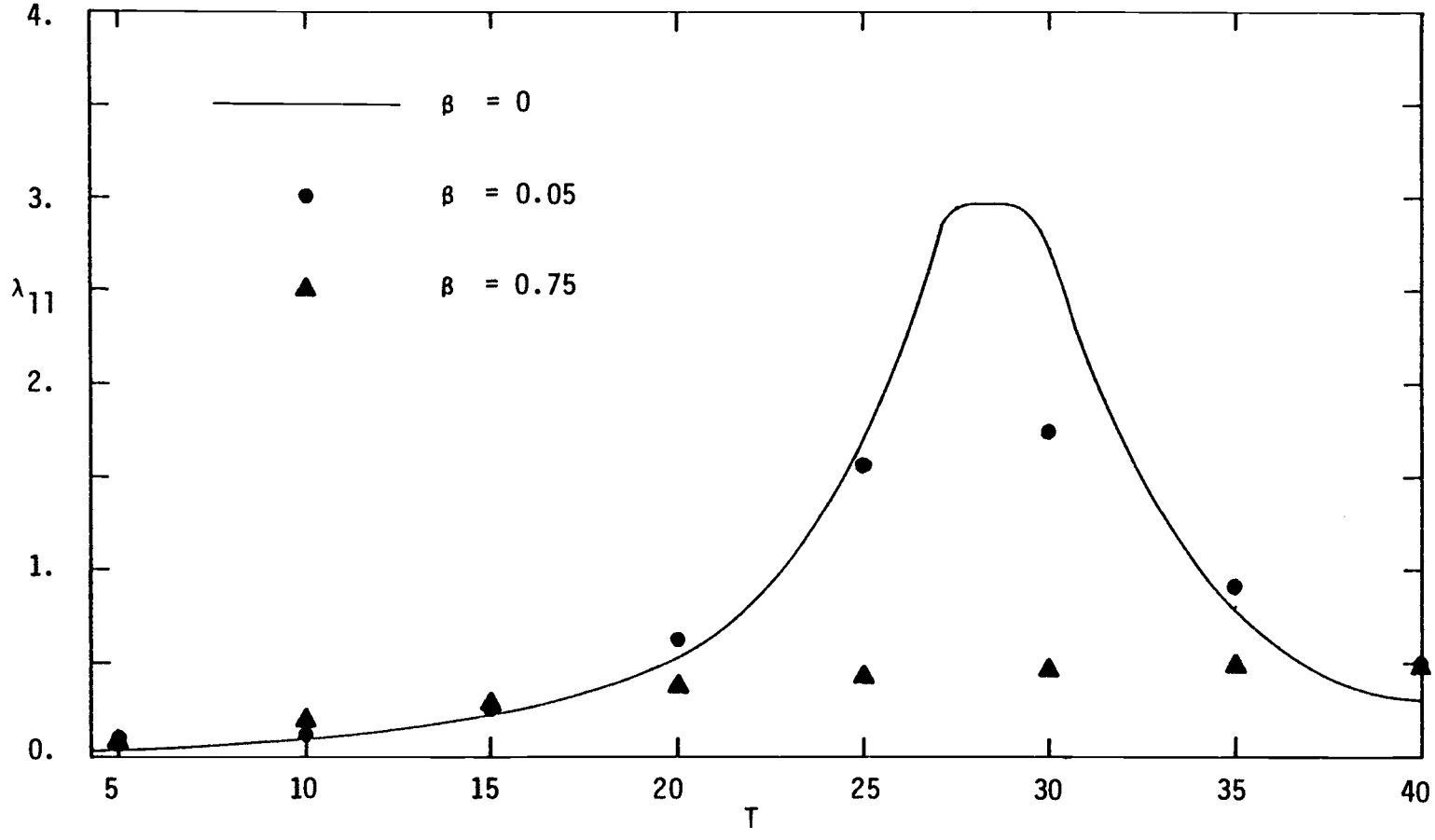

Fig. 3.12. Sway damping coefficient of a rectangular barge adjacent to a vertical wall with permeability β

also illustrated in Fig. 3.9 to show the trend of this effect: the resonance period decreases with increasing permeability and the rate of its influence also decreases with increasing permeability. The resonance phenomena are nearly suppressed for the case of $\beta = 0.25$, where only a small value of negative added mass coefficient was predicted.

3.3.d Catamaran

The hydrodynamics of catamaran type vessels are of particular interest to the naval architect. Numerical solutions of the hydrodynamic coefficients have been reported by Wang and Wahab (73) for a semi-submerged catamaran with circular sections, and by Wang (72) for a fully-submerged catamaran. A method of wave sources and multipoles was employed. Other solution techniques have also been reported by Ohkusu (56) and by Maeda (48).

The hydrodynamic coefficients of a semi-submerged catamaran with two identical circular sections separated by a distance of one cylinder radius in finite water depth (d/a = 10) were calculated using the meshes shown in Fig. 3.5. The sway added mass and damping coefficients (nondimensionalized by ρA_x and $\omega\rho A_x$, respectively) for the case of beam seas are illustrated in Fig. 3.13. The heave added mass and damping coefficients for the case of beam seas are illustrated in Fig. 3.14 and Fig. 3.15, respectively, together with those results of of Wang and Wahab (73) where an infinite water depth was assumed. Good agreement over the frequency range of $\nu a = 0.1$ to 2 is obtained,

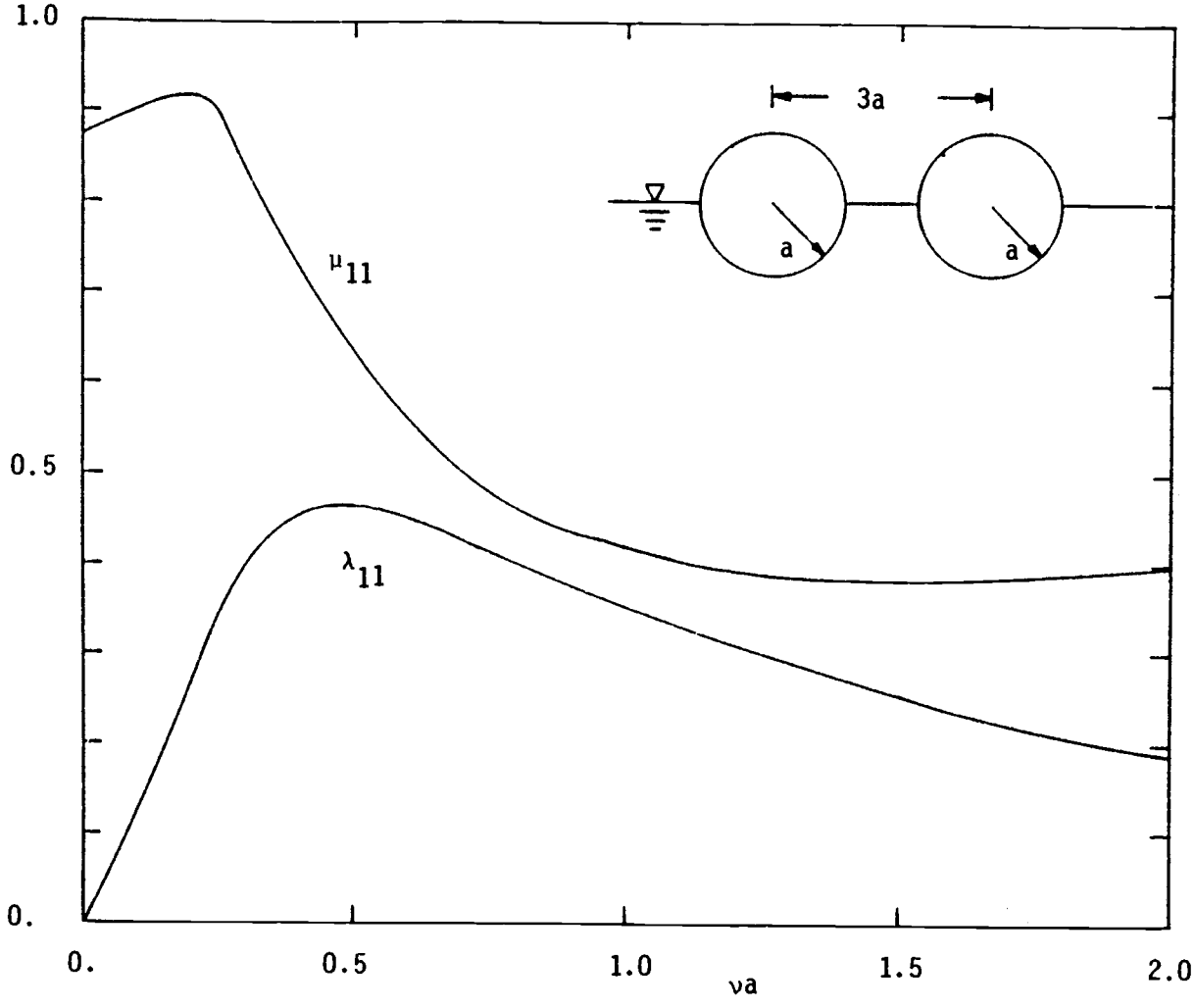

Fig. 3.13. Sway added mass and damping coefficients of catamaran (d/a = 10) in beam seas

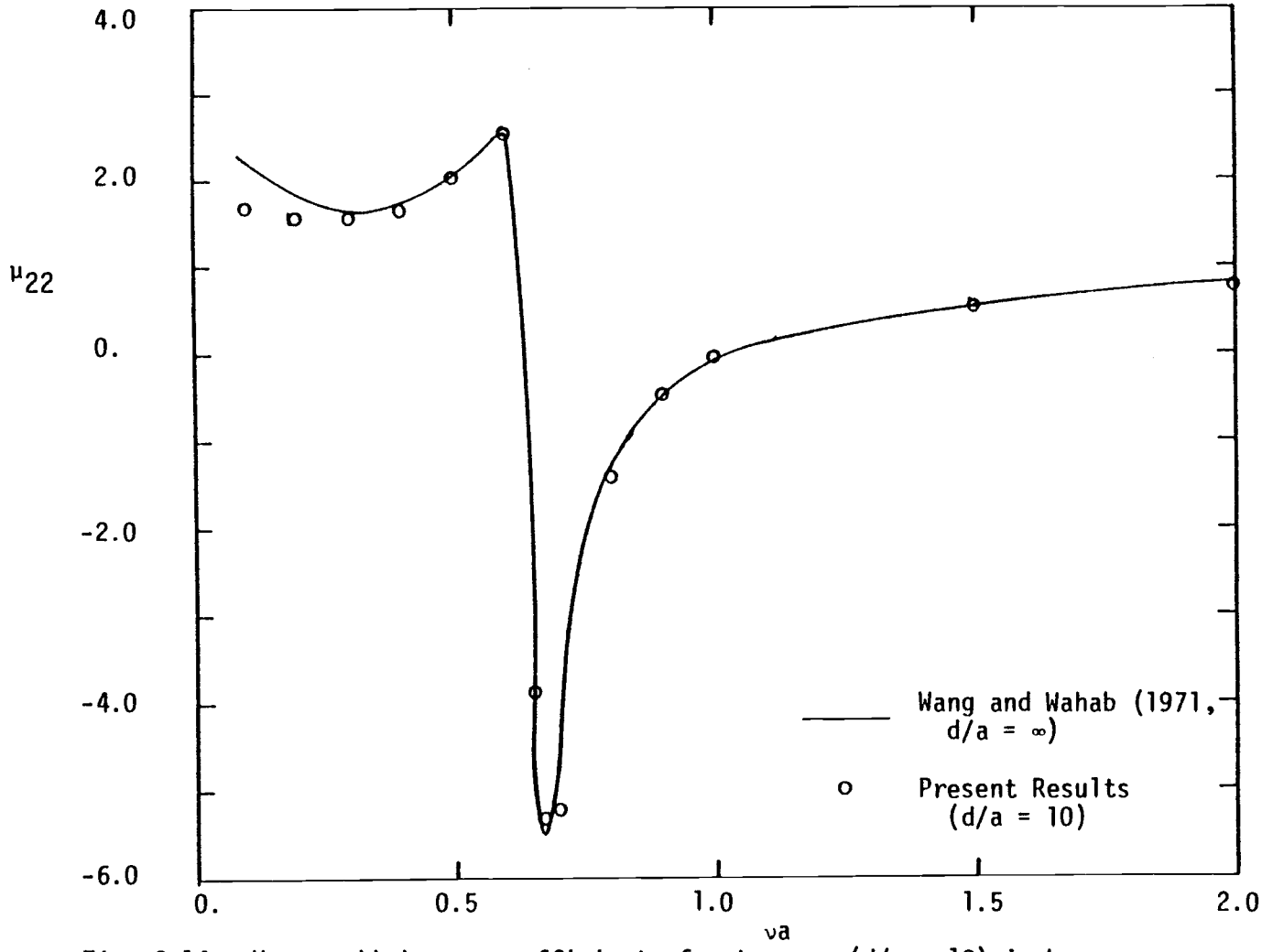

Fig. 3.14. Heave added mass coefficient of catamaran (d/a = 10) in beam seas

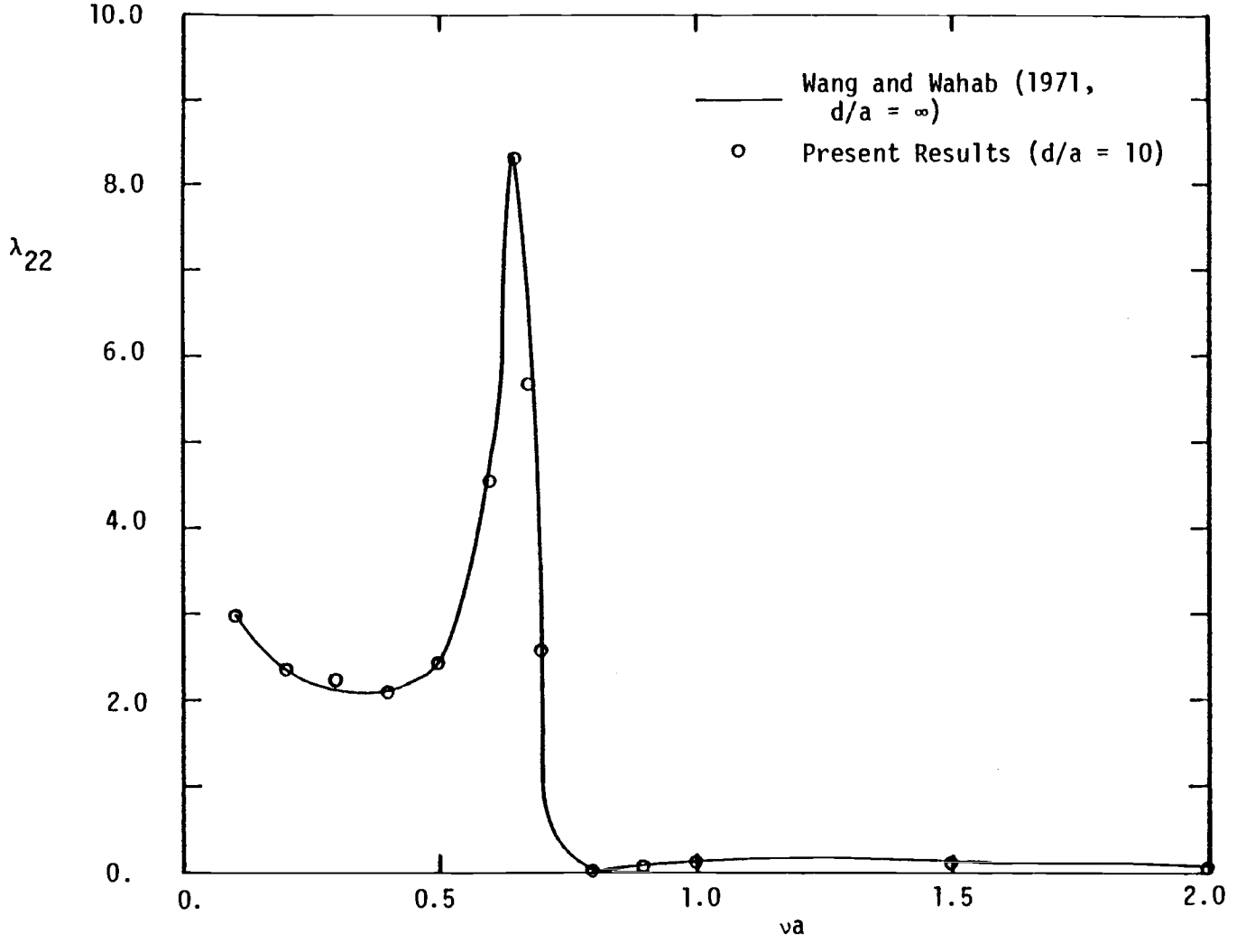

Fig. 3.15. Heave damping coefficient of catamaran (d/a = 10) in beam seas

except at the low frequency range where the finite depth finite element solutions differ from the infinite depth solutions. The phenomenon of wave resonance between the two sections, which happens in a discrete set of characteristic frequencies as shown by Wang and Wahab (73), is predicted using the present finite element method. For the particular case studied, the first resonance corresponds approximately to $\nu a = 0.65$.

3.3.e Two Freely Floating Cylinders

The case of two freely floating cylinders with identical sections, in constrast to the other extreme case of two rigidly connected cylinders of a catamaran, has also been studied. The finite element meshes employed are identical to those used for the case of a catamaran as shown in Fig. 3.5. The hydrodynamic coefficients were calculated for the case of beam seas over a frequency range of $\nu a = 0.1$ to 2. The added mass and damping coefficients are the same for both cylinders since identical sections are used (i.e., $\mu_{k1k1} = \mu_{k2k2}$, $\lambda_{k1k1} = \lambda_{k2k2}$, $k = 1,2$). These coefficients are illustrated in Figs. 3.16-3.19, together with the coefficients corresponding to a single isolated cylinder. The phenomenon of wave resonance is also shown in Figs. 3.16-3.19 to occur approximately at integer multiples of $\nu a = 0.65$. Large negative values of added mass are calculated across the first resonance frequency where the standing wave system between the two cylinders changes its phase about 180 degrees. The hydrodynamic response of cylinders will be significantly affected due to the 180

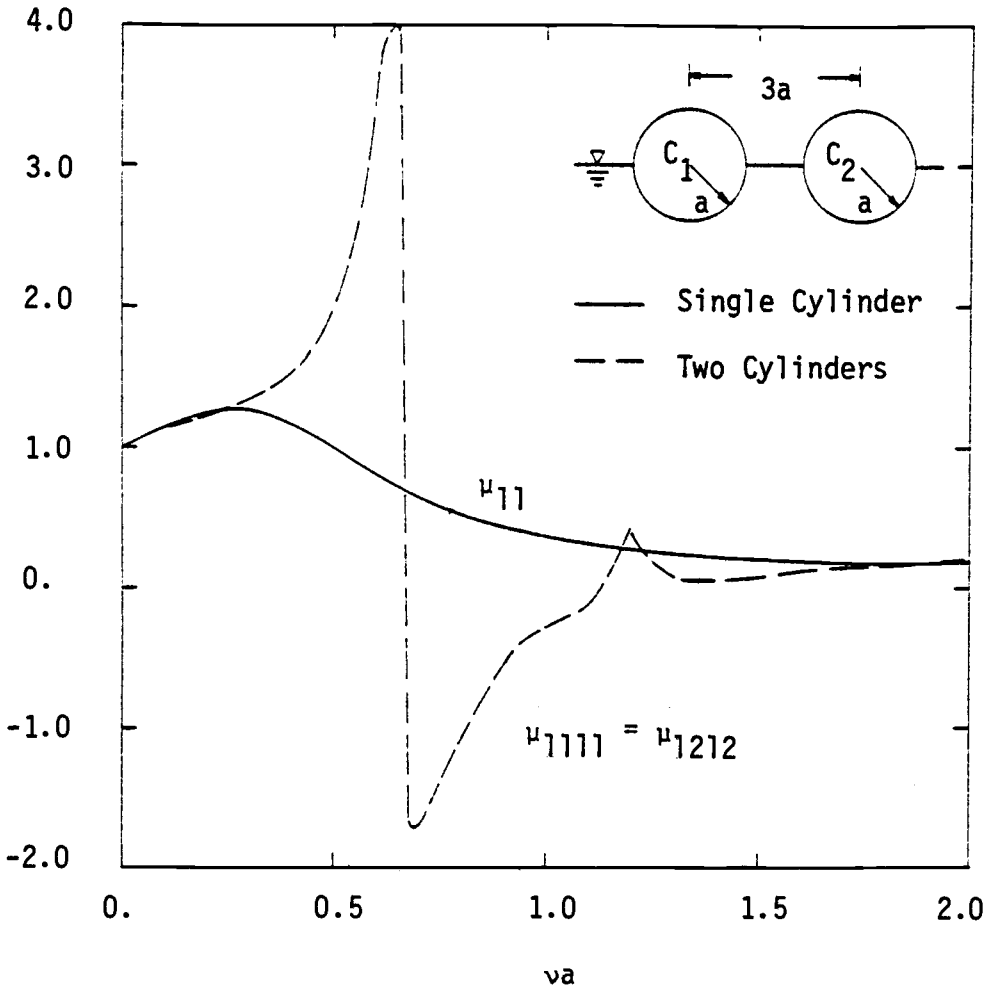

Fig. 3.16. Sway added mass coefficient of two cylinders in beam seas (d/a = 10)

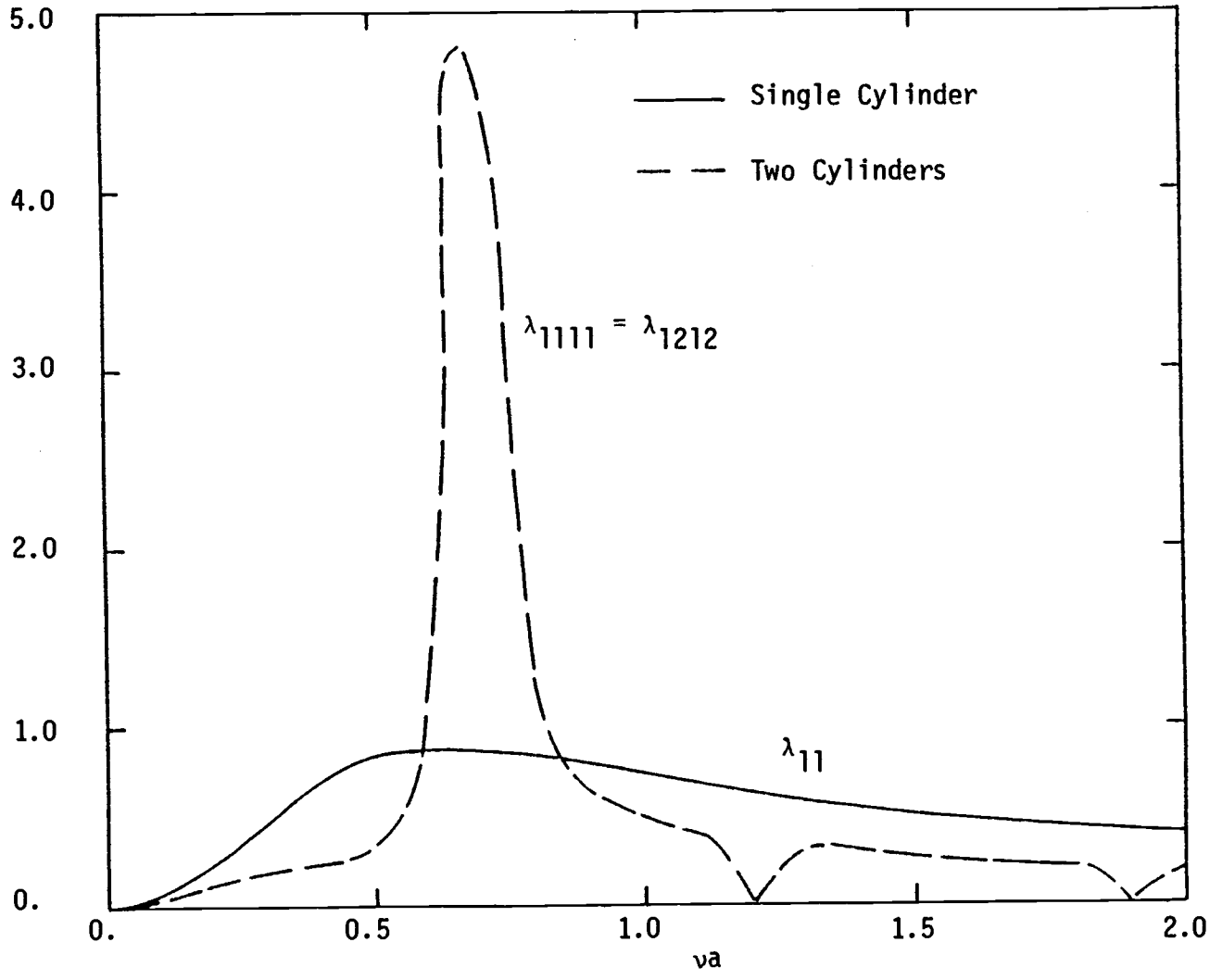

Fig. 3.17. Sway damping coefficient of two cylinders in beam seas (d/a = 10)

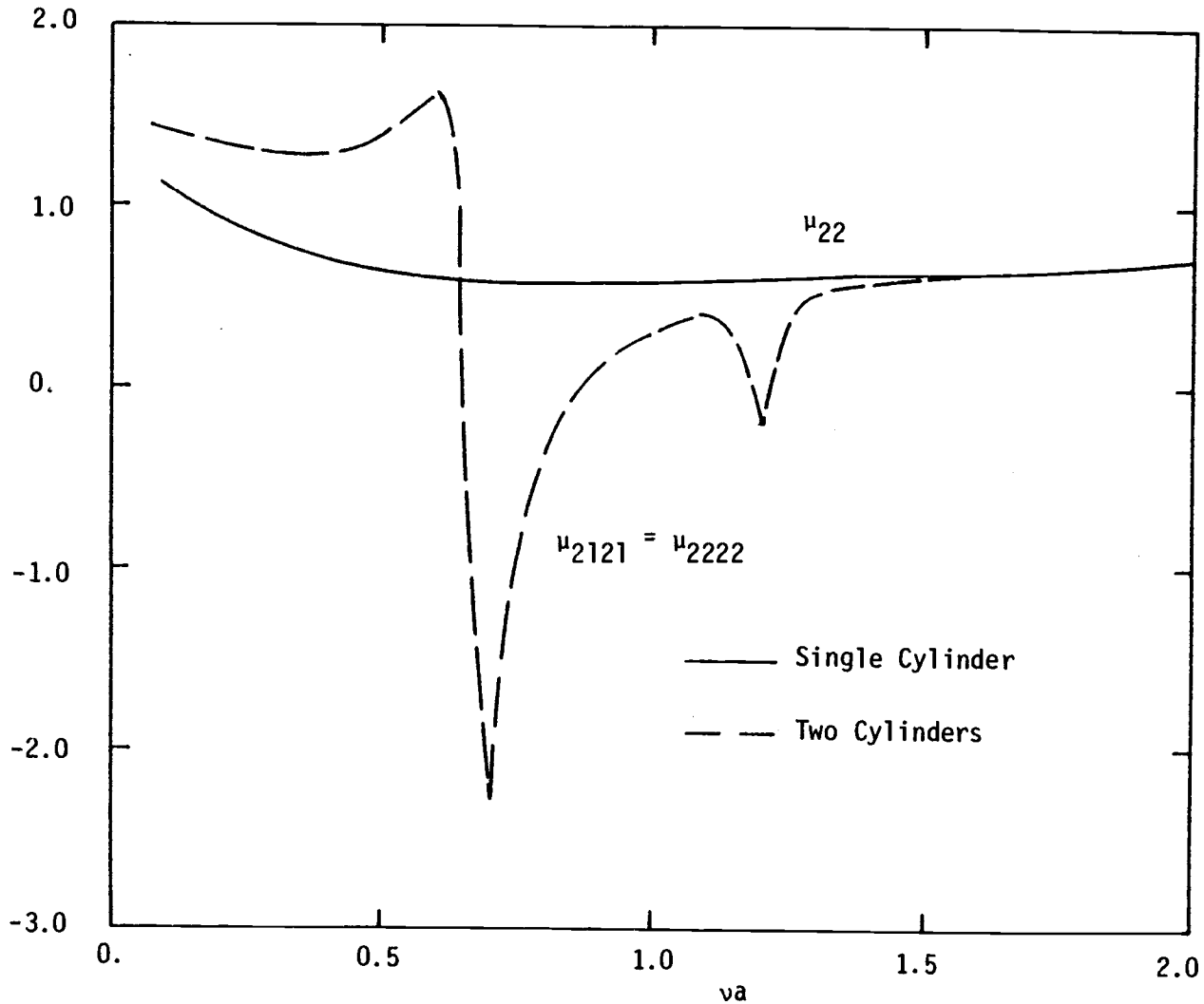

Fig. 3.18. Heave added mass coefficient of two cylinders in beam seas (d/a = 10)

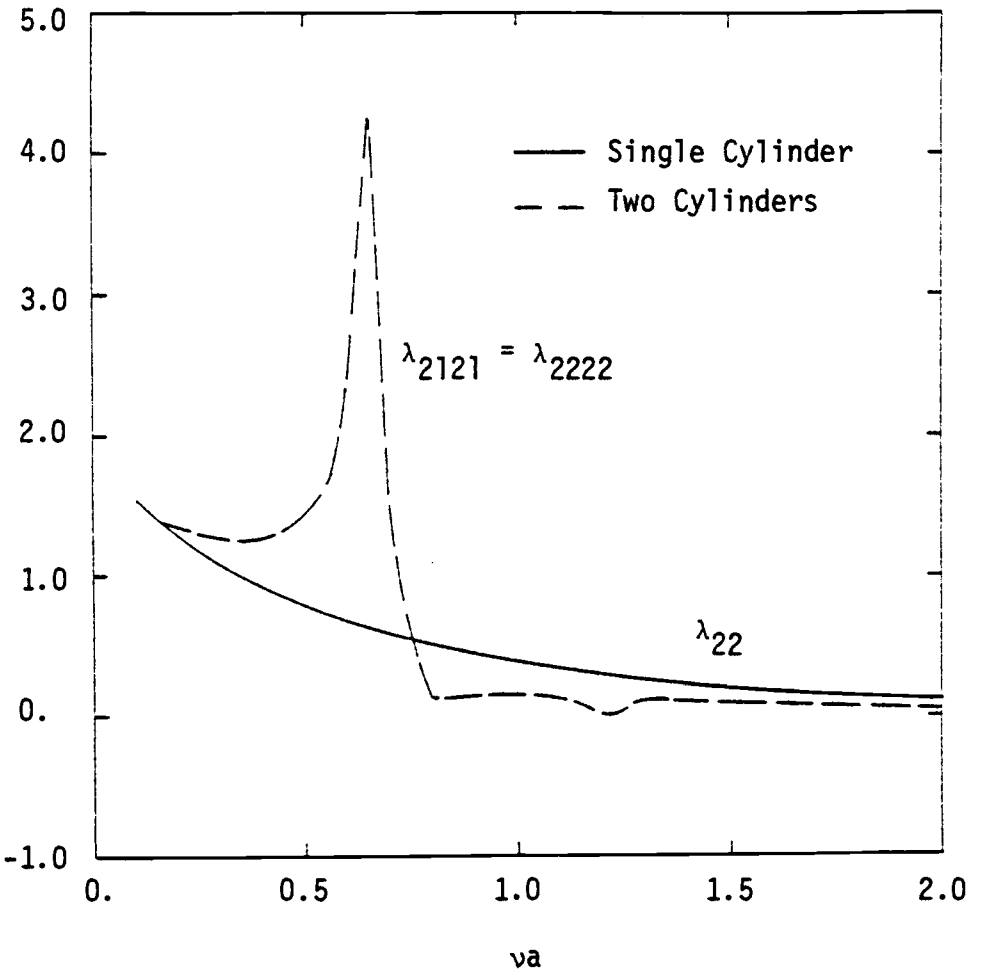

Fig. 3.19. Heave damping coefficient of two cylinders in beam seas (d/a = 10)

degree out-out-phase relative motions.

The absolute and relative responses of cylinders in beam seas are illustrated in Figs. 3.20-3.21 for the sway and heave modes, respectively, together with the responses of a single isolated cylinder. In general, the absolute responses of the cylinder on the downwave side are less than the responses of the cylinder on the upwave side due to wave sheltering effects. The absolute response curves of the upwave cylinder, in both the sway and heave modes, are seen to be oscillating around the response curves of a single isolated cylinder. This is due to the effects of wave reflections from the downwave cylinder, in contrast to the sheltering effects. The relative motions between the adjacent cylinders are seen to have resonance peaks around a discrete set of characteristic frequencies where the motions are 180 degree out-of-phase. These large relative motions should be identified in the design of facilities and operations in offshore and harbor waters, e.g., cargo transfer between adjacent vessels.

There exist relatively few reports in which the responses of a single cylinder or multiple cylinders are calculated. Numerical results of Lee (44) for heave response of a single circular cylinder semi-submerged in an infinite water depth have been compared with the present results. Close agreement to two decimal places was obtained for the frequency range studied. Numerical results of the two-cylinder case by Sayer and Spencer (59), based on a modified method of multipoles similar to that of Wang and Wahab (73), compare fairly well with the present results as shown in Figs. 3.20-3.21. However,

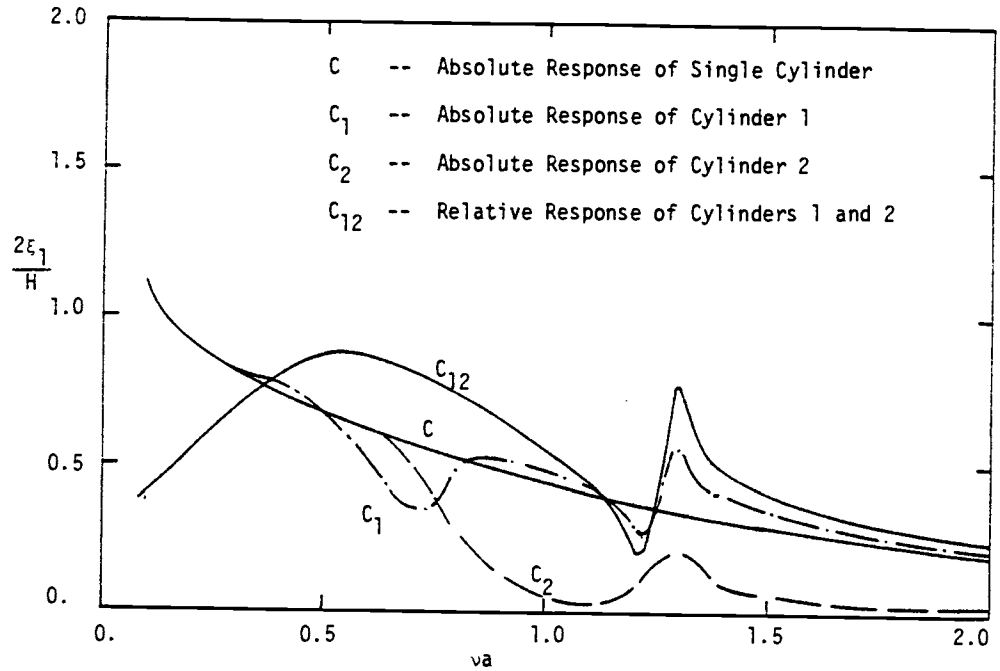

Fig. 3.20. Sway response of two cylinders in beam seas (d/a = 10)

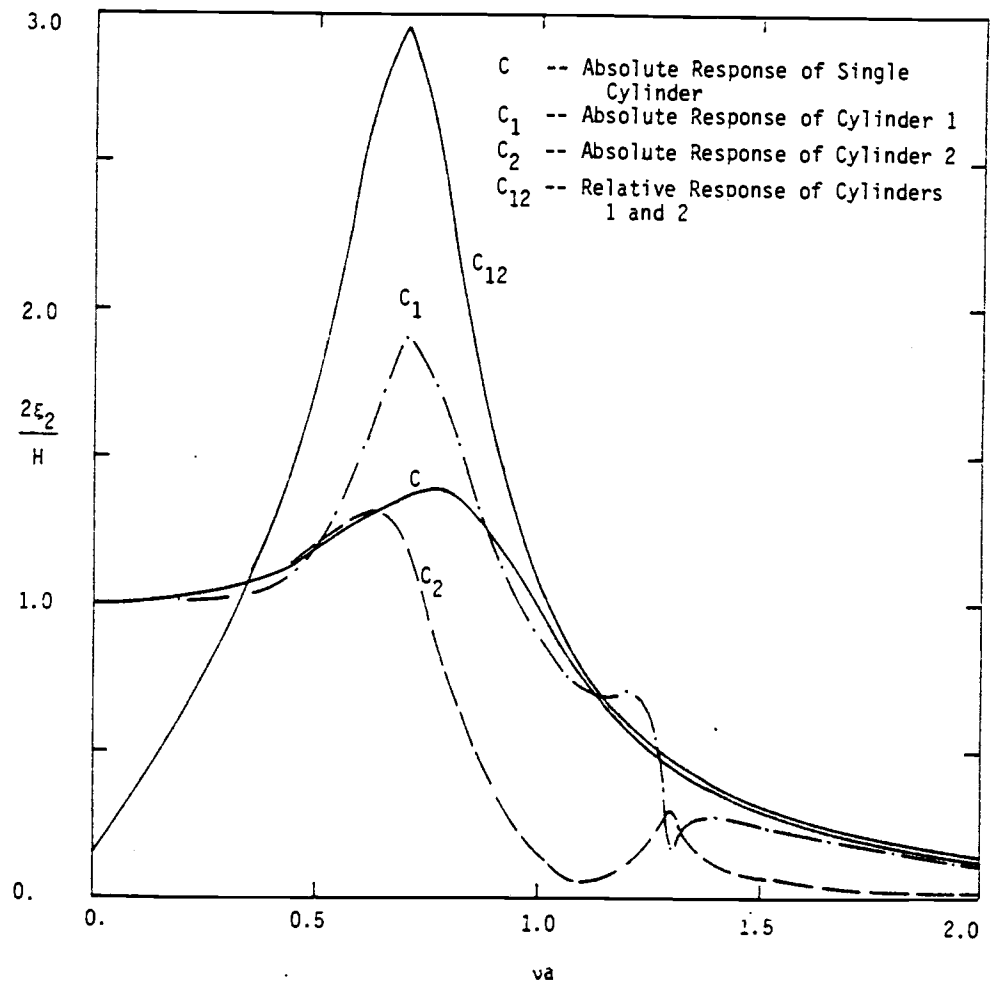

Fig. 3.21. Heave responses of two cylinders in beam seas (d/a = 10)

Sayer and Spencer (59) erroneously reported that the linear superposition of diffraction and radiation problems, as employed in the present method, is inadequate for solving the interference problem between adjacent cylinders. The phase difference between the motions needs to be solved explicitly in the method of Sayer and Spencer in contrast to the present method.

The case of two cylinders has also been studied for the case of obliquely incident waves of $\alpha = 45^{\circ}$. The absolute and relative responses of cylinders are illustrated in Figs. 3.22-3.23 for the sway and heave modes, respectively. The heave response curves are similar to those of beam seas. However, the large sway response is shifted to a higher resonance frequency.

3.3.f Two Floating Cylinders With Inter-Structural Constraint

In order to study the effect of inter-structural restoring force on the structural responses, numerical results were calculated for two floating circular cylinders shown in Fig. 3.5 with varying horizontal linear constraints. Table 3.3 presents the absolute and relative responses of cylinders for the case of beam seas and $\nu a = 0.5$, with different values of dimensionless spring constant for the inter-structural sway constraint, $Q_{1112}/\rho ga$.

For this particular case studied, it is shown that, although the absolute responses oscillate around those of the freely floating case, the relative sway response decreases as the constraint becomes stiffer.

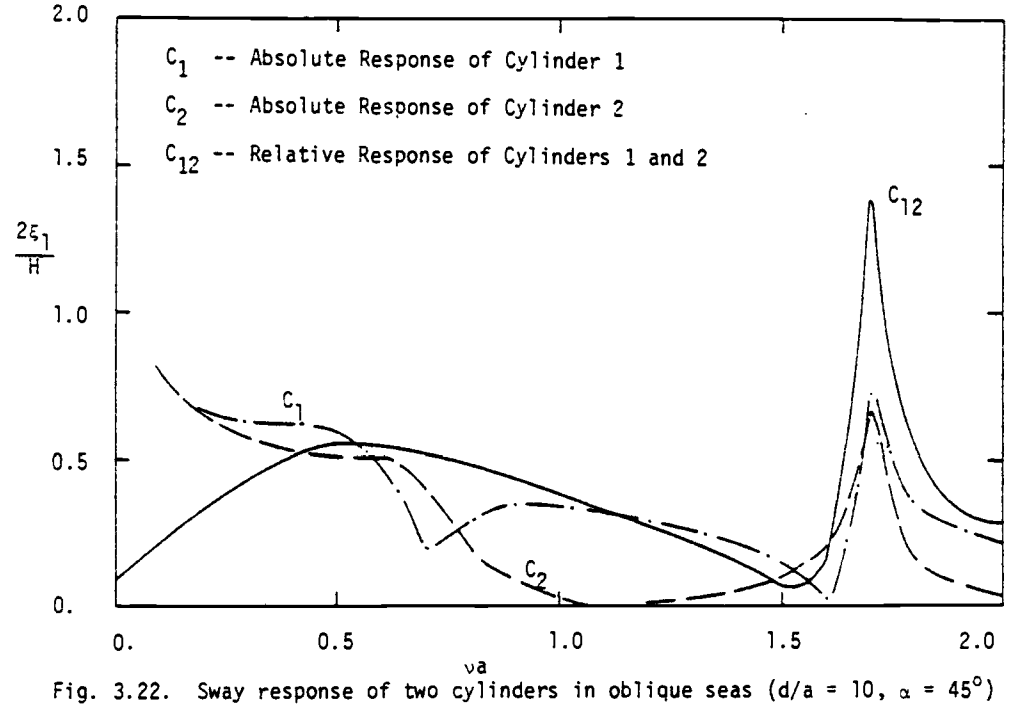

Fig. 3.22. Sway response of two cylinders in oblique seas (d/a = 10, $\alpha = 45^{\circ}$)

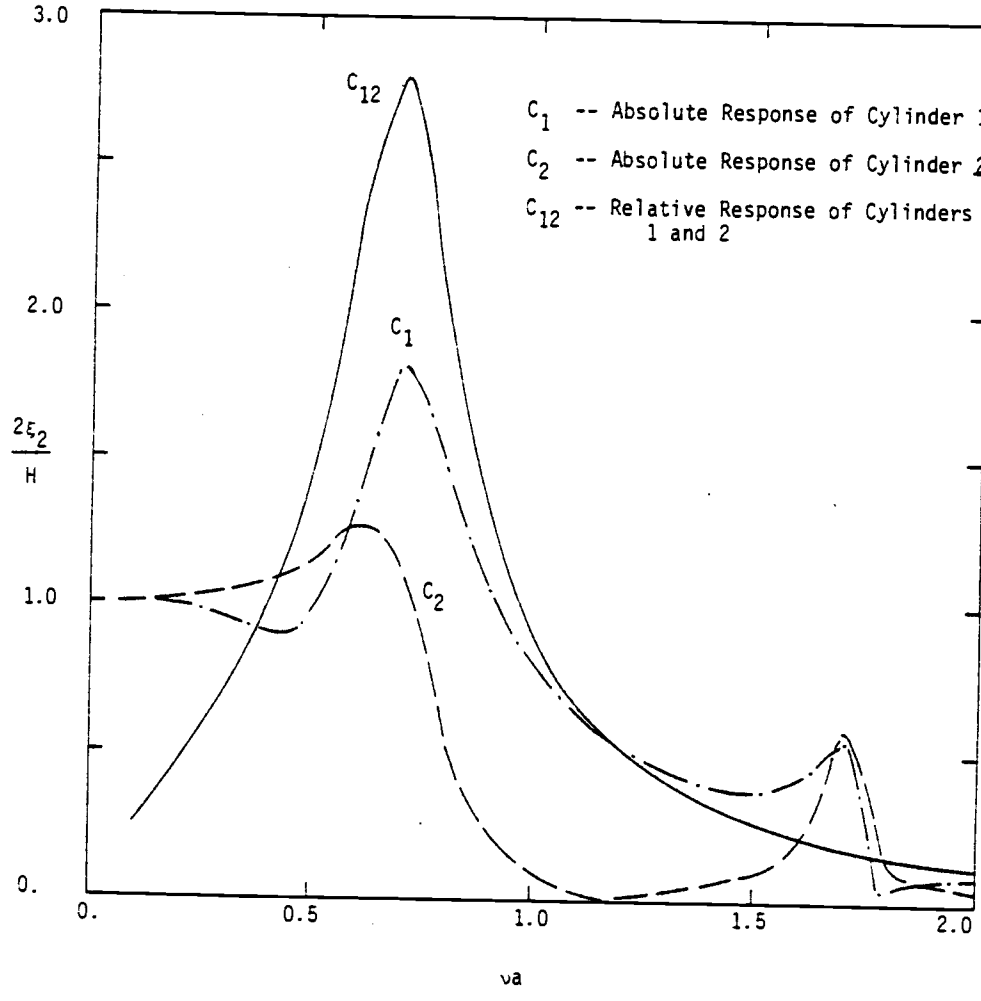

Fig. 3.23. Heave response of two cylinders in oblique seas ($d/a = 10$, $\alpha = 45^\circ$)

This is consistent with the increase of in-phase constraint in the sway motion.

TABLE 3.3 EFFECTS OF INTER-STRUCTURAL CONSTRAINT ON RESPONSES

	Upwave Cylinder		Downwave Cylinder			
	Absolute Response		Absolute Response		Relative Response	
$Q_{1112}/\rho ga$	Sway	Heave	Sway	Heave	Sway	Heave
(1)	(2)	(3)	(4)	(5)	(6)	(7)
0.	0.686	1.173	0.677	1.188	0.878	1.758
0.0264	0.696	1.165	0.679	1.195	0.871	1.757
0.264	0.827	1.084	0.722	1.261	0.808	1.742
2.64	0.489	1.231	0.385	0.941	0.455	1.550
26.4	0.043	1.017	0.050	1.201	0.081	1.692

3.4 Summary

The linear boundary-value problems have been formulated for a multiple two-dimensional structures system interacting with oblique waves in finite water depth. The hydrodynamic interference effects between floating structures and between fixed and floating structures have been calculated using a localized finite element method incorporating plane boundary dampers. Numerical results indicate that:

1) The localized finite element model provides accurate results

over a wide range of frequencies, even when a moderate extent of fluid domain is discretized, when compared with the more exact solution techniques of matching with analytical boundary solutions. This has been validated by comparing the numerical results of the diffraction and radiation problems of a single cylinder with alternative solutions, both in beam seas and in oblique seas.

2) Numerical results of both extreme cases of a catamaran and of two freely floating cylinders compare closely with those obtained by the method of multipoles. Important interference phenomena, such as wave resonance and large relative motions, are identified over a wide range of frequencies. Numerical solutions can therefore be extended to more complicated geometries and arrangements, where numerical difficulties exist and the phenomenon of irregular frequencies are not clearly differentiated from resonance phenomenon in the integral equation method.

3) The interference effects between a mixture of fixed and floating structures have been extended to the case of a permeable wall. Permeability of the wall has a dominant effect on suppressing the wave resonance.

4) Numerical results of taut-moored floating breakwater responses compare closely with those obtained by the boundary element method and by experimental works. The effect of inter-structural restoring force on the responses has been given by varying the magnitude of in-phase linear constraint between two floating cylinders.

Although the numerical results obtained are limited to infinitely

long cylinders, they do provide useful information for incorporation with the semi-empirical strip theory (vide Ref. 10). The hydrodynamic coefficients are estimated by two-dimensional calculations integrated along the cylinder axis without accounting for the three-dimensional end effects. In oblique seas, the hydrodynamic coefficients can be calculated using the present finite element method and applied in the strip theory. This would be more appropriate in comparison to the usual procedure wherein the hydrodynamic coefficients corresponding to beam seas have been used even when the incident waves are oblique (vide Ref. 10). For the case of head seas, an exact three-dimensional model, such as formulated by Van Oortmerssen (71), would be necessary in order to simulate the wave refraction along the cylinder axes.

4.0 THREE-DIMENSIONAL GENERAL PROBLEM

The calculation of hydrodynamic interference between multiple three-dimensional structures interacting with linear waves is treated. A finite element method incorporating radiation boundary dampers and a fictitious bottom boundary is employed to solve the corresponding boundary-value problems. Numerical results are given for the diffraction and radiation problems of a single structure, both fixed and floating, and of two floating vessels adjacent to a semi-impermeable, semi-permeable wharf.

4.1 Theoretical Formulation

Consider the diffraction and radiation of monochromatic linear waves of height, H, and angular frequency, ω, by three-dimensional multiple structures adjoining each other as shown in Fig. 4.1. The problem formulation follows closely that of Chapter 3, without a flexural wave approximation in the three-dimensional case.

A Cartesian coordinate system (x,y,z) is employed in which the z coordinate is measured positive upwards from the still water level. An ideal fluid is assumed. Thus the velocity potential, for linear wave theory, may be expressed by linear superposition of the incident, scattered and radiation potential as

$$\Phi(x,y,z,t) = \mathrm{Re}\{-i\omega[(\phi_I + \phi_S)\frac{H}{2} + \sum_{j=1}^{M_c}\sum_{k=1}^{6}\phi_{kj}\xi_{kj}]\ \exp -i\omega t\} \tag{4.1}$$

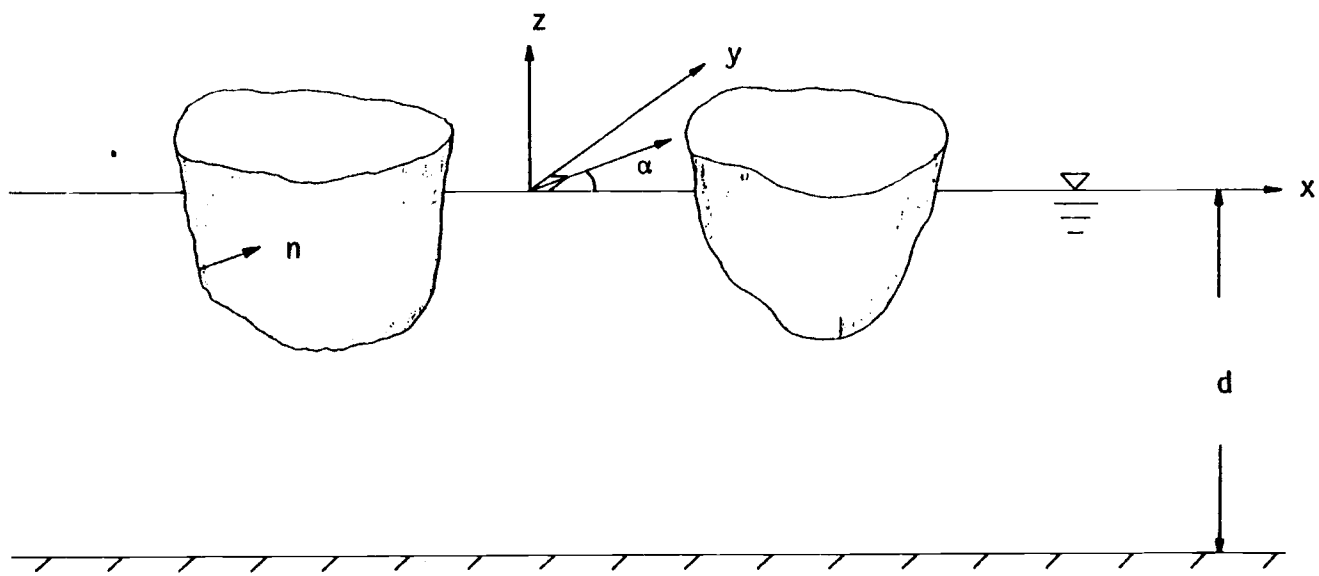

Fig. 4.1. Definition sketch of three-dimensional problem

in which M_c = number of structures. The spatial velocity potential of the incident wave is expressed as

$$\phi_I = \frac{1}{\nu} \frac{\cosh K(z+d)}{\cosh Kd} \exp i(Kx \cos\alpha + Ky \sin\alpha) \tag{4.2}$$

in which $\nu = \omega^2/g$ and α = incident wave angle. ϕ_s = spatial velocity potential of the scattered wave, ϕ_{kj} = velocity potential of the radiated wave due to unit amplitude motion in the k^{th} mode by the j^{th} structure in which k = 1,...6 corresponds to the surge, sway, heave, roll, pitch and yaw modes, respectively. ξ_{kj} = response amplitude of the j^{th} structure in the k^{th} mode. K is the wave number which satisfies the dispersion equation, Eq. (2.4).

The individual velocity potential satisfies the Laplace equation

$$\nabla^2 \phi_\ell = 0 \; ; \quad \ell = I, s, kj \tag{4.3}$$

and the following free-surface and bottom boundary conditions:

$$\frac{\partial \phi_\ell}{\partial z} - \nu \phi_\ell = 0 \; ; \quad z = 0, \ell = I, s, kj \tag{4.4}$$

$$\frac{\partial \phi_\ell}{\partial z} = 0 \; ; \quad z = -d, \ell = I, s, kj \tag{4.5}$$

The scattered and radiated potentials satisfy the radiation boundary condition of

$$\lim_{r\to\infty} r^{1/2} \left[\frac{\partial \phi_\ell}{\partial r} - (iK - \frac{1}{2r}) \phi_\ell\right] = 0 \; ; \quad \ell = s, kj \tag{4.6}$$

in which $r = (x^2 + y^2)^{1/2}$, and the body boundary conditions of

$$\frac{\partial \phi_S}{\partial n_j} + \frac{\partial \phi_I}{\partial n_j} = 0 \quad \text{on } B_j, \quad j = 1,\ldots M_c \tag{4.7}$$

$$\frac{\partial \phi_{kj}}{\partial n_j} - n_{kj} = 0 \quad \text{on } B_j,$$

$$m,j = 1,\ldots M_c \tag{4.8}$$

$$\frac{\partial \phi_{kj}}{\partial n_m} = 0 \qquad \text{on } B_m,\ m \neq j$$

in which n_j = unit inward normal on structure B_j, and n_{kj} = the x, y and z components of the unit normal on the j^{th} structure for k = 1,2, 3, respectively; and

$$\begin{aligned} n_{4j} &= (y_j - y_{cj})n_{3j} - (z_j - z_{cj})n_{2j} \\ n_{5j} &= (z_j - z_{cj})n_{1j} - (x_j - x_{cj})n_{3j} \\ n_{6j} &= (x_j - x_{cj})n_{2j} - (y_j - y_{cj})n_{1j} \end{aligned} \tag{4.9}$$

where x_{cj}, y_{cj} and z_{cj} are the coordinates of the center of rotation.

The physical wave field quantities of pressure, exciting forces and hydrodynamic restoring forces may be expressed by

$$p(x,y,z,t) = \mathrm{Re}\{\rho\omega^2 [(\phi_I+\phi_S)\frac{H}{2} + \sum_{j=1}^{M_c} \sum_{k=1}^{6} \phi_{kj}\xi_{kj}] \exp -i\omega t\} - \rho g z \tag{4.10}$$

$$F_{kj}(x,y,z,t) = \text{Re}\{ \rho\omega^2 \frac{H}{2} \iint_{B_j} (\phi_I + \phi_s)\, n_{kj}\, dD \exp -i\omega t\}$$

$$= \text{Re}\{ f_{kj} \exp -i\omega t\} \tag{4.11}$$

$$R_{kj}(x,y,z,t) = \text{Re}\{ \rho\omega^2 \sum_{m=1}^{M_c} \sum_{\ell=1}^{6} \xi_{\ell m} \iint_{B_j} n_{kj}\phi_{\ell m}\, dD \exp -i\omega t\}$$

$$= \text{Re}\{\sum_{m=1}^{M_c} \sum_{\ell=1}^{6} \xi_{\ell m} P_{kj\ell m} \exp -i\omega t\} \tag{4.12}$$

in which ρ = fluid density and dD = differential area of the immersed body surface. The property of symmetry between the hydrodynamic coefficients $P_{kj\ell m}$ is still valid in the three-dimensional formulation and may be expressed by Eqs. (3.21-3.24) where it is understood that area integrations are now performed.

The responses of the structures in waves may be calculated by Eq. (3.25) with the mode indices of ℓ, k = 1,...6.

4.2 Finite Element Formulation

Solutions for the three-dimensional diffraction and radiation boundary-value problems are now formulated using the standard finite element method where boundary dampers are applied at moderate distance, $r = r_D$, from the structures. Cylindrical and plane dampers are used here to model the radiation boundary condition. In the case

of deep water or infinite water depth, a slight modification of the bottom boundary condition is necessary to avoid extensive fluid domain discretization. A bottom boundary condition of

$$\frac{\partial \phi_\ell}{\partial z} - K \tanh K(z+d)\, \phi_\ell = 0 \; ; \; \ell = s \, , \, kj \tag{4.13}$$

is assumed at a fictitious water depth of $z = -d_f$. The true bottom boundary condition for arbitrary water depth, Eq. (4.5), may be obtained from Eq. (4.13) by extending the fluid domain down to $z = -d$. Finite element functionals may then be expressed as

$$\begin{aligned}
\Pi(\phi_s) = {} & \iiint_V \frac{1}{2} \left\{ \left(\frac{\partial \phi_s}{\partial x}\right)^2 + \left(\frac{\partial \phi_s}{\partial y}\right)^2 + \left(\frac{\partial \phi_s}{\partial x}\right)^2 \right\} dV \\
& - \iint_{z=0} \frac{1}{2} \nu \phi_s^2 \, dD - \iint_{z=-d_f} \frac{1}{2} \tanh K(z+d)\, \phi_s^2 \, dD \\
& - \iint_{r=r_D} \frac{1}{2} \left(iK - \frac{1}{2r_D}\right) \phi_s^2 \, dD + \sum_{j=1}^{M_c} \iint_{B_j} \frac{\partial \phi_I}{\partial n_j} \phi_s \, dD
\end{aligned} \tag{4.14}$$

$$\begin{aligned}
\Pi(\phi_{kj}) = {} & \iiint_V \frac{1}{2} \left\{ \left(\frac{\partial \phi_{kj}}{\partial x}\right)^2 + \left(\frac{\partial \phi_{kj}}{\partial y}\right)^2 + \left(\frac{\partial \phi_{kj}}{\partial z}\right)^2 \right\} dV \\
& - \iint_{z=0} \frac{1}{2} \nu \phi_{kj}^2 \, dD - \iint_{z=-d_f} \frac{1}{2} \tanh K(z+d)\, \phi_{kj}^2 \, dD \\
& - \iint_{r=r_D} \frac{1}{2} \left(iK - \frac{1}{2r_D}\right) \phi_{kj}^2 \, dD - \iint_{B_j} n_{kj} \phi_{kj} \, dD
\end{aligned} \tag{4.15}$$

for the diffraction and radiation problems, respectively, by using the cylindrical dampers. V = finite element fluid domain, dV = differential area on the free surface, z = 0, body surface, B_j, or cylindrical boundary dampers, r = r_D. The functionals in the plane damper approach may be obtained from Eqs. (4.14-4.15) by assuming $r_D \to \infty$.

The fluid domain is now discretized into 3-D rectangular prism volume elements and 2-D quadrilateral area elements. Two isoparametric finite elements with quadratic shape functions are used in this study: these are the 20-noded prisms and 8-noded quadrilaterals. The minimization and assemblage of functional derivatives to formulate the system matrix and vectors follow closely those of Sections 2.2 and 3.2, and will not be repeated here. The system matrix, although symmetric and banded, is in general very large for three-dimensional problems. An efficient Gauss elimination solution technique with blockform using secondary computer storages (vide Ref. 76) is adopted in this study to solve the diffraction and radiation problems.

Numerical results based on the above formulations have been calculated for a variety of problems. These results are discussed in the next section.

4.3 Numerical Results

A three-dimensional finite element computer algorithm incorpo-

rating a blockform solution technique has been developed and applied to several example problems. The diffraction problem of a fixed, surface-piercing circular cylinder is again used to verify the accuracy of the present finite element model.

4.3.a Single Fixed Vertical Circular Cylinder

Finite element solutions of a fixed circular cylinder diffraction problem have been calculated for the case of a/d = 1 (in which a = cylinder radius) over a range of Ka from 0 to 3, using cylindrical damper formulation. Both 1-ring, 8-segment and 2-ring, 8-segment finite element models with a radial size of 0.2a were used in this study. Numerical prediction of the horizontal diffraction force coefficient, C_h, together with the analytical solutions of MacCamy and Fuchs (47), are illustrated in Fig. 4.2. As would be expected, the 2-ring model gives more accurate predictions over the whole diffraction range. In general, good agreement between the finite element solutions and the analytical solutions over the range of Ka > 0.5 is obtained. The three-dimensional finite element solutions overestimate the diffraction forces below the range of Ka = 0.5 (or 2a/L = 0.16) where the hydrodynamic pressure forces are less inertially dominated. Similar predictions are also indicated in the two-dimensional formulation, as shown in Fig. 2.2.

The runup profile around the cylinder is illustrated in Fig. 4.3 for the case of Ka = 1 by using the 2-ring, 8-segment finite element

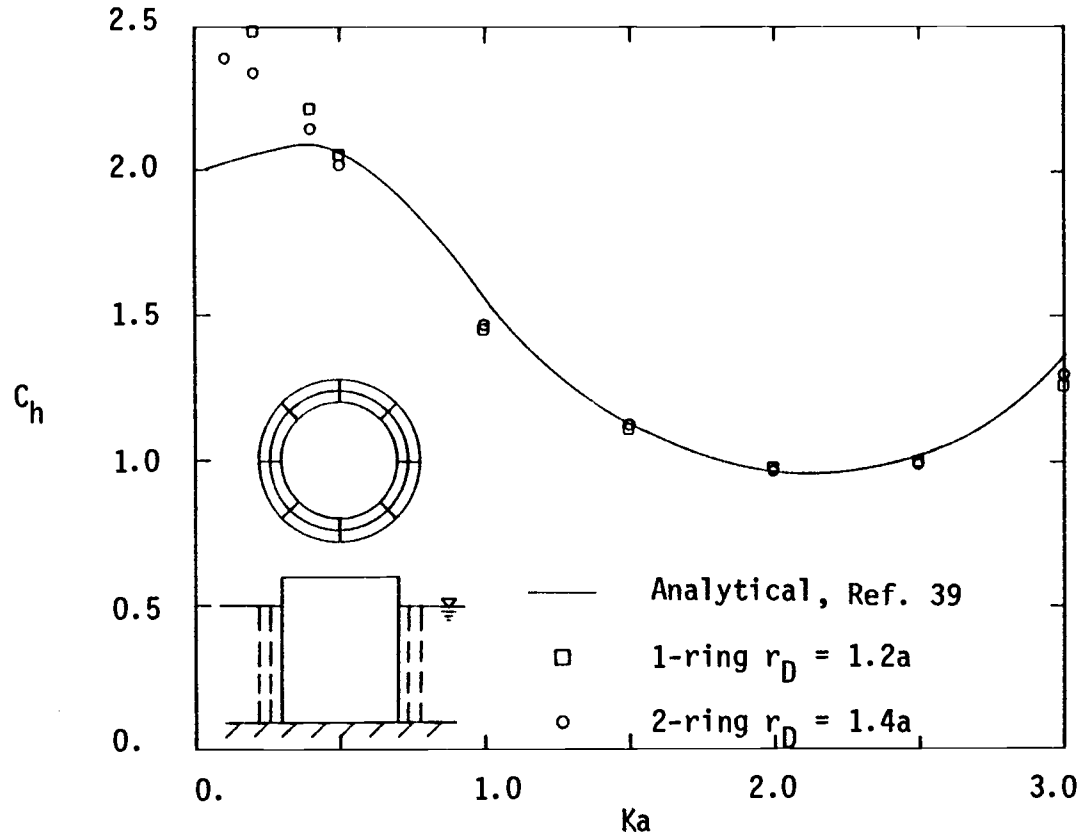

Fig. 4.2. Horizontal diffraction force coefficient, C_h, for a single circular cylinder (a/d = 1, 3-D)

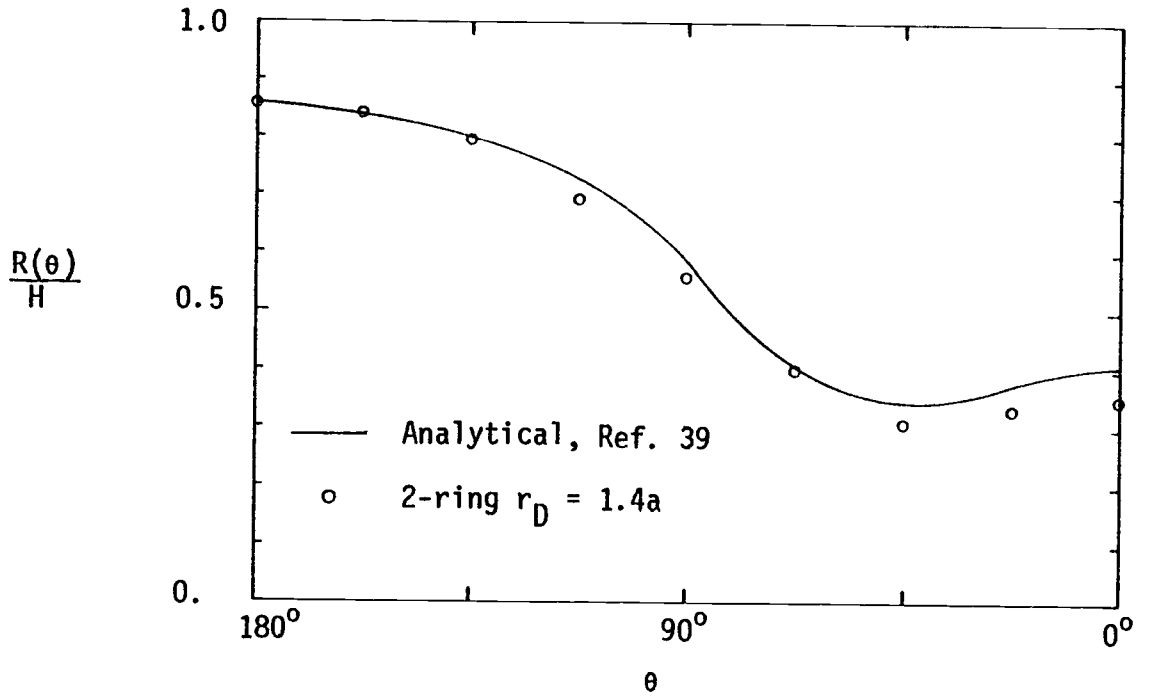

Fig. 4.3. Runup profile for a single surface-piercing circular cylinder (Ka = 1, a/d = 1, 3-D)

model. Good agreement between the present results and the analytical form is shown. The three-dimensional finite element solutions underestimate runups at the leeside, similar to the prediction by using the two-dimensional formulation as shown in Fig. 2.3.

4.3.b Single Floating Vertical Circular Cylinder

The scattering of linear waves by a floating vertical circular cylinder has been solved in an analytical form by Garrett (21). Numerical solutions have also been calculated for a particular geometry shown in Fig. 4.4 (with $d/a = 0.75$, $d_1/a = 0.5$, d_1 = draft of cylinder) by Yue, et al. (80) using the boundary series method (BSM). Specifically, the finite element model chosen by Yue, et al. (80) has a total of 99 boundary series terms, 56 volume elements and 435 nodes with greater node density near sharp edges. Numerical solutions have also been calculated for this particular case by using the cylindrical damper finite element formulation. The finite element model chosen in this study has a total of 28 volume elements and 219 nodes. The meshes used in this study are shown in Fig. 4.4, together with those of Yue, et al. (80).

Accurate prediction of the hydrodynamic pressure (or velocity potential) distribution is necessary to evaluate second-order wave drift forces by direct integration of pressures on the submerged surface of floating structure. Details of pressure distribution are often poorly resolved in the integral equation method since a uniform

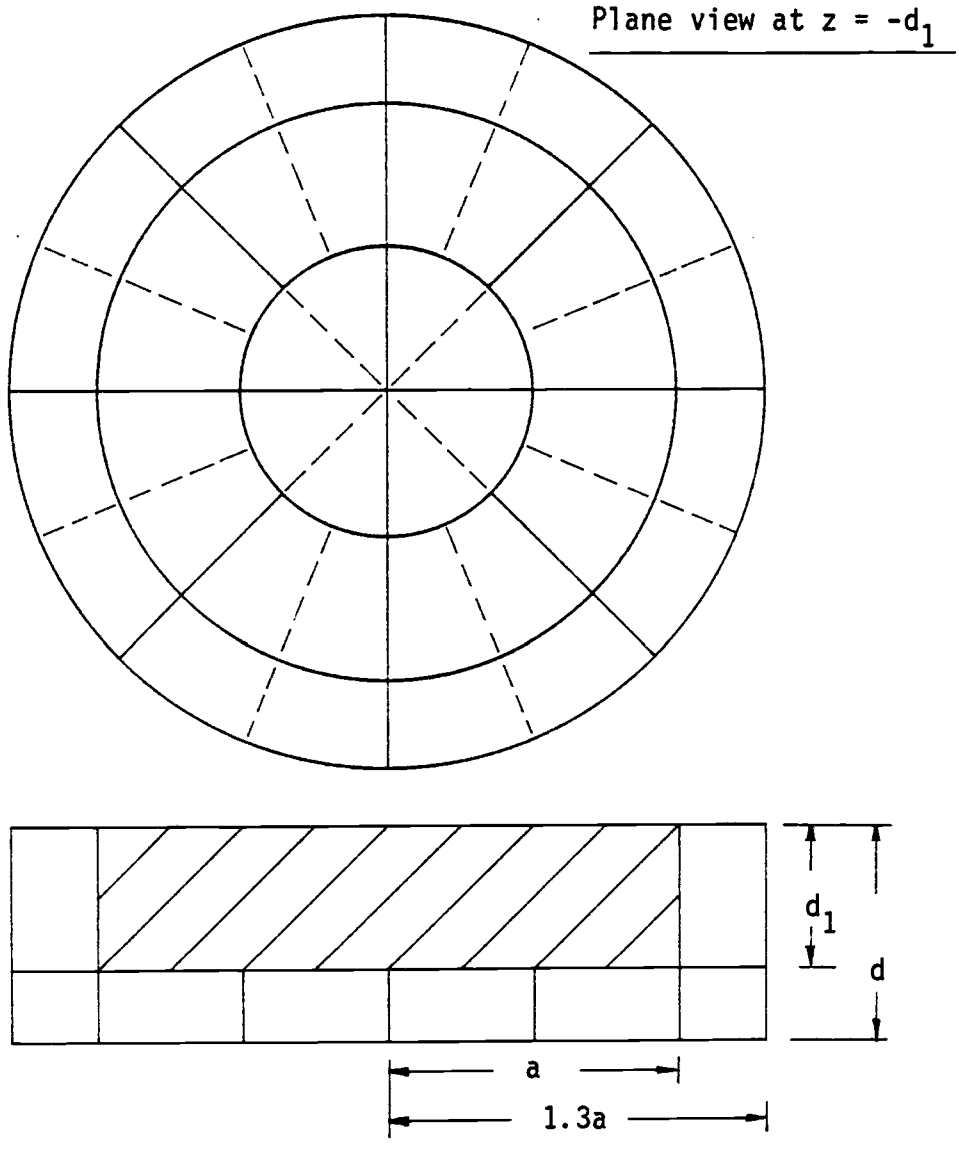

Fig. 4.4. Mesh for floating vertical circular cylinder (d/a = 0.75, d_1/a = 0.5) {—— = present mesh, ---- and —— = mesh in Ref. 80}

distribution of source strength is usually assumed (vide Ref. 17). It is therefore of interest to compare the pressure of velocity potential distribution between different solution methods. Numerical results of the total velocity potential distribution at the dock's bottom plate from Yue, et al. (80) and this study are shown in Fig. 4.5, for the case of Ka = 1. Good agreement between the two numerical techniques is obtained. It is important to note that a relatively coarse mesh is employed in this study.

Numerical results of both the horizontal and vertical exciting force coefficients, C_{FX} and C_{FZ}, over a range of Ka from 0 to 6 are given in Fig. 4.6, where the exciting forces are nondimensionalized by $\rho g \pi a d_1 H/2$. Both the analytical solutions of Garrett (21) and the BSM solutions of Yue, et al. (80) are also illustrated in Fig. 4.6. Close agreement among these three studies is obtained with slight discrepancy at Ka = 6, where the present study underestimates the horizontal exciting force. Finer meshes are necessary to improve the solution accuracy in the range of very short waves.

The diffraction and radiation problems of a floating vertical circular cylinder have also been studied by Garrison (22,24,25) using the three-dimensional integral equation method with point source distribution, and by Hudspeth, et al. (35) using the axisymmetric Green's function integral equation method. Finite element solutions for the case of $d/a = 1$, $d_1/a = 0.5$ have been calculated over a frequency range of νa from 0 to 3 in this study using the two meshes shown in Fig. 4.7. Meshes 1 and 2 employed cylindrical and plane dampers,

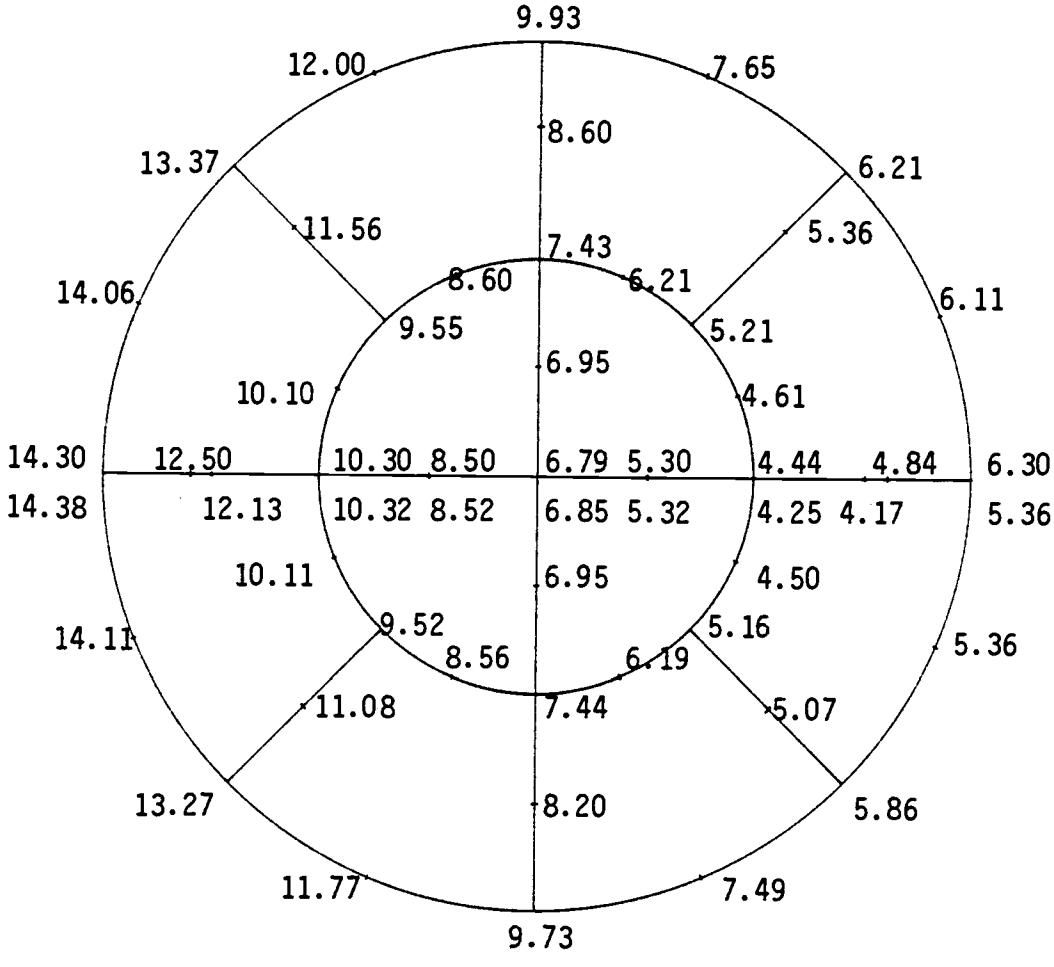

Fig. 4.5. Distribution of velocity potential at the bottom plate of a floating vertical circular cylinder (Ka = 1, d/a = 0.75, d_1/a = 0.5) {upper part = Ref. 80, lower part = present results}

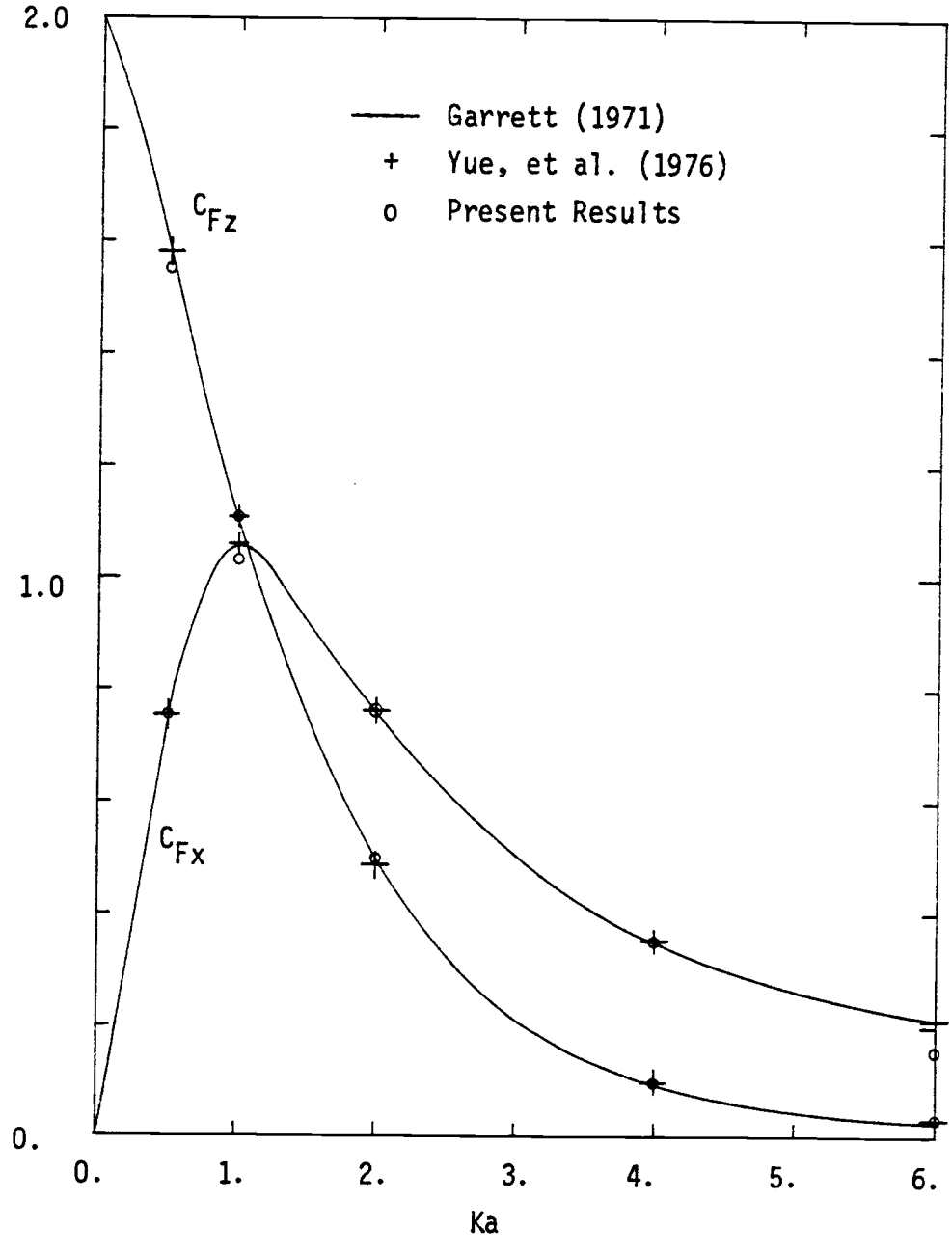

Fig. 4.6. Horizontal and vertical exciting force coefficients for a floating vertical circular cylinder (d/a = 0.75, $d_1/a = 0.5$)

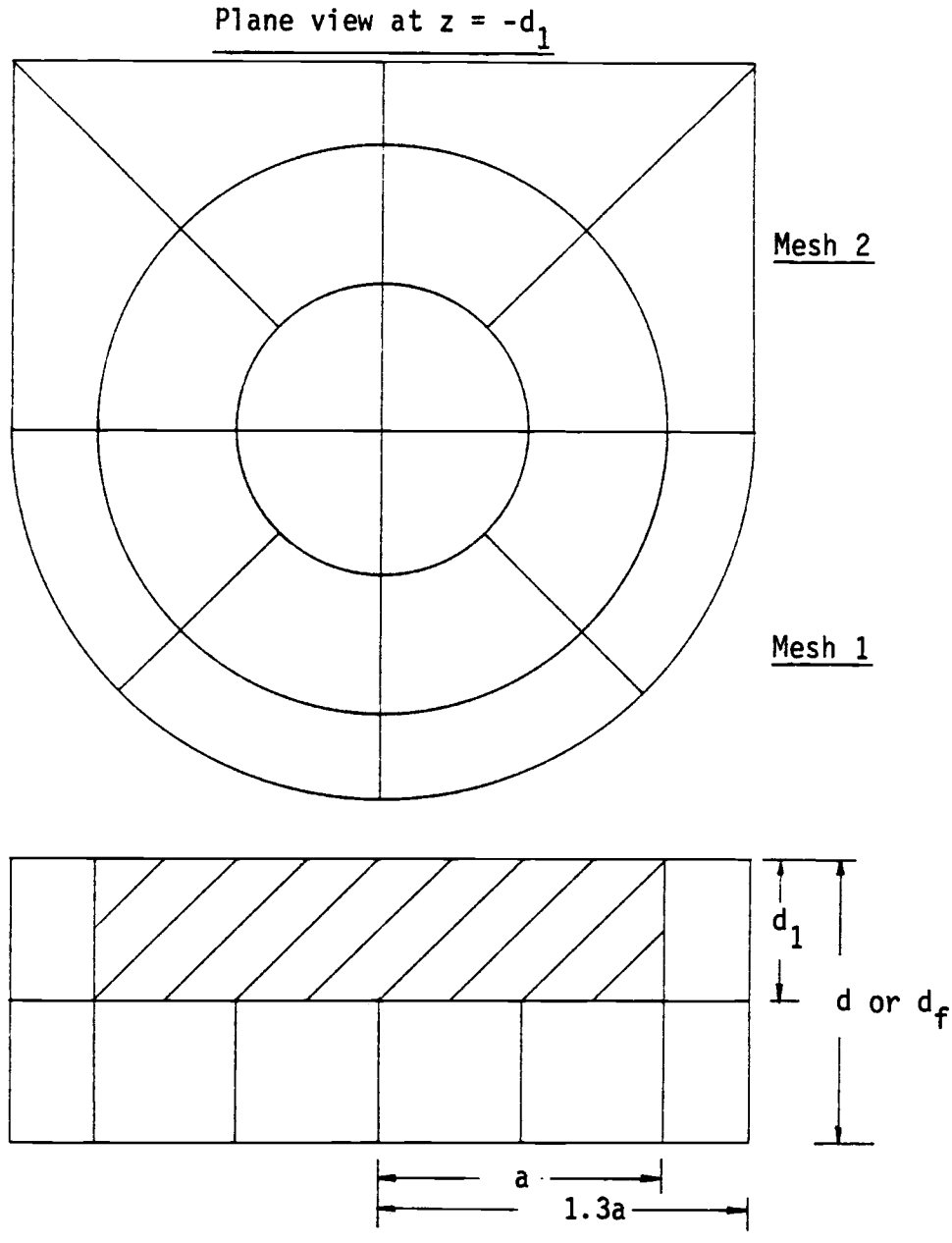

Fig. 4.7. Meshes for floating vertical circular cylinder ($d/a = 1$, $d_1/a = 0.5$ and $d/a = \infty$, $d_f/a = 1$, $d_1/a = 0.5$)

respectively, to model the radiation boundary condition. Numerical results of the added mass and damping coefficients in surge (M_{11}, N_{11}), heave (M_{33}, N_{33}) and pitch (M_{55}, N_{55}) are given in Fig. 4.8, together with the results of Garrison (22). Close agreement has been obtained between the two integral equation solutions for this particular case, except that Hudspeth, et al. (35) have predicted smaller surge added mass coefficient in the long wave range. Therefore, the results of Hudspeth, et al. (35) are not shown in Fig. 4.8. The added mass and damping coefficients are nondimensionalized by ρa^3 and $\omega\rho a^3$, respectively, in the surge and heave modes. In pitch mode, they are nondimensionalized by ρa^5 and $\omega\rho a^5$, respectively.

Agreement between the present Mesh 1 results and solutions based on the integral equation is found to be generally good, the greatest discrepancies arising in the heave mode: the present results appear to be converging to different lines from the integral equation solutions. Smaller added mass coefficients, M_{33}, and larger damping coefficients, N_{33}, are predicted by the finite element method. Smaller surge added mass coefficient, M_{11}, are also predicted by the finite element solutions. The variation of pitch added mass coefficient, M_{55}, varies from 0.206 to 0.192 as νa varies from 0.5 to 3, slightly smaller than the integral equation solutions. A constant value of pitch damping coefficients, $N_{55} = 0.01$ is predicted, this is consistent with the integral equation solutions. Slightly different hydrodynamic coefficients have been obtained by using the Mesh 2 finite element solutions. In general, the discrepancies in these

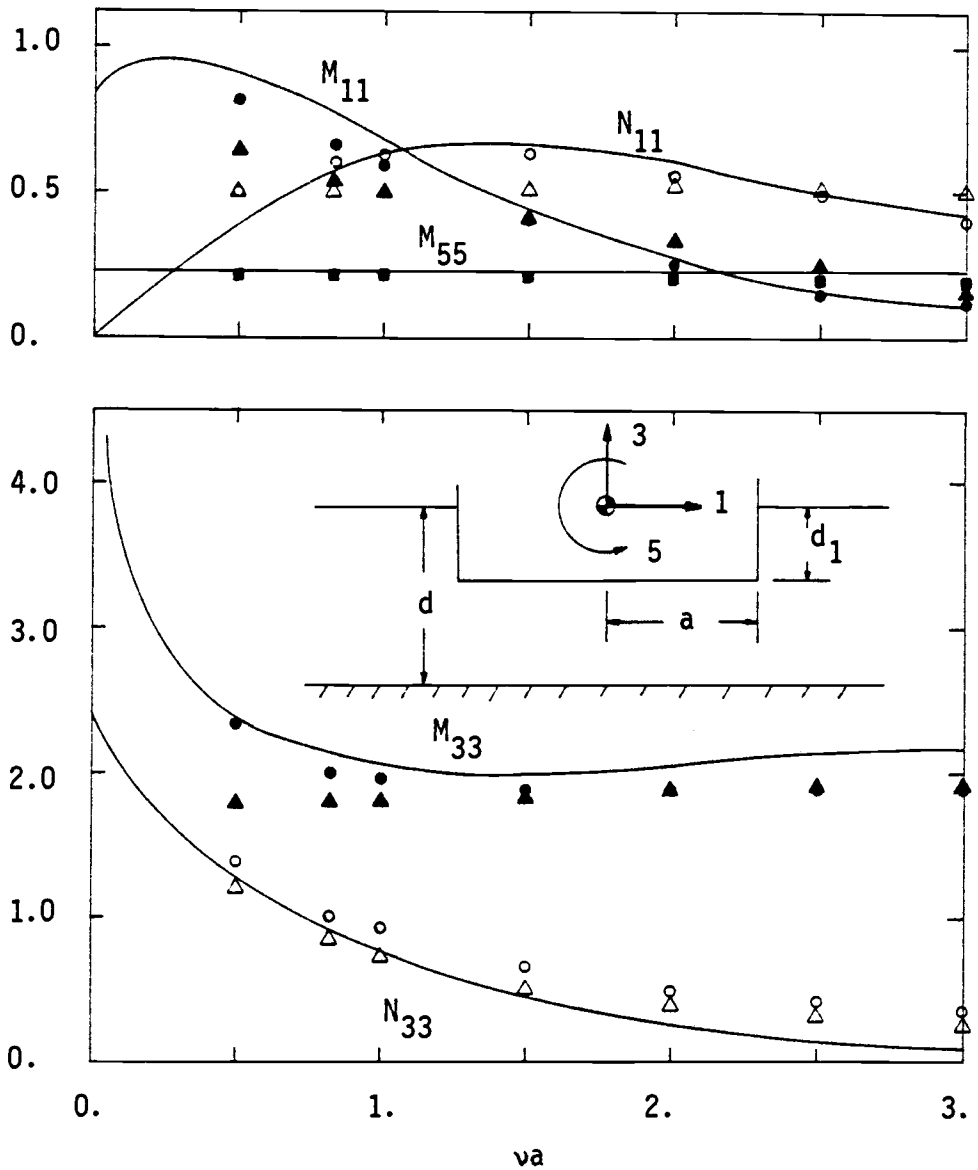

Fig. 4.8. Added mass and damping coefficients of a floating vertical circular cylinder (d/a = 1, d_1/a = 0.5) {—— = Ref. 22, ● , ○ , ■ = present results using Mesh 1; ▲ ,△= present results using Mesh 2}

coefficients are relatively irrelevant to the computation of first order response, although they are likely to have greater influence on drift forces.

Numerical results of the dimensionless surge and heave exciting forces, $C_{F1} = 2F_{1max}/\rho g a^2 H$ and $C_{F3} = 2F_{3max}/\rho g a^2 H$, and pitch exciting moment, $C_{F5} = 2F_{5max}/\rho g a^3 H$, are given in Fig. 4.9. Good agreement between the present Mesh 1 results and the axisymmetric Green's function integral equation solutions of Hudspeth, et al. (35) is obtained. Garrison (22) only reported the results of surge exciting force coefficient, which are slightly larger than the results of this study and Hudspeth, et al. (35). In general, smaller surge forces and larger heave forces are predicted by using the Mesh 2 finite element solutions.

Numerical calculations of the hydrodynamic responses are based on taking the center of gravity at the still water level and the pitching radius of gyration as 0.691a, which corresponds to a pitch moment of inertia of $0.75\rho a^5$. These responses are shown in Figs. 4.10-4.12 for the surge, heave and pitch modes, respectively, together with those obtained by Garrison (22). Good agreement between the two results is obtained for all the responses, except at the heave resonance approximately at $\nu a = 0.83$. Smaller heave resonance is predicted by the present Mesh 1 finite element solution probably due to a smaller heave added mass calculated. The pitch response has a very large peak at resonance because of the very small damping.

Finite element solutions for the case of infinite water depth (

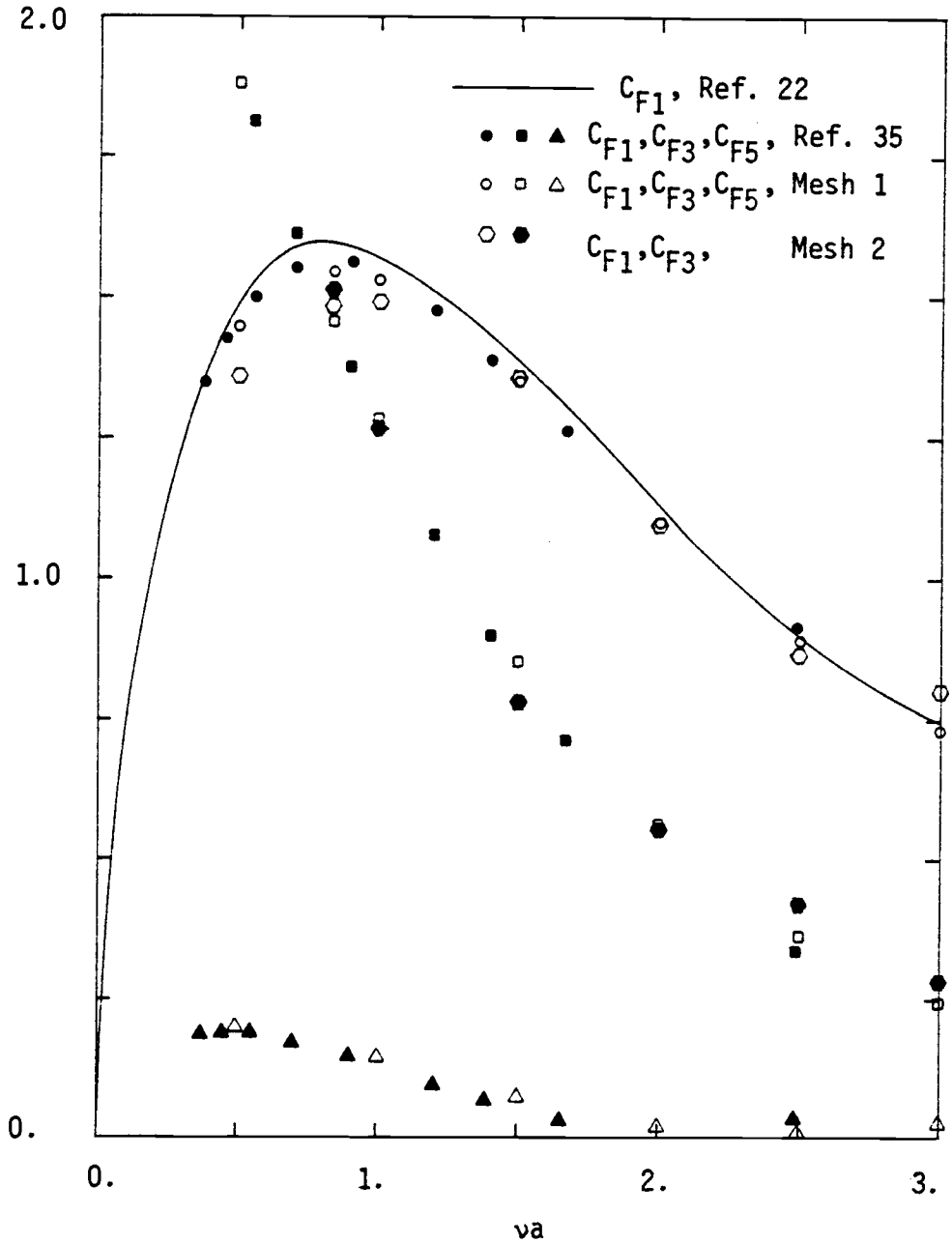

Fig. 4.9. Exciting force coefficients for a floating vertical circular cylinder (d/a = 1, d_1/a = 0.5)

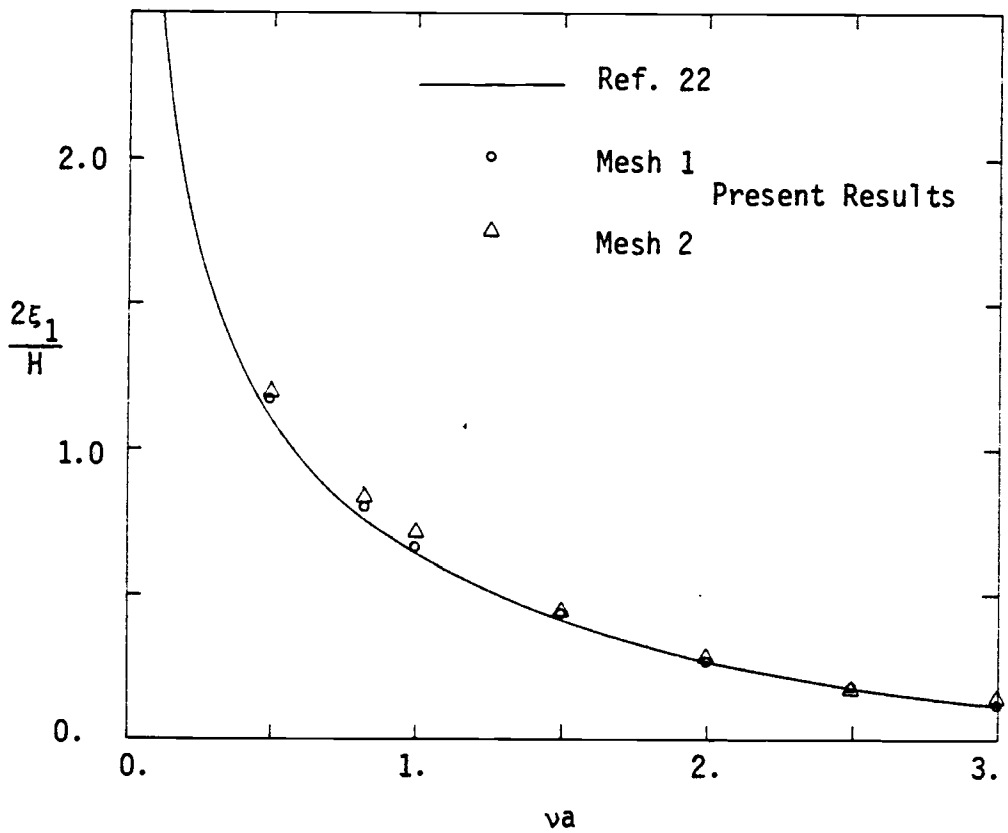

Fig. 4.10. Surge response of a floating vertical circular cylinder ($d/a = 1$, $d_1/a = 0.5$)

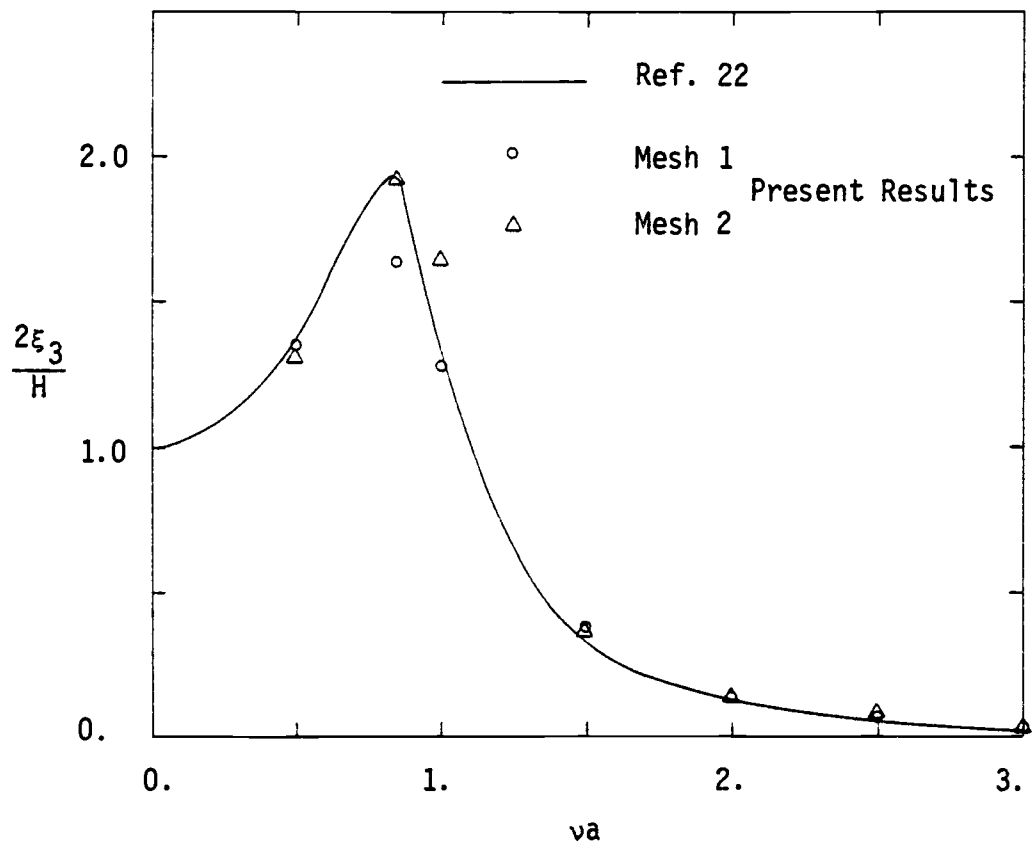

Fig. 4.11. Heave response of a floating vertical circular cylinder ($d/a = 1$, $d_1/a = 0.5$)

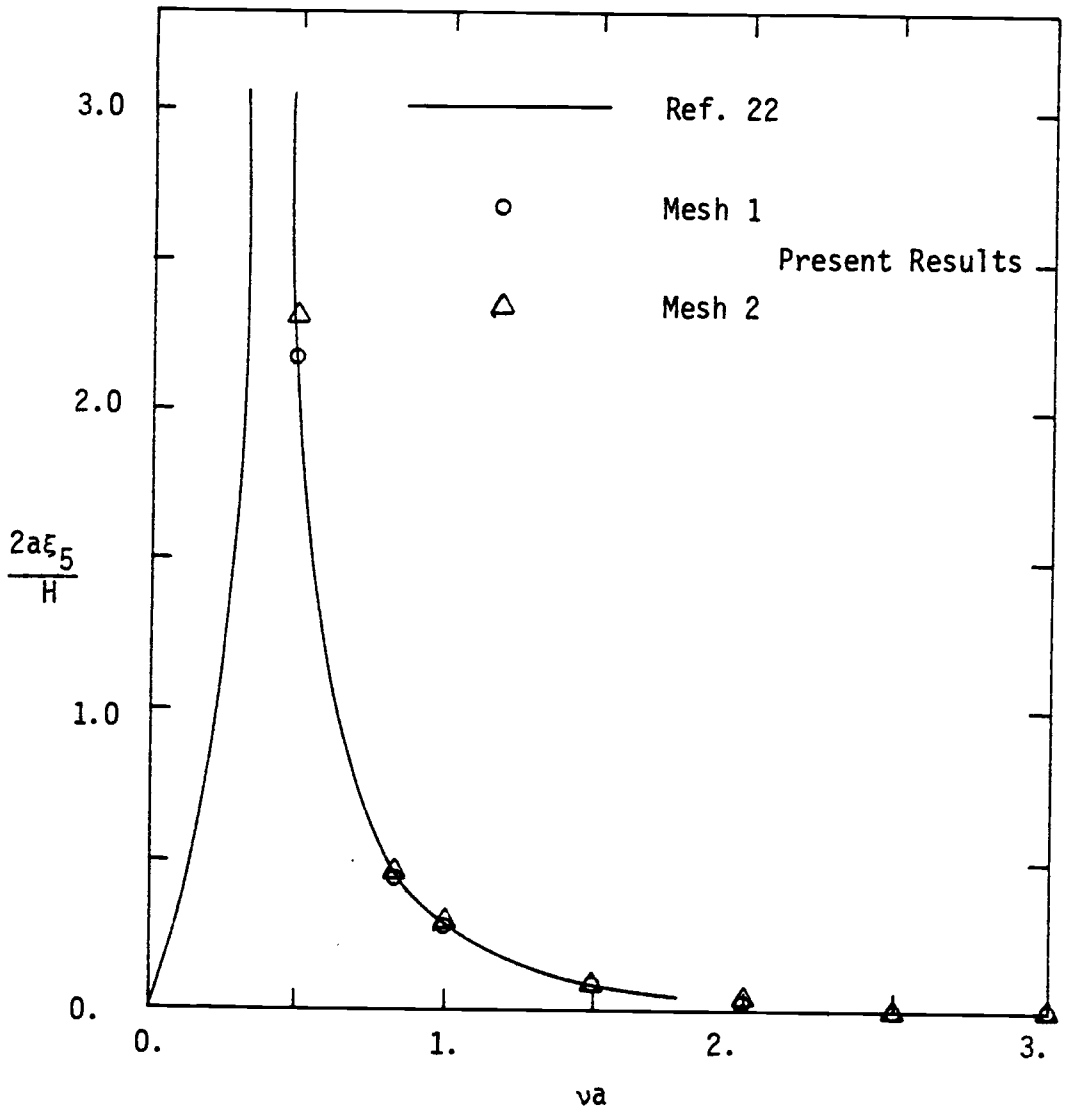

Fig. 4.12. Pitch response of a floating vertical circular cylinder ($d/a = 1$, $d_1/a = 0.5$)

$d/a = \infty$, $d_1/a = 0.5$) have also been calculated over a frequency range of νa from 0 to 3 by using a fictitious water depth of $d_f/a = 1$ and the two meshes shown in Fig. 4.7. Numerical results for added mass and damping coefficients are given in Fig. 4.13, where they are seen to converge to different lines from the results of Garrison (22). The pitch damping coefficient varies from 0.005 to 0.007 over the whole frequency range. Numerical results of the exciting forces and moment are shown in Fig. 4.14 which indicate smaller finite element surge force predictions near the peak, compared with Garrison's (22) results. The hydrodynamic responses of the cylinder are calculated and illustrated in Figs. 4.15-4.17. These responses compare fairly well with those obtained by Garrison (22) except at the heave resonance. Smaller heave resonance is again predicted by the present Mesh 1 finite element solution, larger heave resonance is predicted by Mesh 2 finite element solution. No experimental work has been reported for this particular case to compare with different numerical predictions.

4.3.c Floating Disc Buoy

Hoffman, et al. (31) have published their experimental results for a large shallow-draft disc buoy. The geometry of the disc buoy is shown in Fig. 4.18. Numerical computations of the buoy heave and pitch responses have been reported by Garrison (22). Detail calculations have also been performed by Hudspeth (36) using the axisymmetric

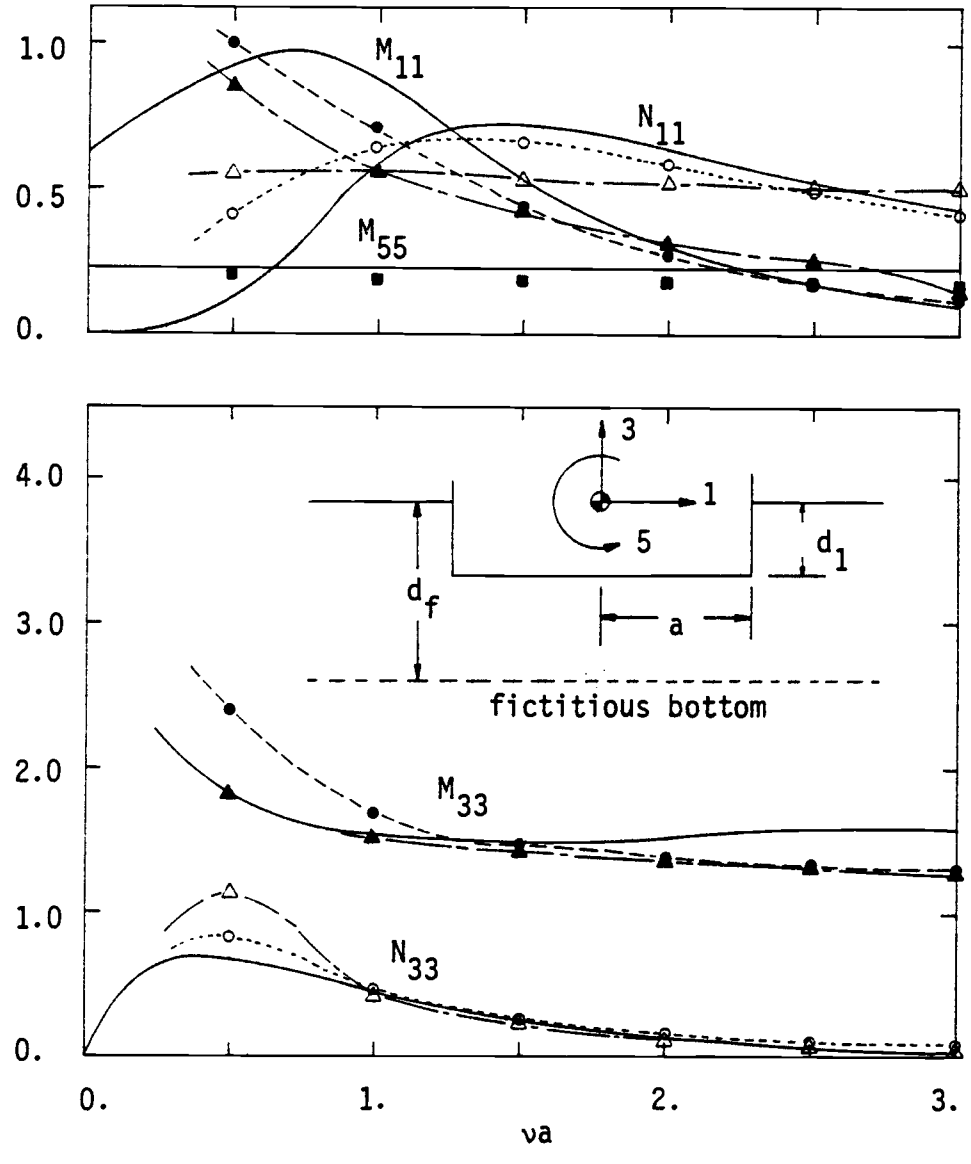

Fig. 4.13. Added mass and damping coefficients of a floating vertical circular cylinder ($d/a = \infty$, $d_f/a = 1$, $d_1/a = 0.5$) {—— = Ref. 22, ●, ○, ■ = present results using Mesh 1; ▲, △ = present results using Mesh 2}

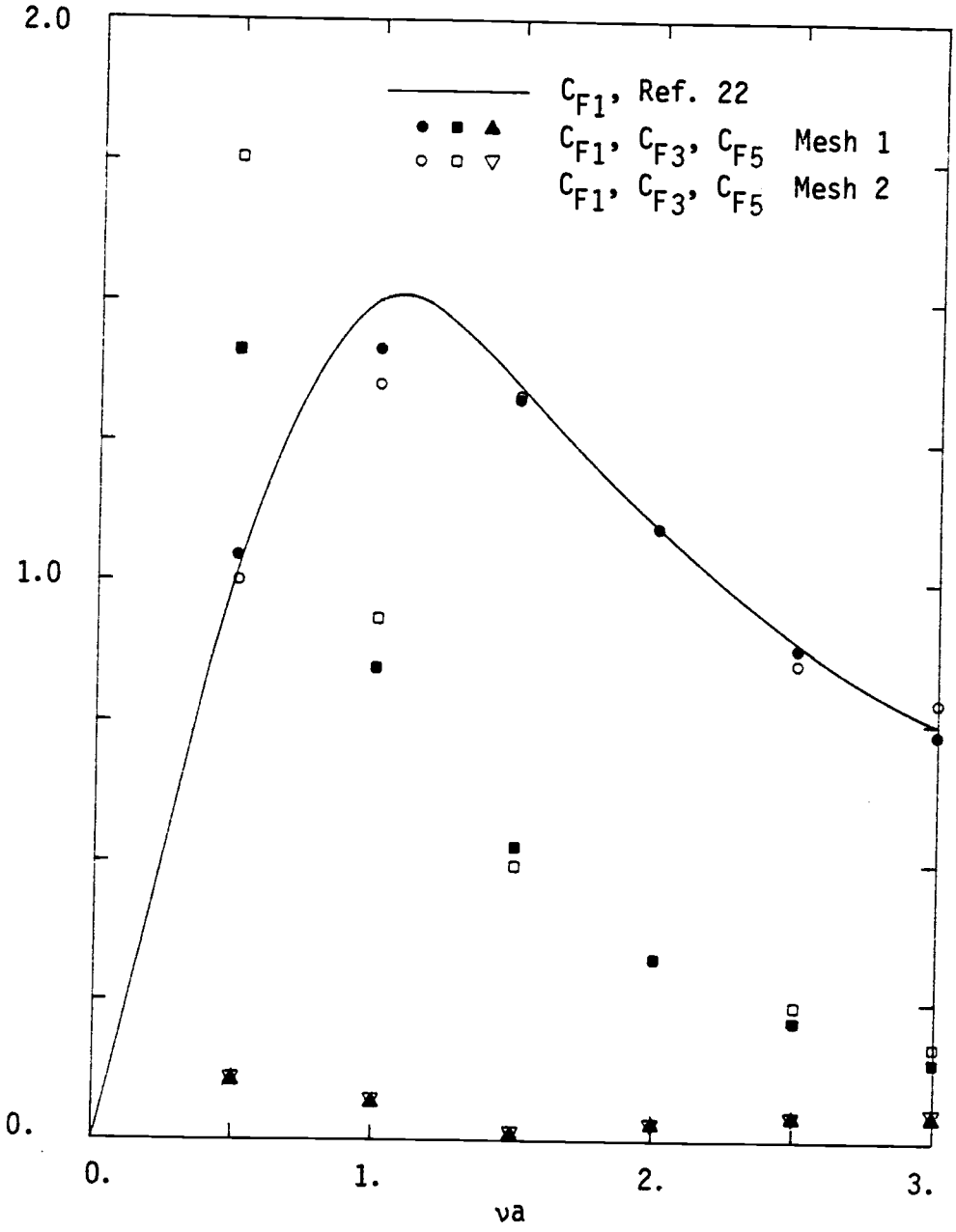

Fig. 4.14. Exciting force coefficients for a floating vertical circular cylinder in infinite water ($d/a = \infty$, $d_f/a = 1$, $d_1/a = 0.5$)

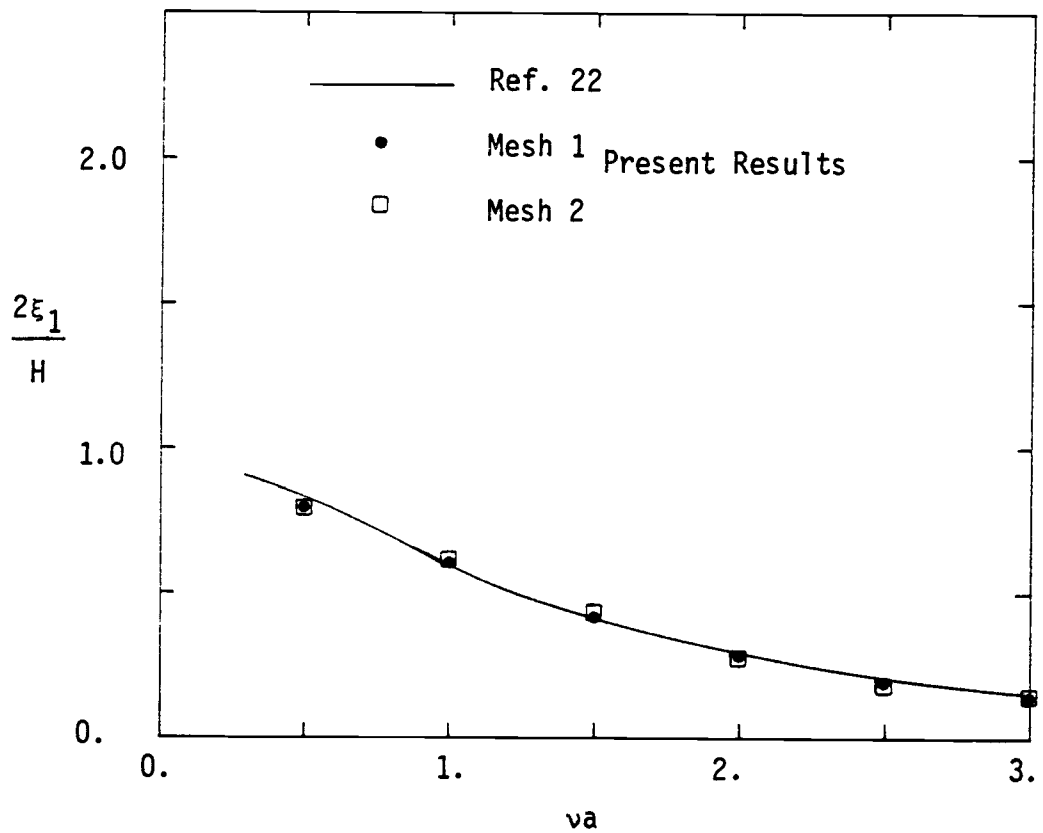

Fig. 4.15. Surge response of a floating vertical circular cylinder in infinite water ($d/a = \infty$, $d_f/a = 1$, $d_1/a = 0.5$)

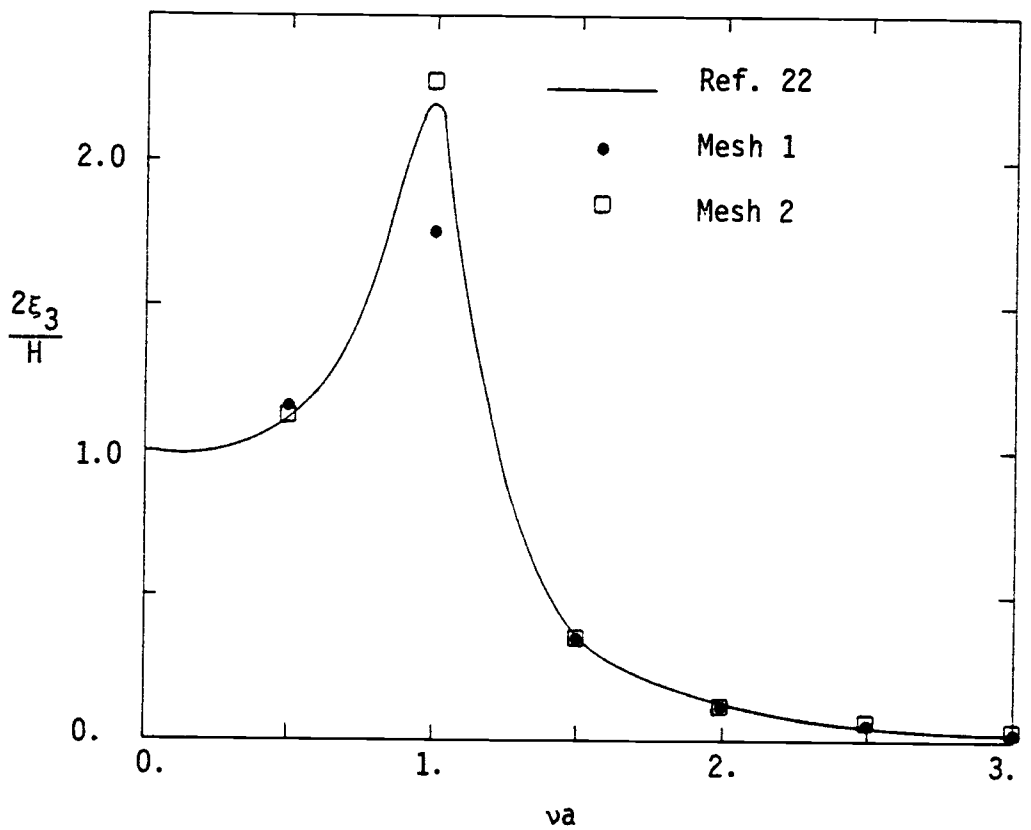

Fig. 4.16. Heave response of a floating vertical circular cylinder in infinite water ($d/a = \infty$, $d_f/a = 1$, $d_1/a = 0.5$)

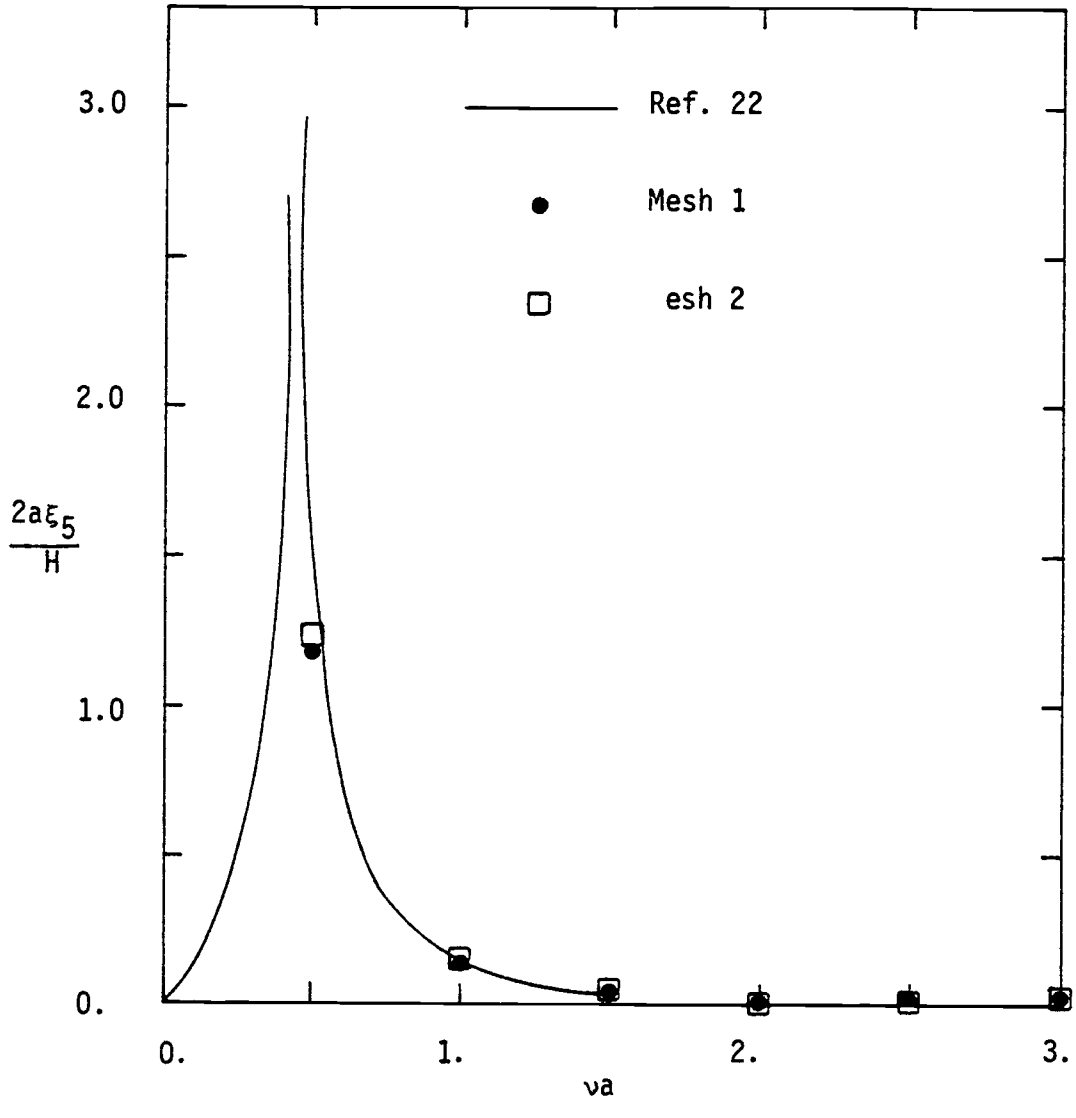

Fig. 4.17. Pitch response of a floating vertical circular cylinder in infinite water ($d/a = \infty$, $d_f/a = 1$, $d_1/a = 0.5$)

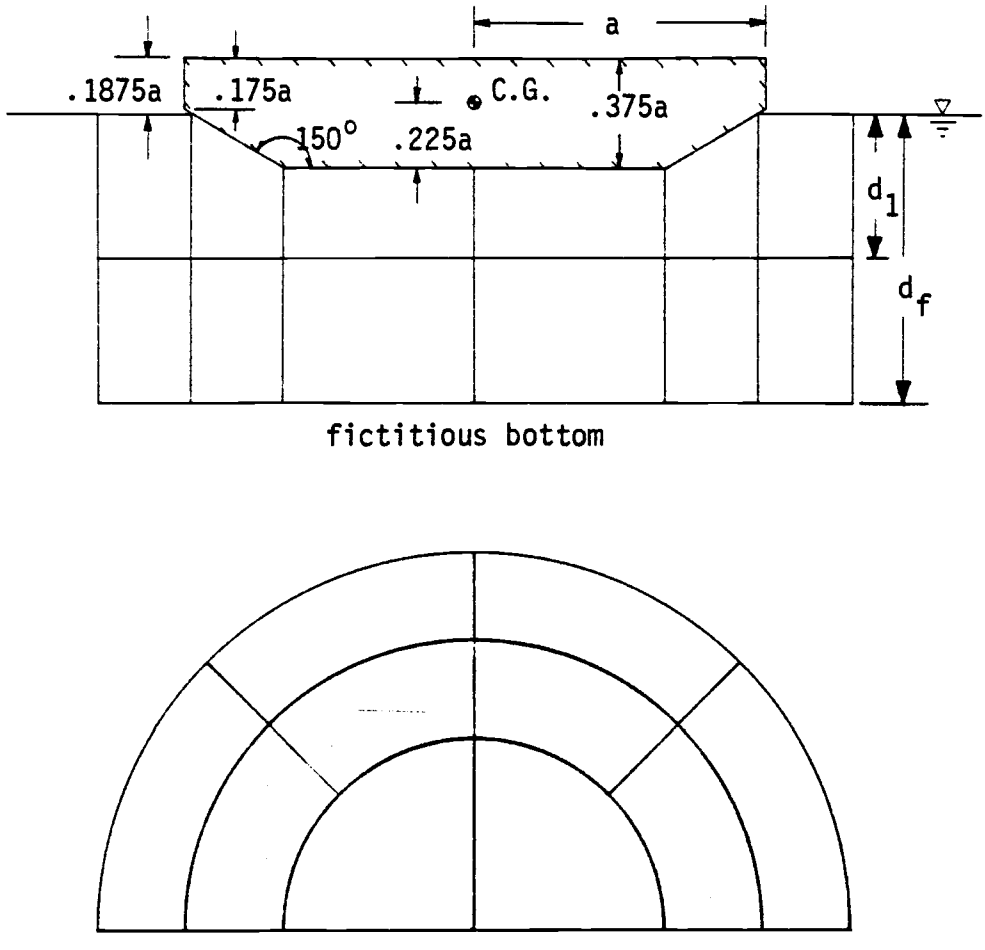

Fig. 4.18. Mesh for floating disc buoy ($d/a = \infty$, $d_f/a = 0.5$, $d_1/a = 1$)

Green's function formulation. The finite element solutions have been calculated by using the meshes shown in Fig. 4.18, where cylindrical dampers and a fictitious bottom were applied at 1.3a and 1a, respectively. The exciting forces calculated from this study are compared with those of Hudspeth (36) in Fig. 4.19. Close agreement between the two studies is obtained, except for the heave force in the low frequency range. The hydrodynamic coefficients from these two studies are compared in Figs. 4.20-4.24 where some discrepancies are illustrated. The hydrodynamic responses are shown in Fig. 4.24, where good agreement between Hudspeth's results (36) and the present finite element solutions is obtained. The discrepancy between the two forms of integral equation method (the axisymmetric and three-dimensional Green's functions) at the pitch resonance is not clear.

4.3.d Three-Dimensional Catamaran

The interference effects between the two hulls of a catamaran have been calculated in Chapter 3 by using a two-dimensional approximation, where a strong heave resonance phenomenon at $\nu a = 0.65$ was shown. For the three-dimensional study of the end effects, a length of 5a and infinite water depth have been used in the calculations. Finite element solutions for this case have been calculated by using the meshes shown in Fig. 4.25, where plane dampers and a fictitious bottom were applied at 3a and 2a, respectively. Numerical solutions have been calculated for the case of beam seas only, and compared

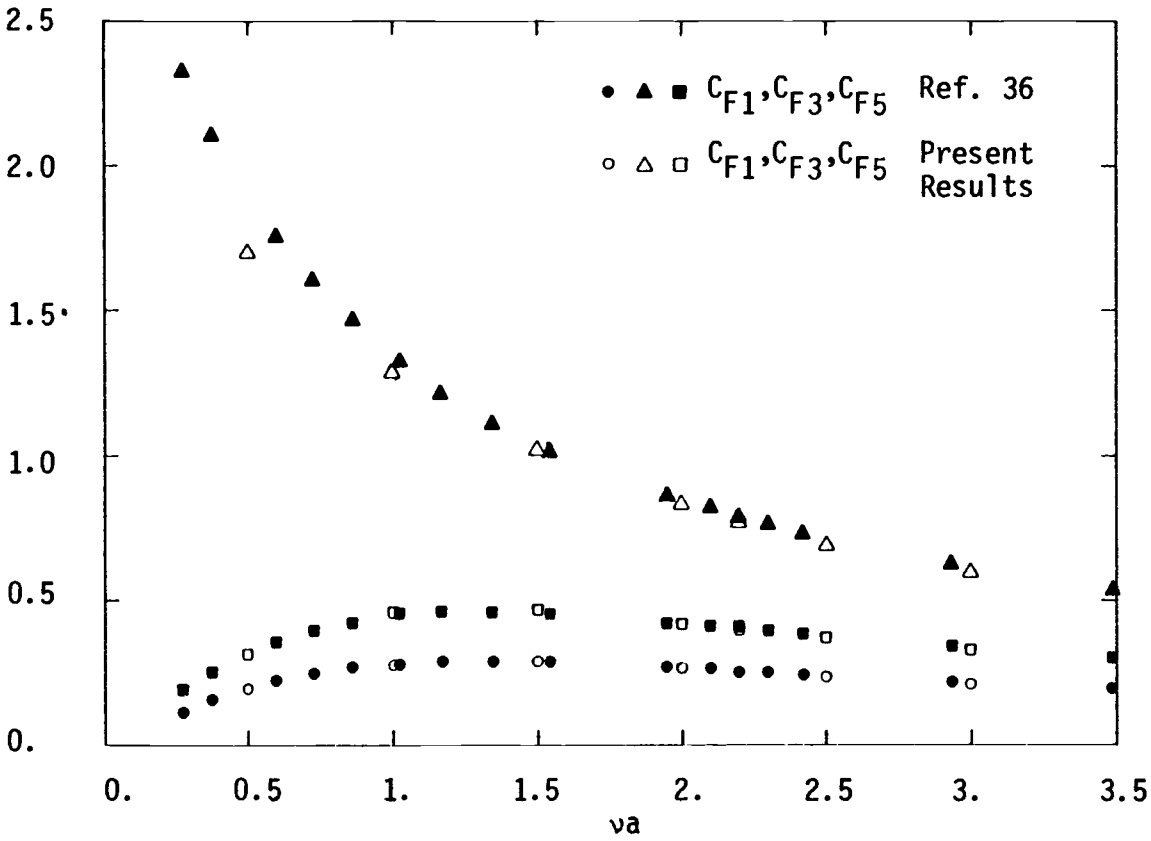

Fig. 4.19. Exciting force coefficients for a floating disc buoy ($d/a = \infty$, $d_f/a = 1$, $d_1/a = 0.5$)

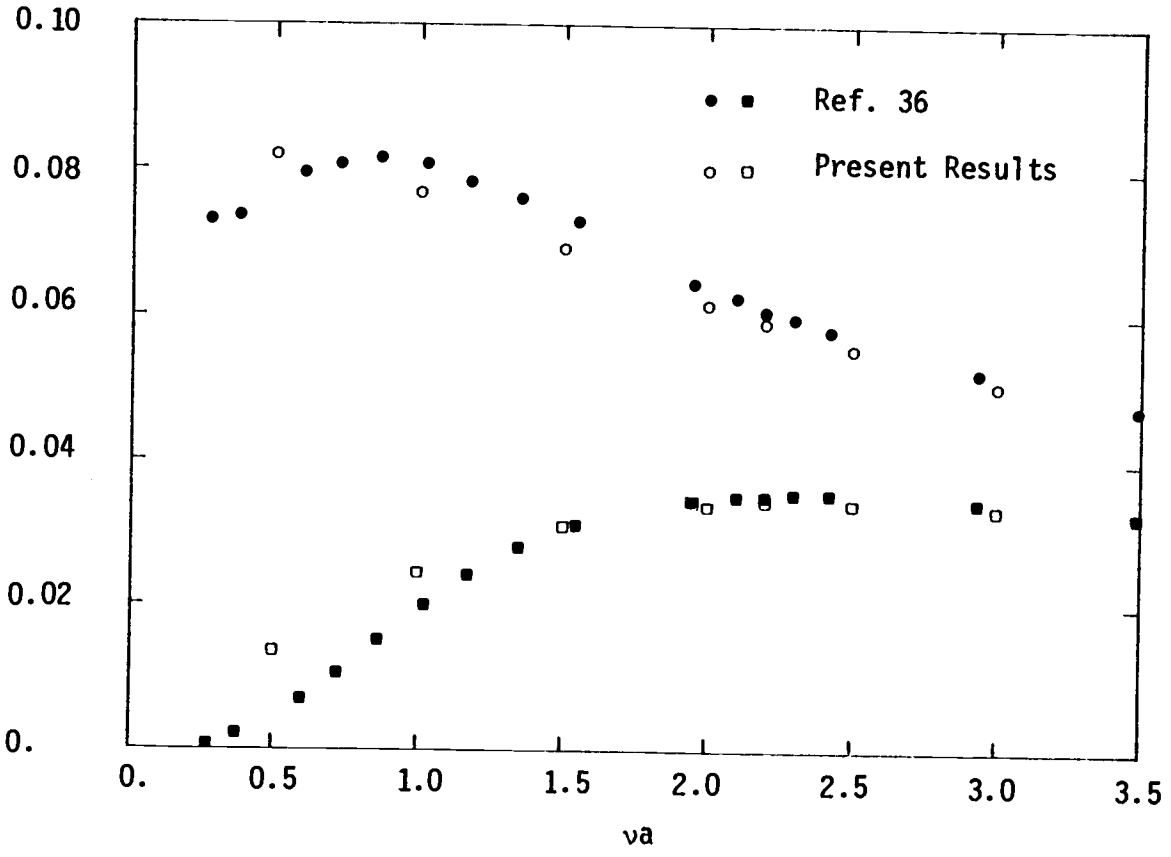

Fig. 4.20. Surge added mass and damping coefficients of a floating disc buoy ($d/a = \infty$, $d_f/a = 1$, $d_1/a = 0.5$) {circle = added mass, square = damping}

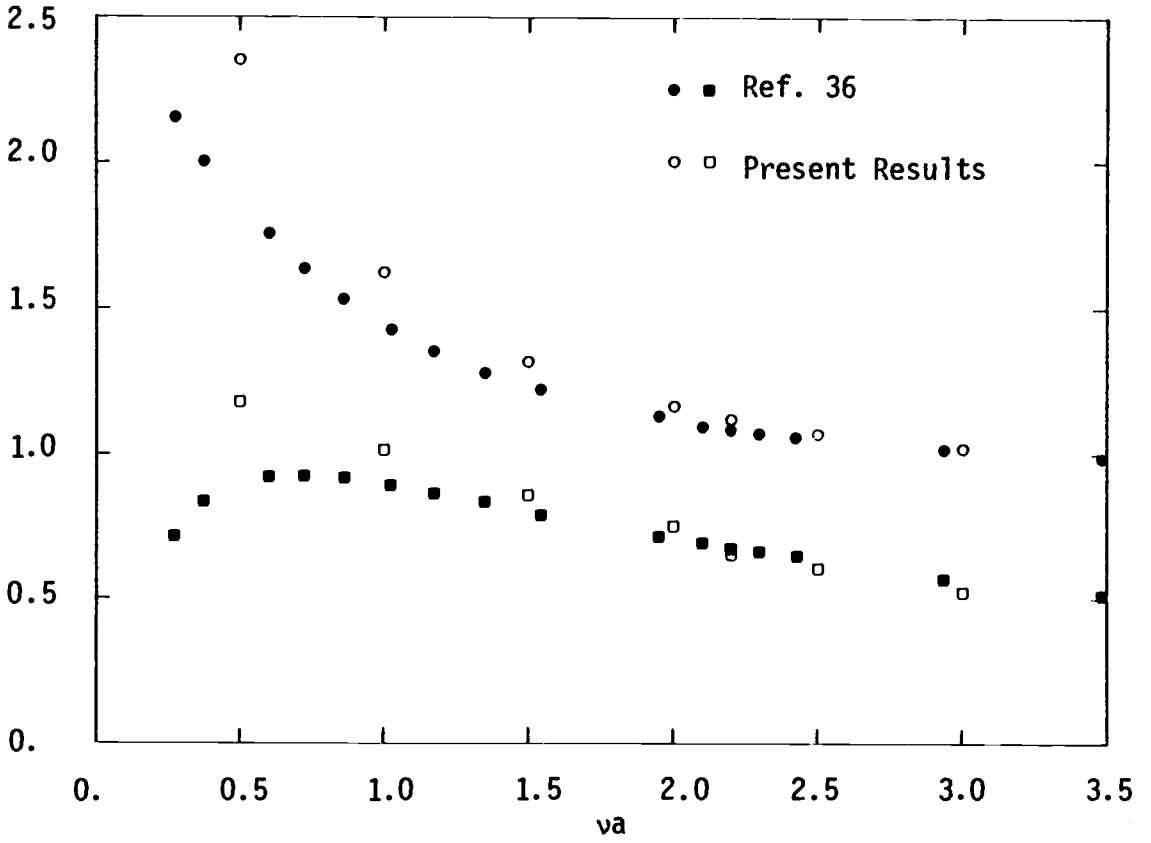

Fig. 4.21. Heave added mass and damping coefficients of a floating disc buoy ($d/a = \infty$, $d_f/a = 1$, $d_1/a = 0.5$) {circle = added mass, square = damping}

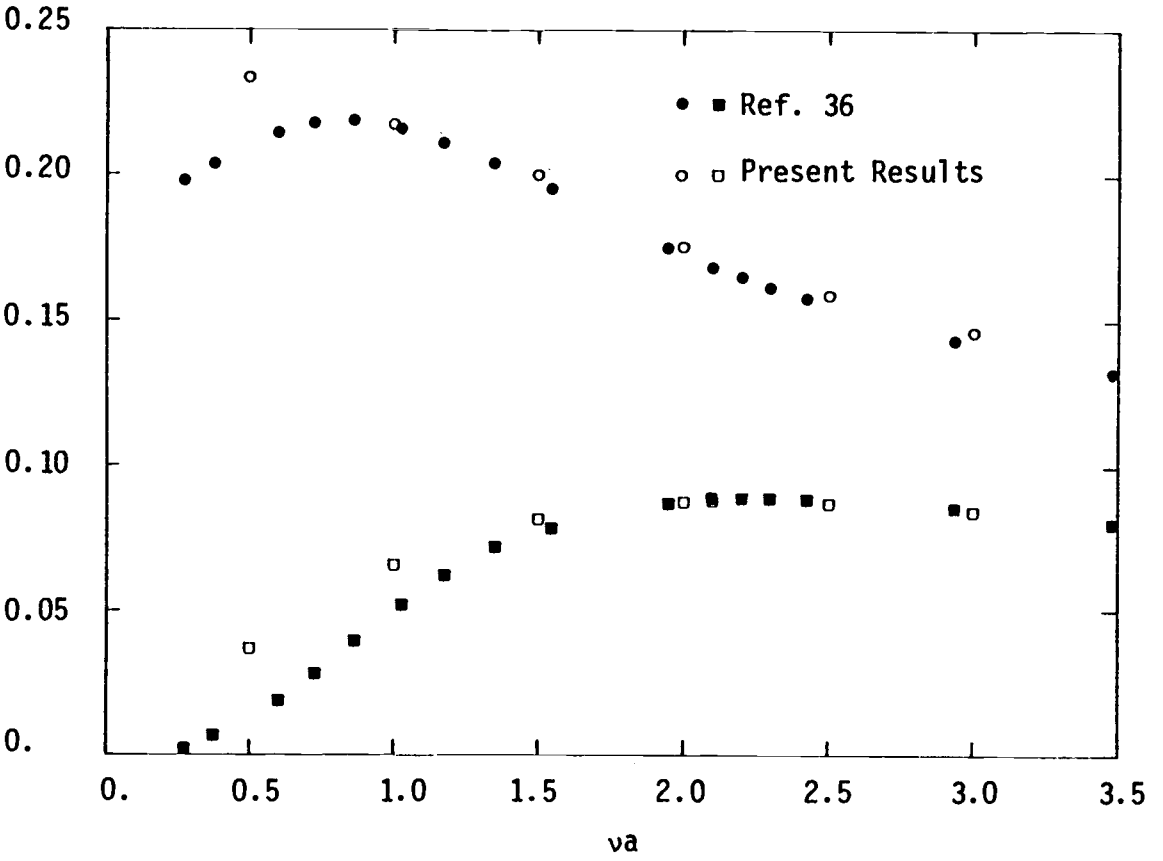

Fig. 4.22. Pitch added mass and damping coefficients of a floating disc buoy ($d/a = \infty$, $d_f/a = 1$, $d_1/a = 0.5$) {circle = added mass, square = damping}

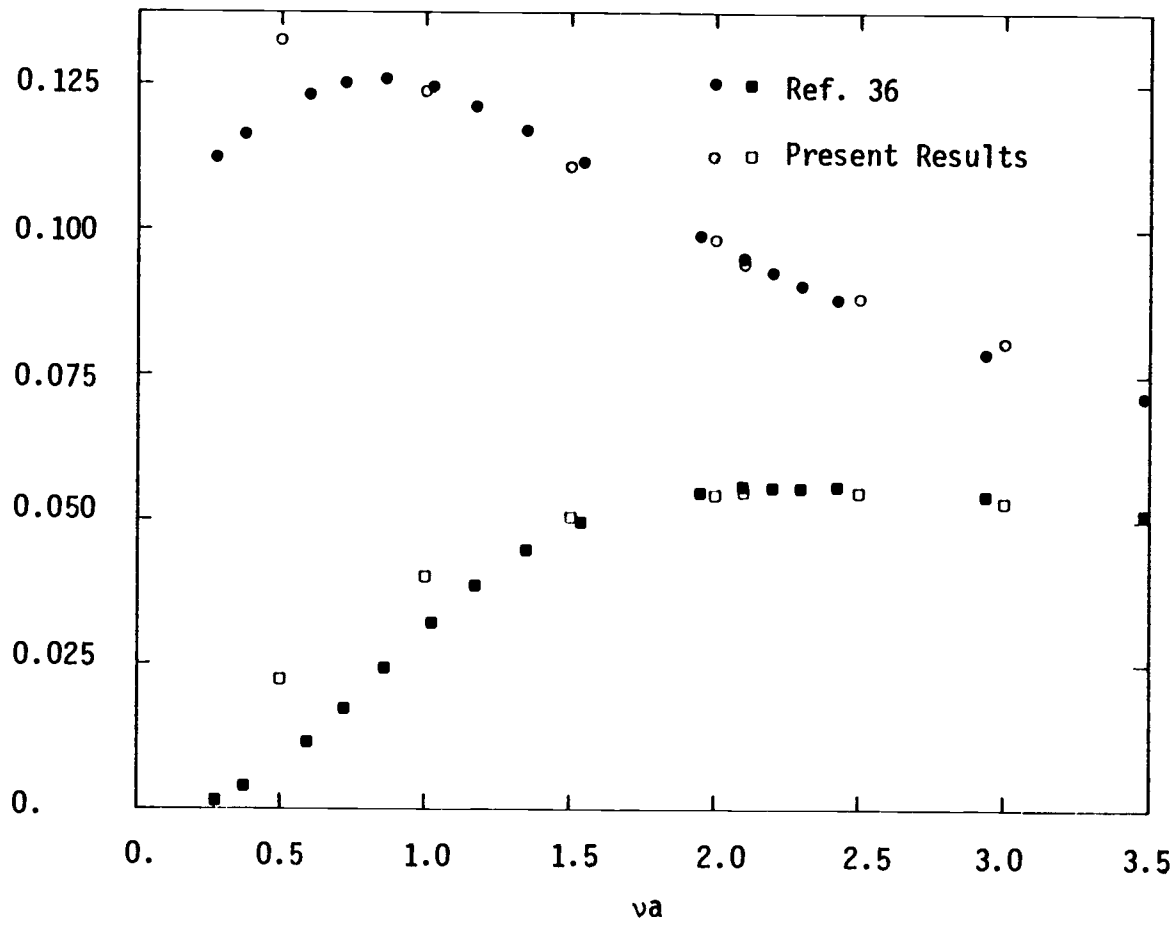

Fig. 4.23. Surge-pitch coupling added mass and damping coefficients of a floating disc buoy ($d/a = \infty$, $d_f/a = 1$, $d_1/a = 0.5$) {circle = added mass, square = damping}

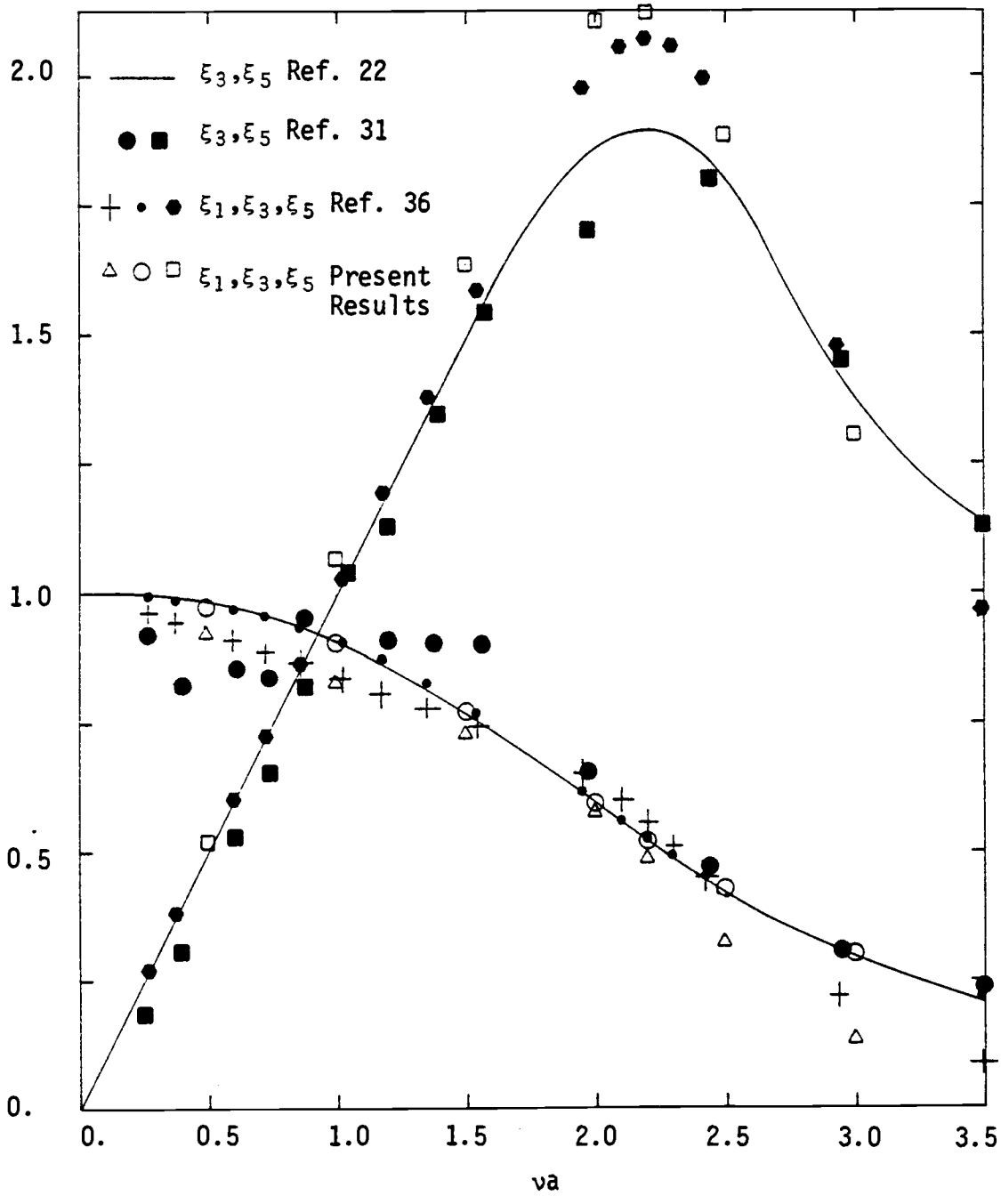

Fig. 4.24. Hydrodynamic responses of a floating disc buoy ($d/a = \infty$, $d_f/a = 1$, $d_1/a = 0.5$)

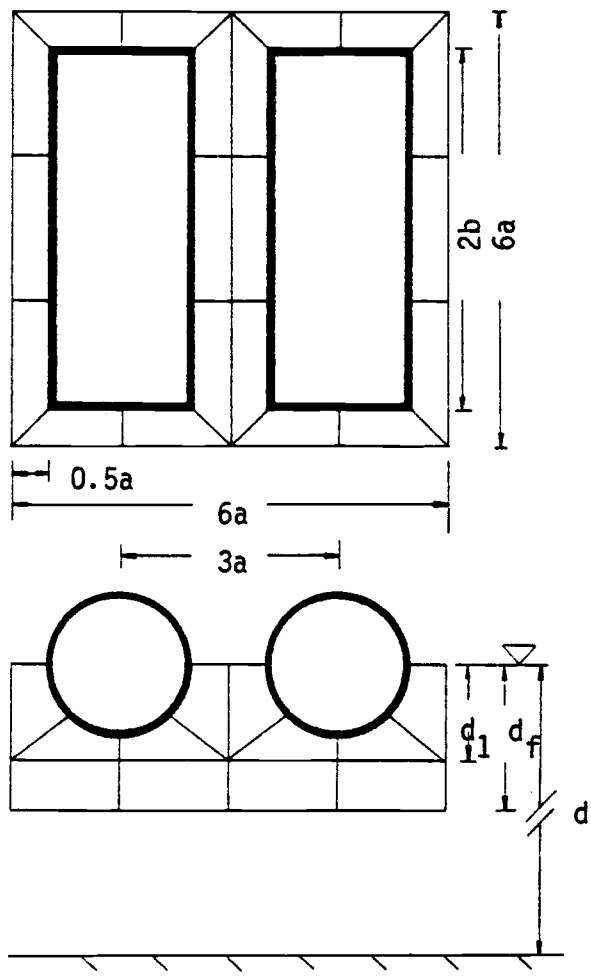

Fig. 4.25. Mesh for three-dimensional catamaran

($d/a = \infty$, $d_1/a = 4/3$, $d_f/a = 2$, $2b/a = 5$)

with the two-dimensional solutions to illustrate the end effects of a three-dimensional catamaran. The hydrodynamic coefficients in the sway mode are shown in Fig. 4.26, where end effects are shown to be small. The heave added mass and damping coefficients are shown in Figs. 4.27-4.28 where the end effects are clearly demonstrated. The standing waves between the two hulls become smaller as a result of flow around the ends of the catamaran. The heave resonance frequency also increases to approximately $\nu a = 0.9$. Similar prediction has been calculated recently by Eatock-Taylor and Zietsman (17) by using the boundary integral method (BIM). Numerical results of the sway and heave exciting forces are shown in Figs. 4.29-4.30, together with those results obtained from the two-dimensional approximation. The end effects are again illustrated by sharp decrease of the heave forces near the two-dimensional resonance frequency and an increase of three-dimensional resonance frequency.

4.3.e Loading/Unloading Facilities

One concept for cargo loading/unloading operations under consideration by engineers is that of a floating derrick barge moored between a vessel and a wharf connected by a long causeway to shore. The wharf and causeway would be supported by piles or some other permeable structures. An understanding of the wave interference phenomena between the two floating vessels, the wharf and the supporting structures are essential to the design of moorings and other forms of

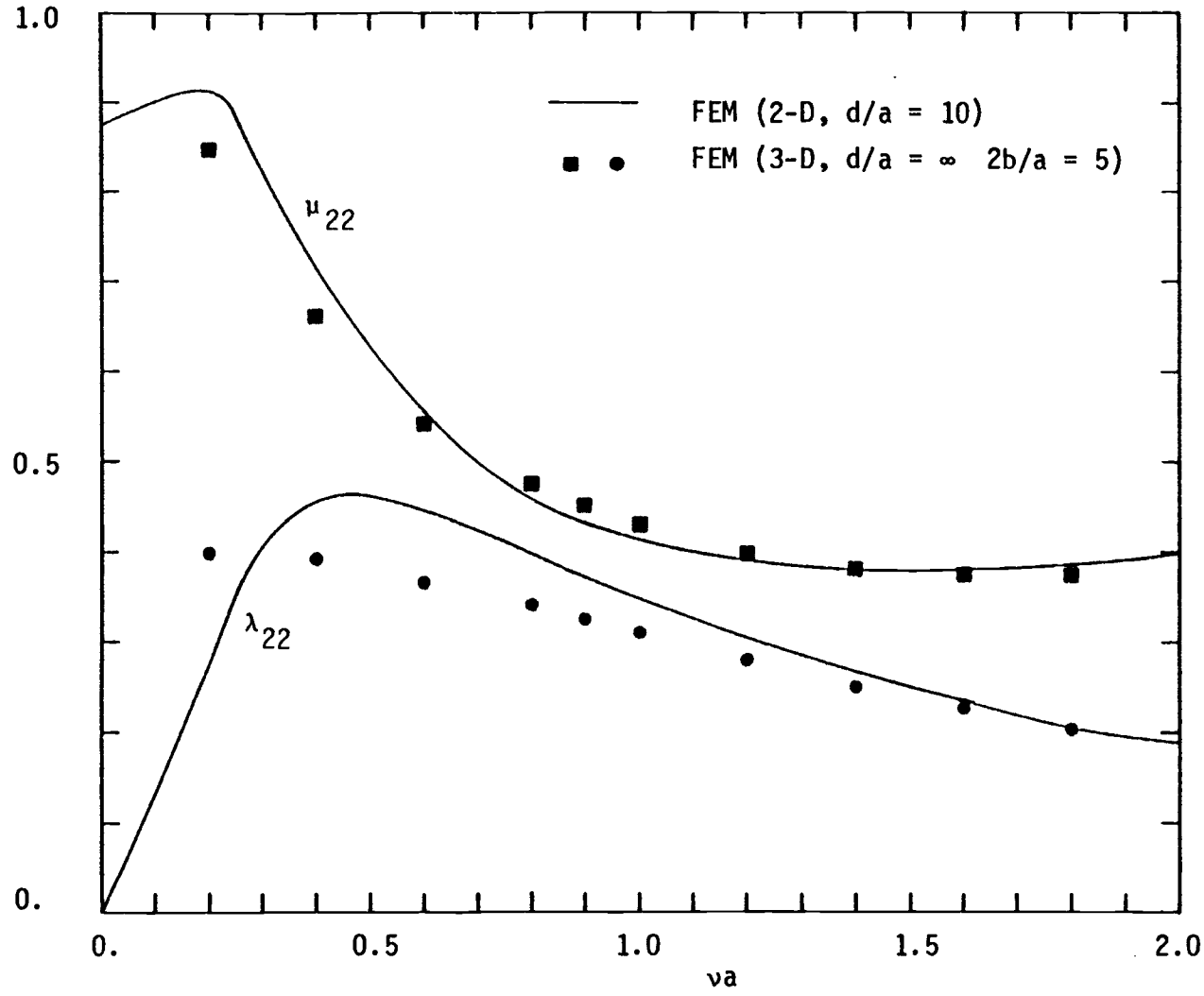

Fig. 4.26. Sway added mass and damping coefficients of catamaran

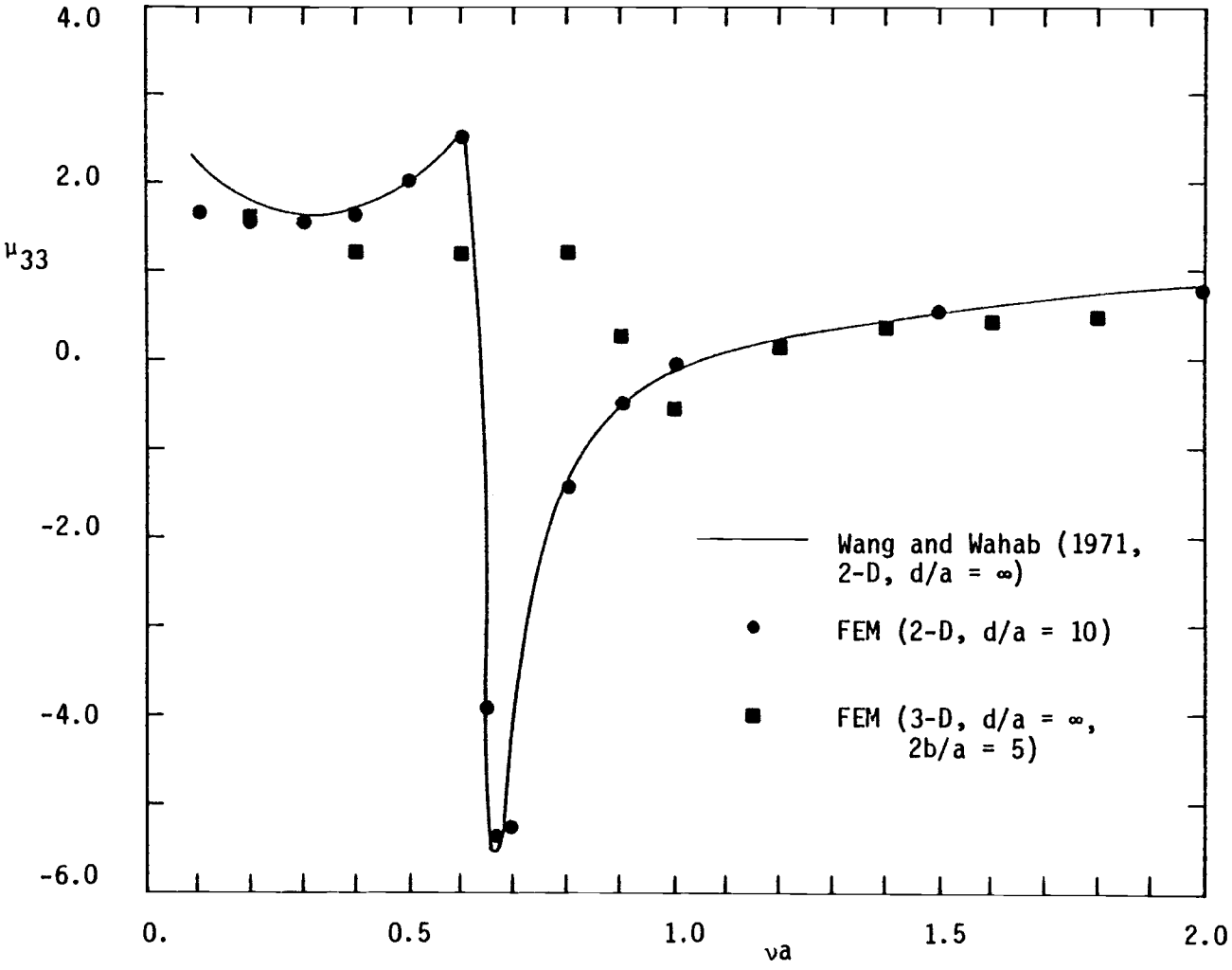

Fig. 4.27. Heave added mass coefficient of catamaran

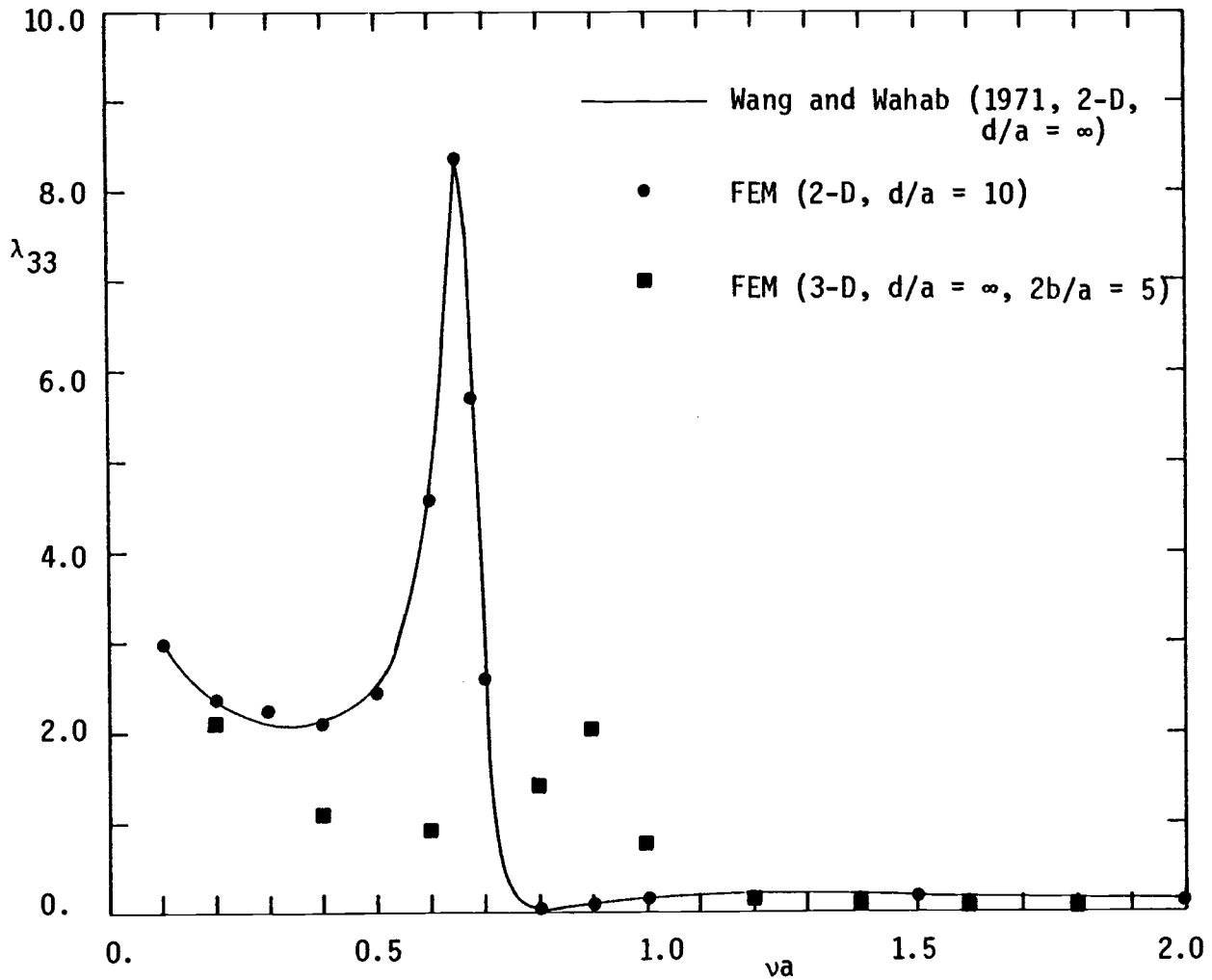

Fig. 4.28. Heave damping coefficient of catamaran

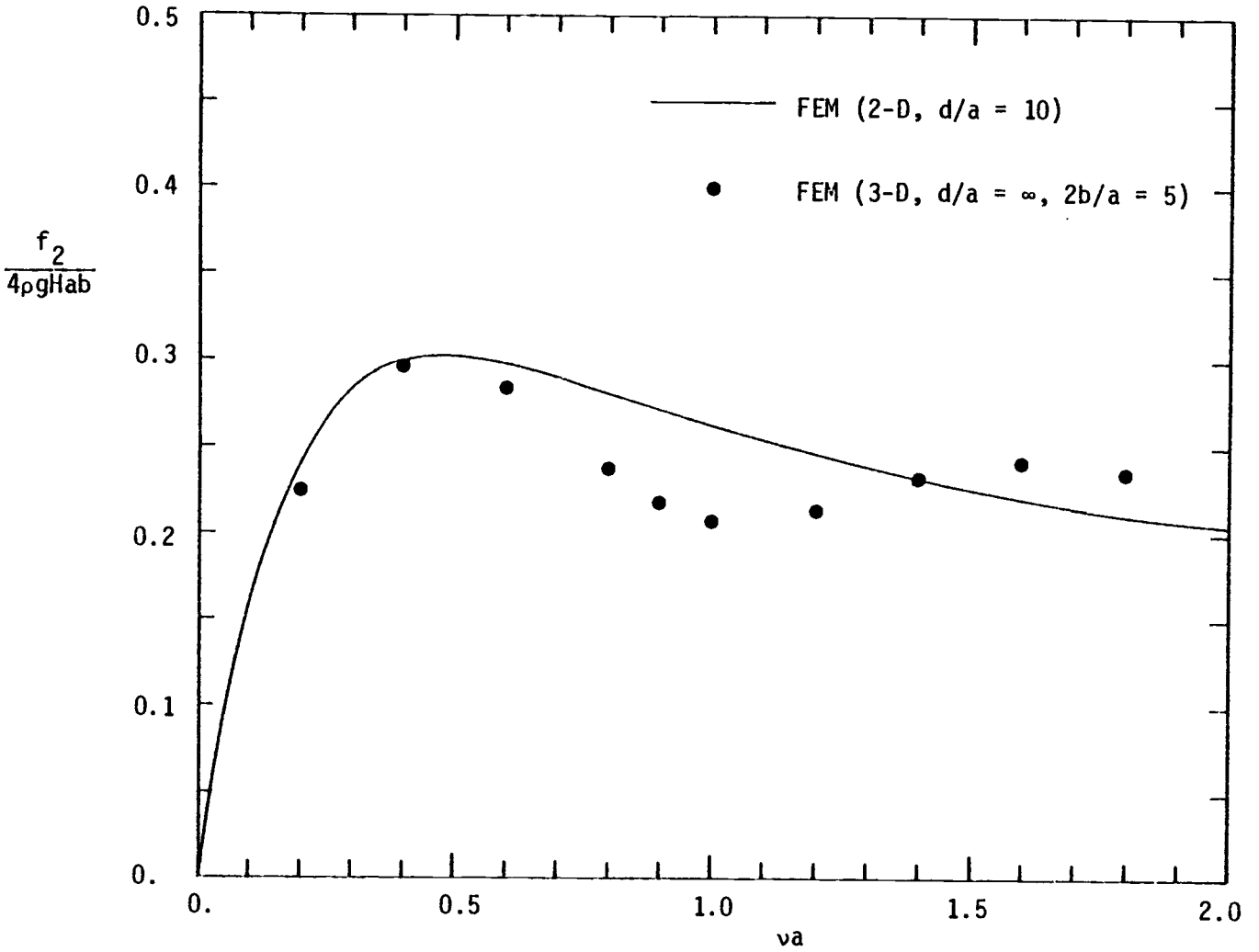

Fig. 4.29. Sway exciting force for a catamaran

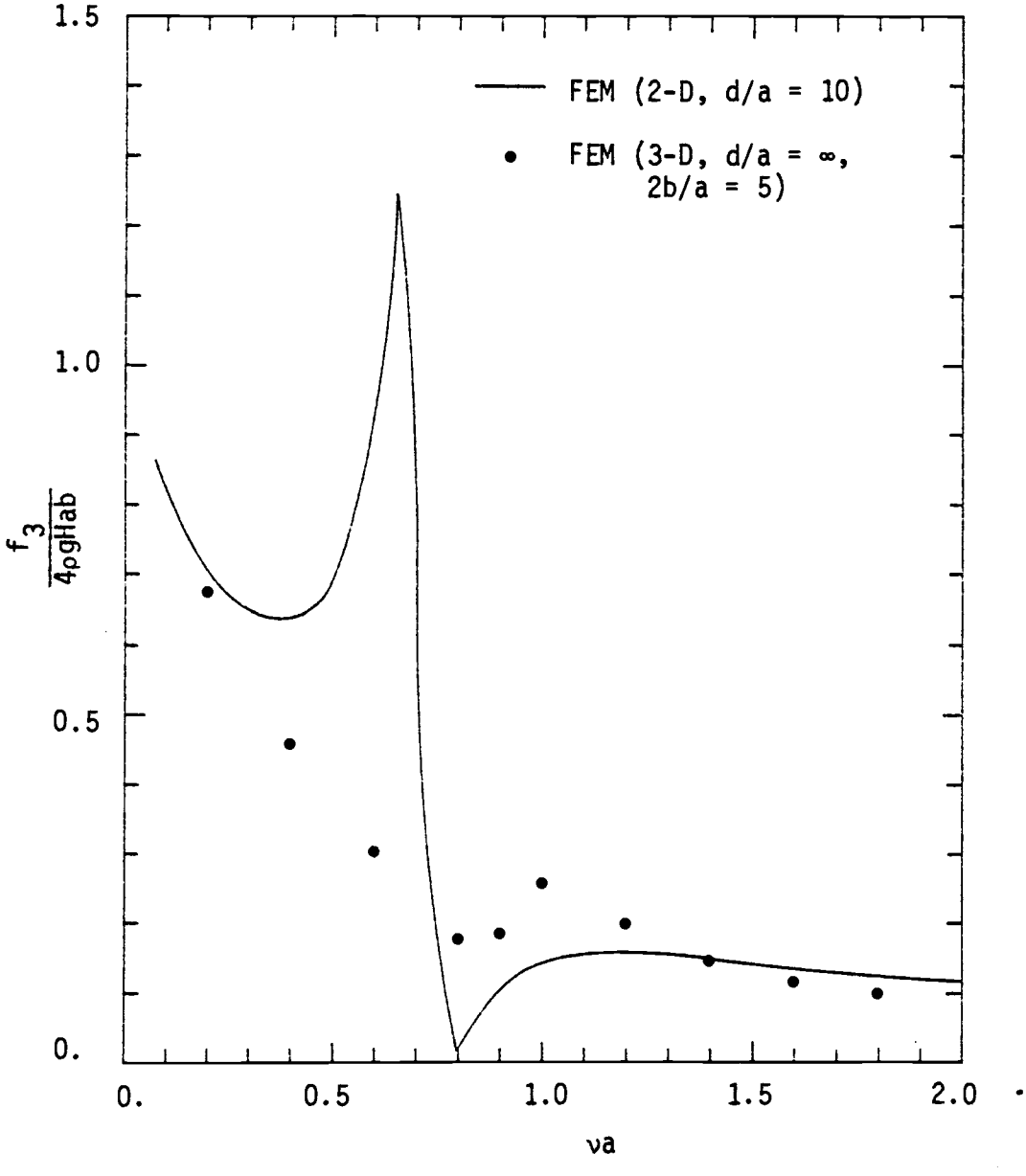

Fig. 4.30. Heave exciting force for a catamaran

inter-structural constraints.

For purpose of illustration, the interference phenomena in such a system have been calculated for the case shown in Fig. 4.31. A permeability of 0.75 was assumed for the supporting pile structure. The geometries and spacing of the two vessels are identical to the three-dimensional catamaran studied previously. Numerical solutions have been calculated for the case of beam seas, by using the meshes shown in Fig. 4.31. The predictions of the sway and heave exciting forces are illustrated in Fig. 4.32. Sharp variations of exciting forces, in both vessels and in both modes, are predicted near νa = 0.9, the resonance frequency of the three-dimensional catamaran. The sway forces are larger than the heave forces near νa = 0.9. As would be expected, large exciting forces are exerted on vessel 1 near the resonance frequency, since vessel 1 is stationed in the standing wave system between the wharf and vessel 2. One important interference phenomenon exists for this particular case: the sway resonance is more pronounced than the heave resonance, due to the effect of the permeable supporting structure under the wharf. As studied earlier in a two-dimensional structure adjacent to a permeable wall, the heave and sway resonance phenomena are strongly suppressed by increasing the permeability of the wall. For this particular case of a highly permeable supporting structure under the wharf , the transmitted waves provide a suction effect on both vessels, therefore, large sway responses.

The hydrodynamic coefficients calculated form the radiation

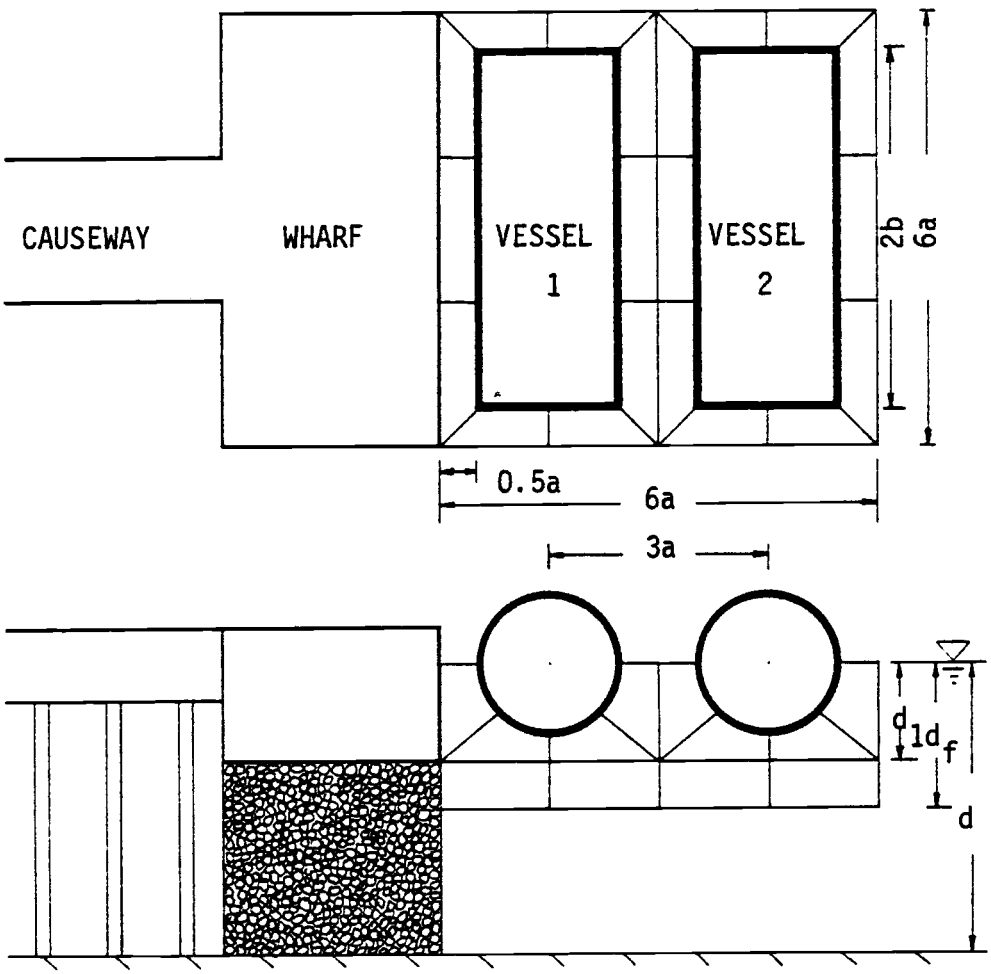

Fig. 4.31. Definition sketch for loading/unloading facilities ($d/a = 4$, $d_1/a = 4/3$, $d_f/a = 2$, $2b/a = 5$)

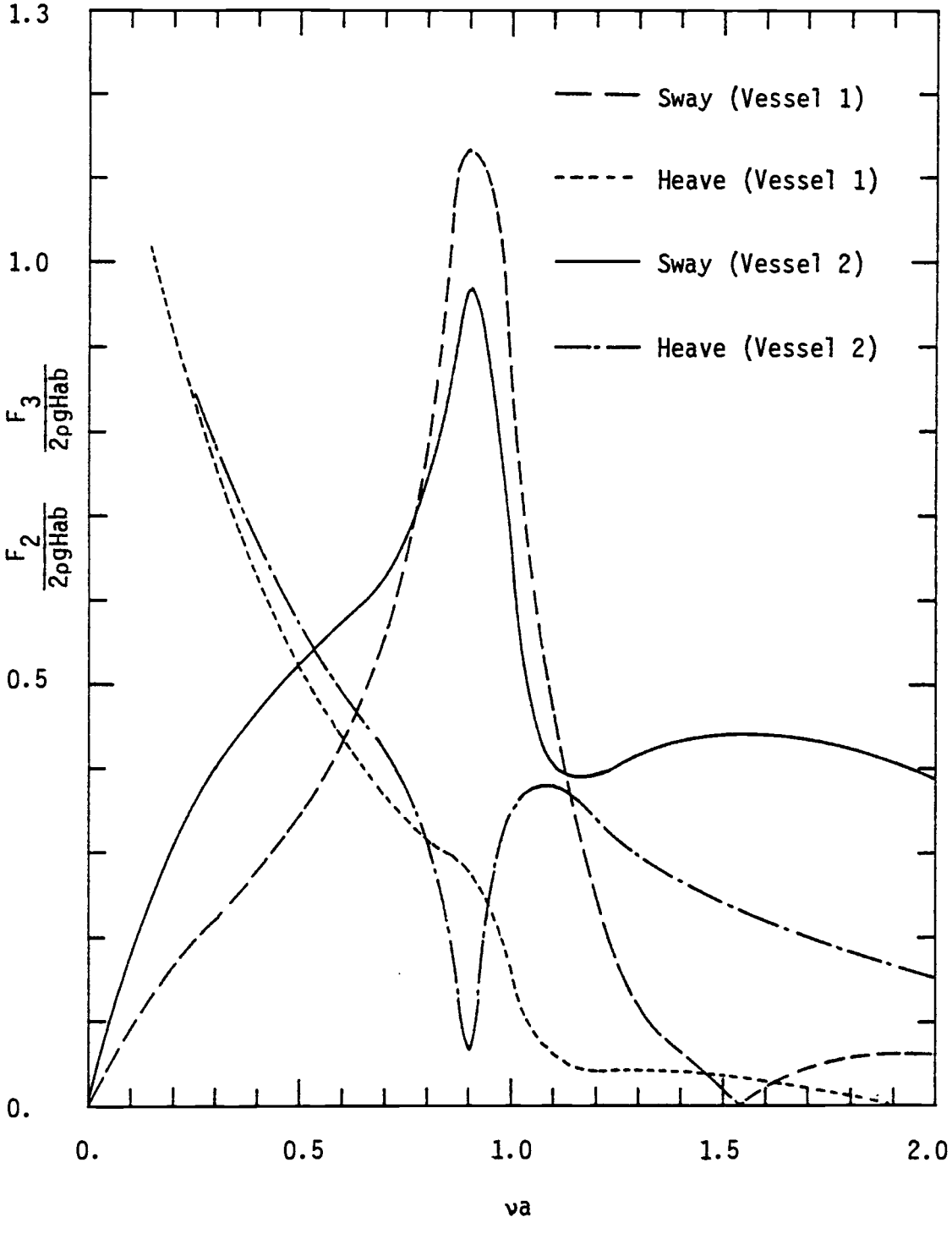

Fig. 4.32. Exciting forces on the two vessels in loading/unloading facilities in beam seas

problems are illustrated in Figs. 4.33-4.36. The resonance phenomena near $\nu a = 0.9$ are also clearly demonstrated. The coupled sway-heave restoring forces, induced by each vessel's own motions and the neighboring vessel's motions, are shown in Figs. 4.35-4.36. It should be pointed out here that these coupled restoring forces only exist in a multiple structures system. An important interference phenomenon exists for this case: negative added mass and very small damping coefficients are predicted in the range of $\nu a > 1.2$, especially in the sway mode. This is in contrast to the catamaran problems studied earlier (both two-dimensional and three-dimensional formulations, as shown in Fig. 4.26) The hydrodynamic responses of the vessels are strongly affected by these coefficients, large responses are associated with small fluid resistance (small damping) and water pressure force acting in the same direction as the vessel's motion (negative added mass). These responses are shown in Figs. 4.37-4.38. Large sway responses are predicted near $\nu a = 1.3$-1.4 for both vessels. The relative sway motions between the two vessels are also seen to have resonance peak at $\nu a = 1.4$ where the motions are 180 degrees out-of-phase. The relative heave response is seen to have a small resonance peak near $\nu a = 1.4$.

4.4 Summary

The linear diffraction and radiation of waves by multiple three-

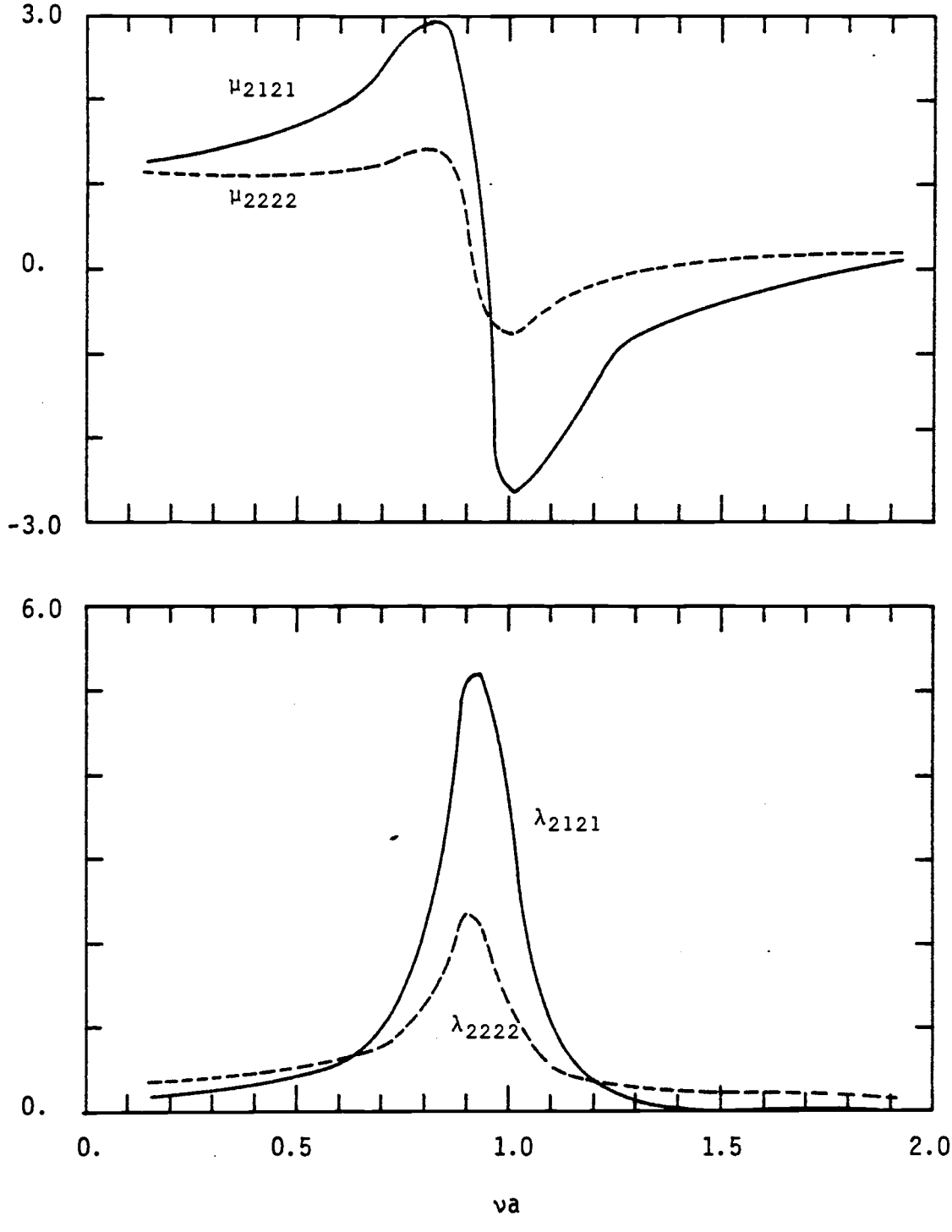

Fig. 4.33. Sway added mass and damping coefficients of the two vessels in loading/unloading facilities

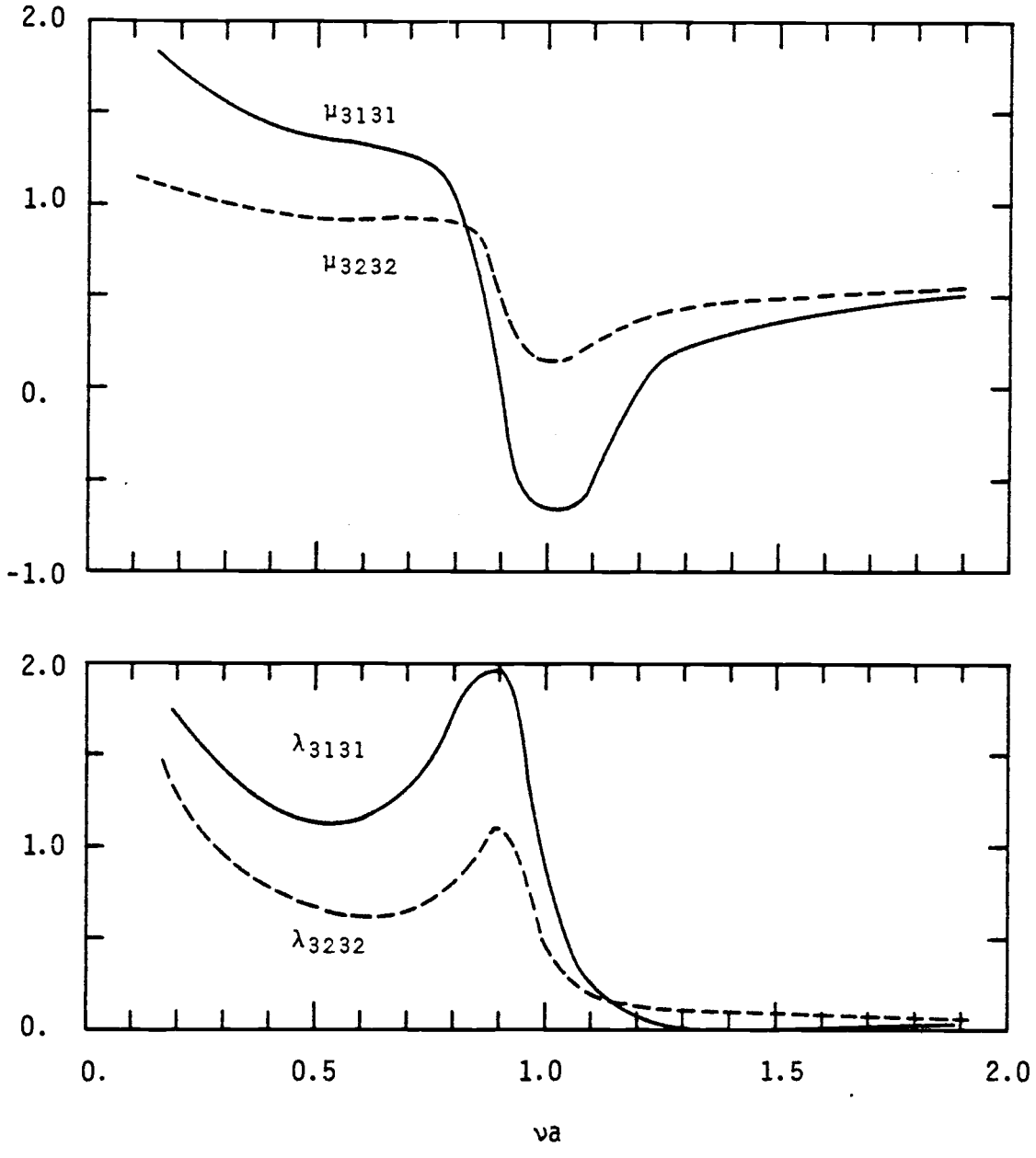

Fig. 4.34. Heave added mass and damping coefficients of the two vessels in loading/unloading facilities

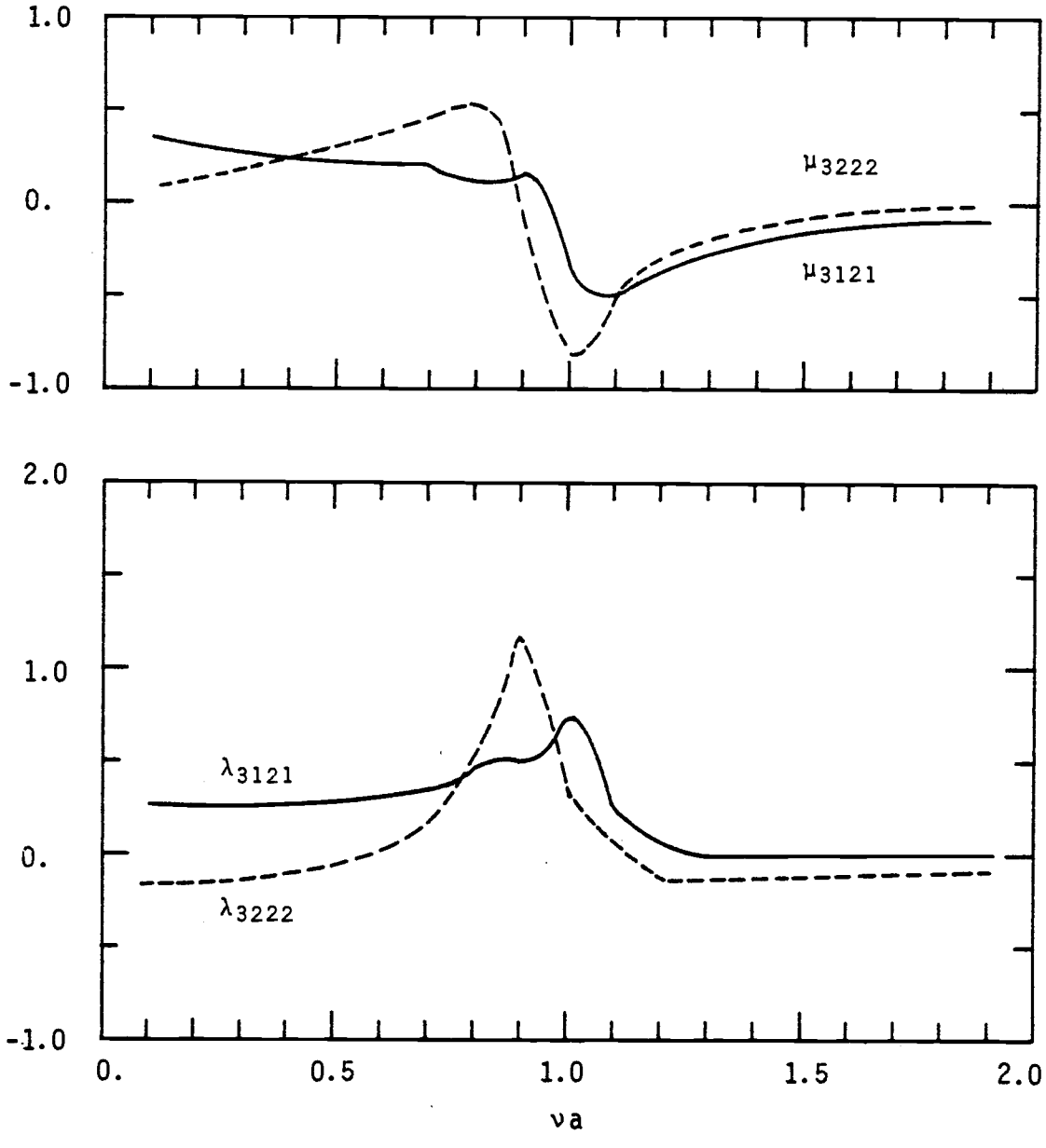

Fig. 4.35. Sway-heave coupled added mass and damping coefficients of the two vessels in loading/unloading facilities

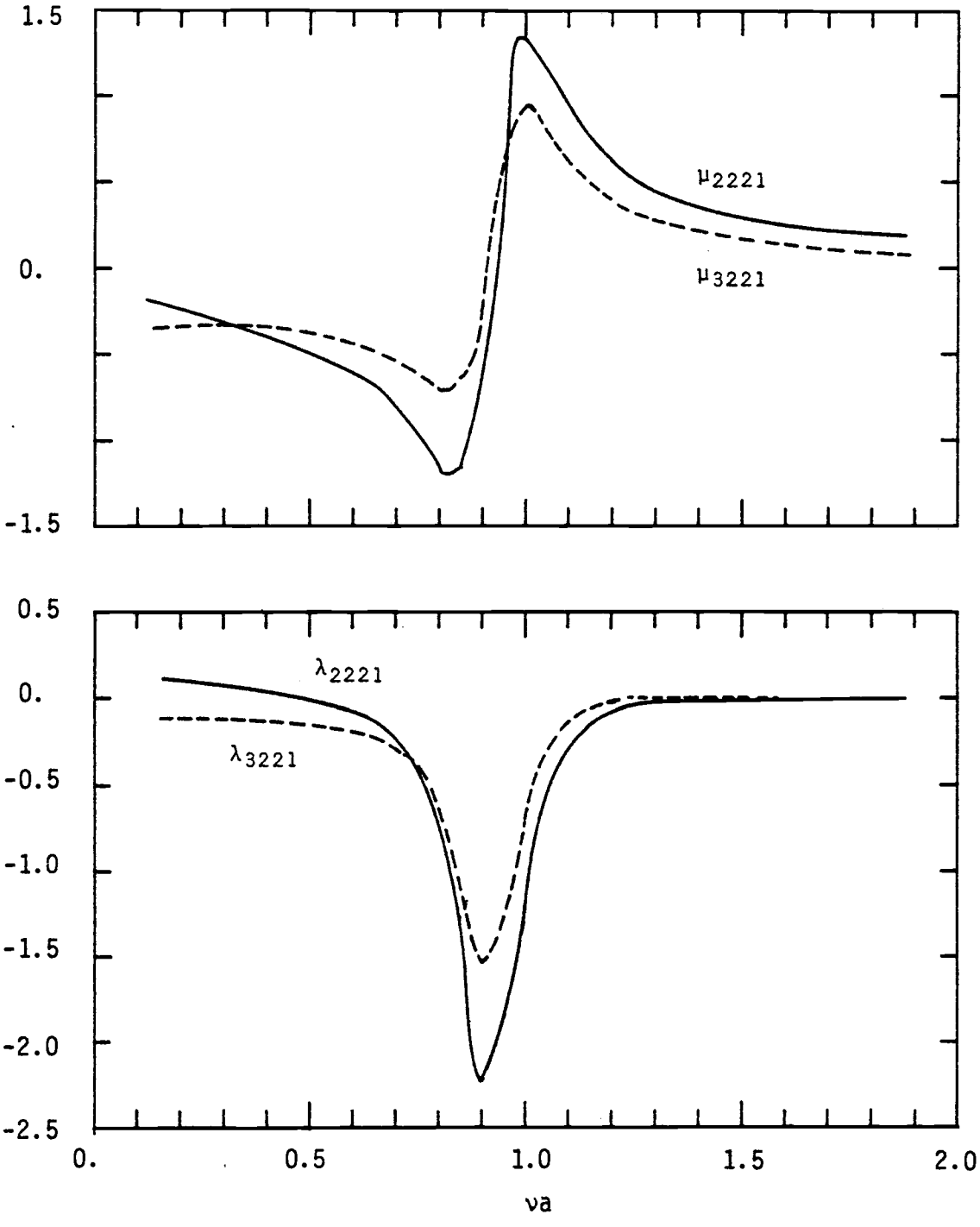

Fig. 4.36. Coupled added mass and damping coefficients between the two vessels in loading/unloading facilities

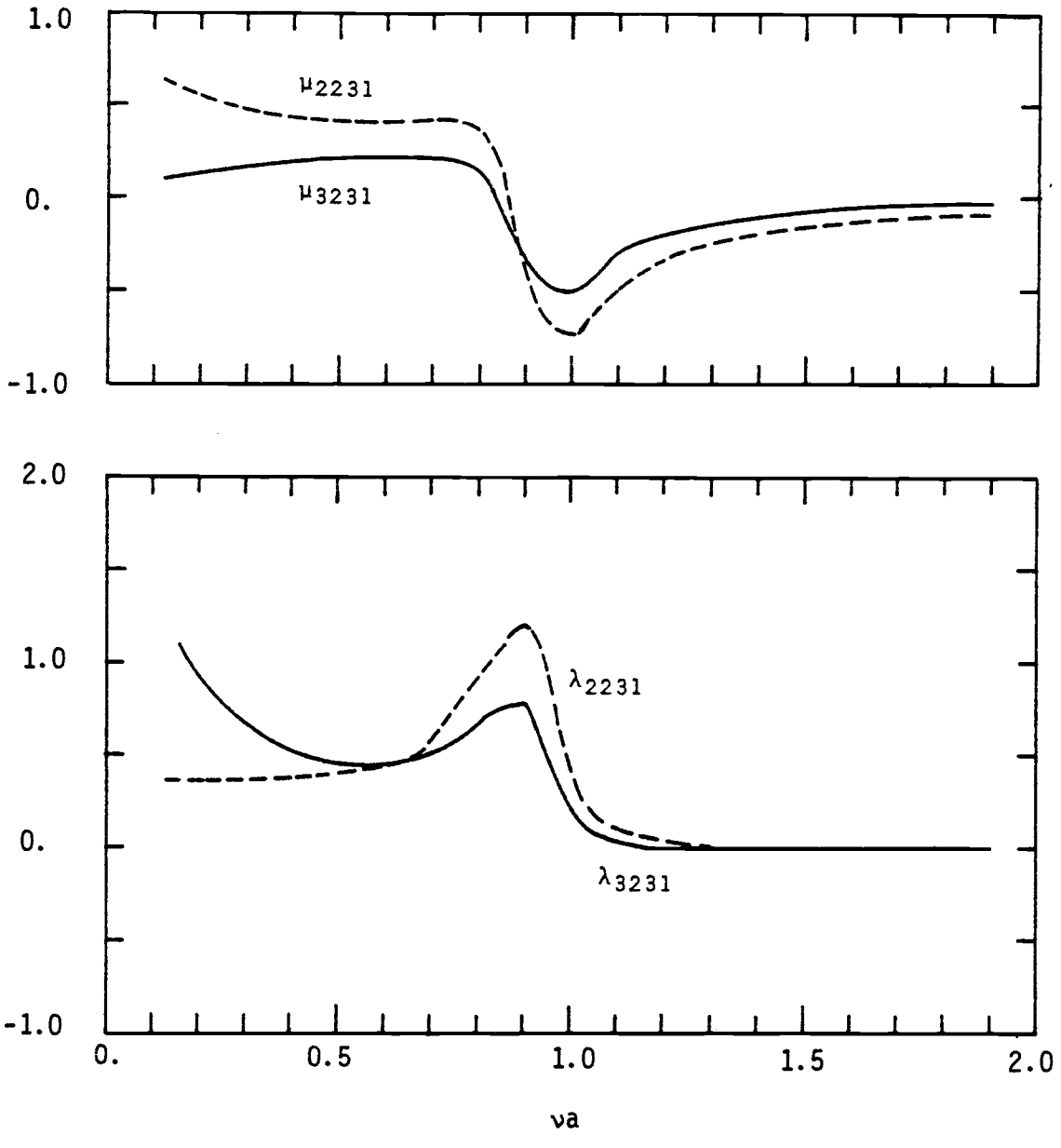

Fig. 4.36. (Continued)

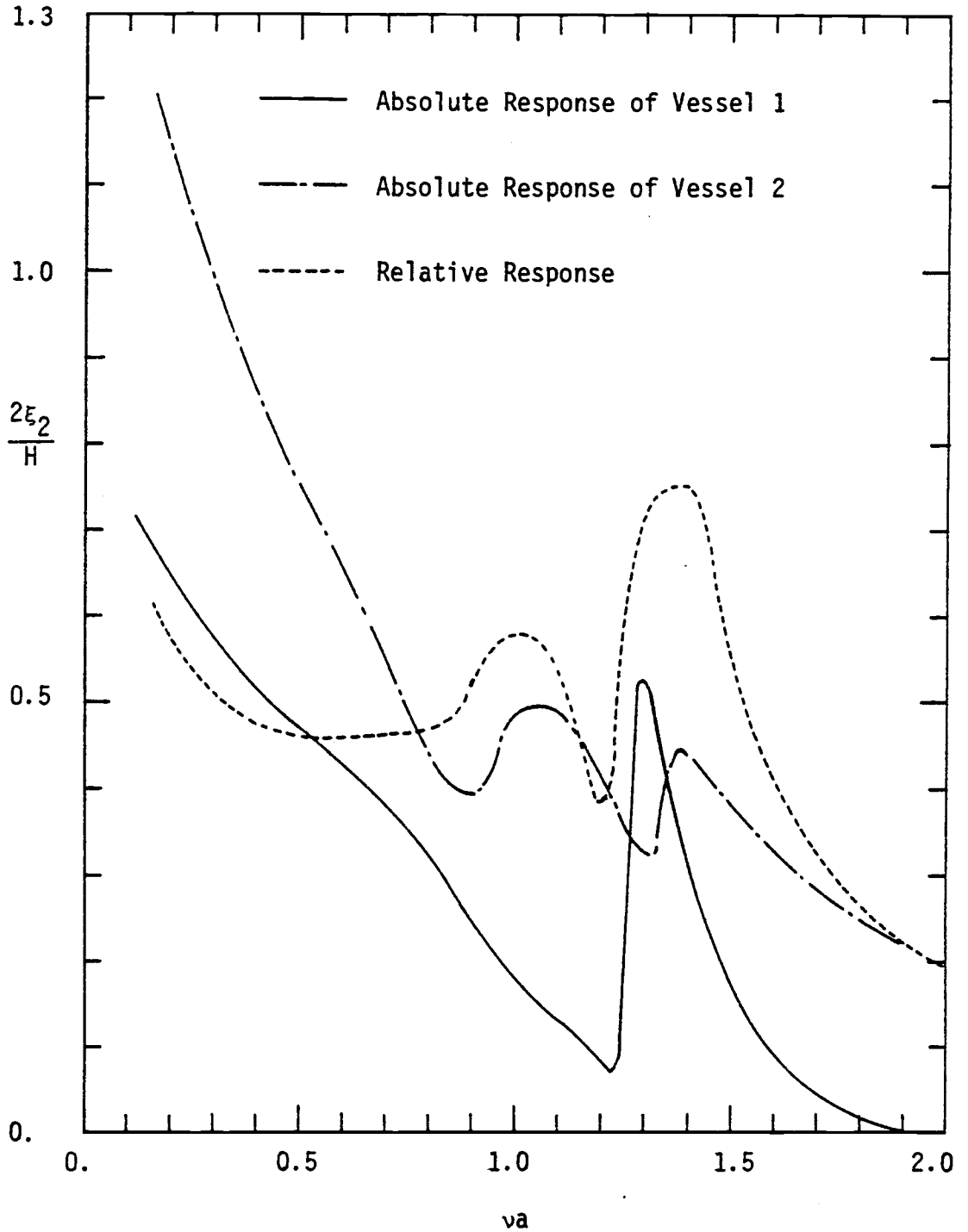

Fig. 4.37. Sway responses for the two vessels in loading/unloading facilities in beam seas

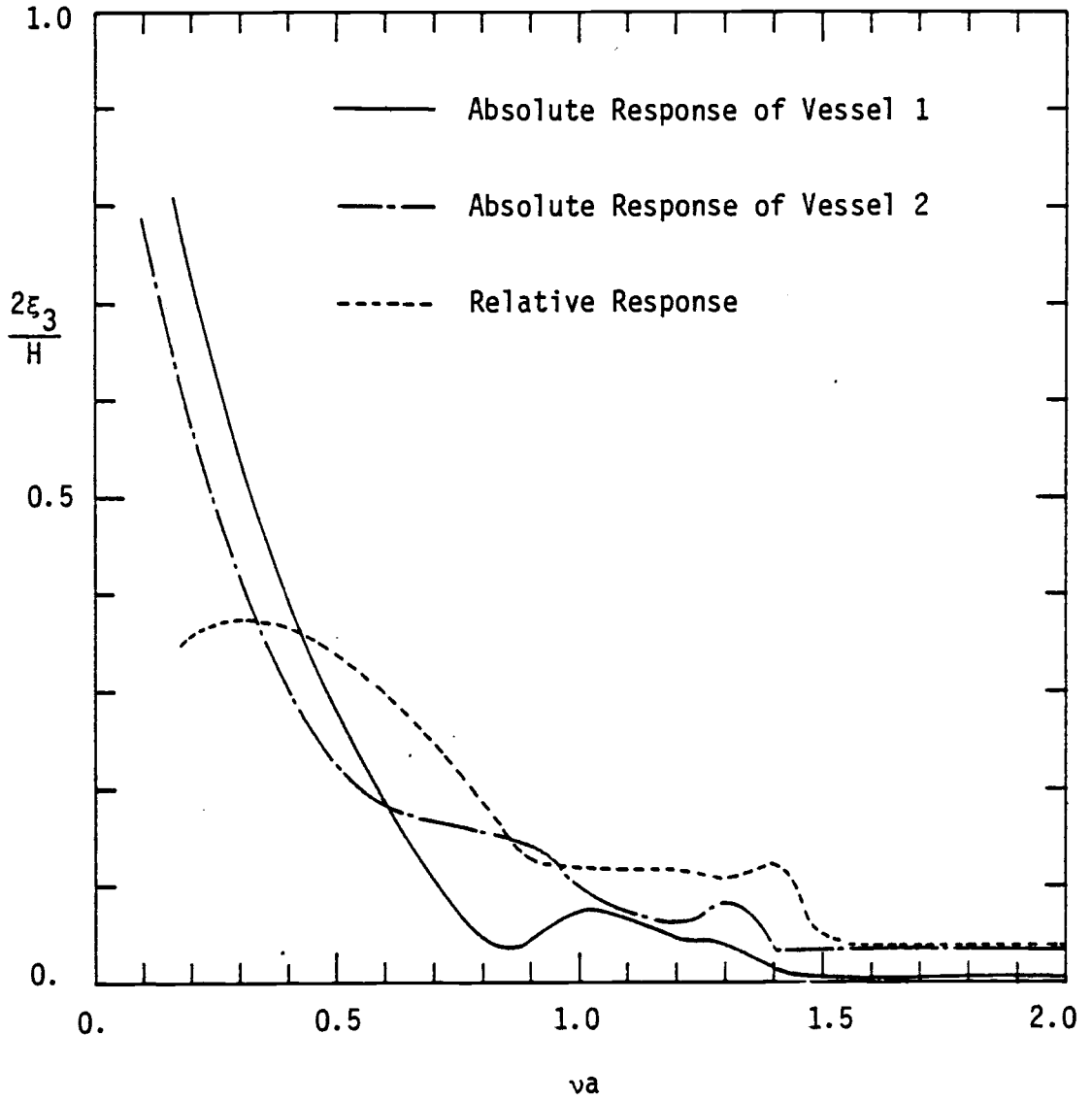

Fig. 4.38. Heave responses for the two vessels in loading/unloading facilities in beam seas

dimensional structures have been considered. A finite element method which incorporates radiation dampers, permeable boundary dampers and a fictitious bottom boundary has been developed with which the wave field variables are calculated for multiple structures system. The validity of the finite element model has been demonstrated for a variety of examples. This is summarized below:

1) For a structure floating in shallow water, the fluid domain is extended to the true bottom in the finite element discretization. Comparisons between the present diffraction solutions and analytical solutions, and boundary series method (BSM) solutions are very good in general. Comparisons between the present solutions and the integral equation solutions indicate some discrepancies in the diffraction and radiation calculations. However, the hydrodynamic responses are not greatly affected -- comparisons are generally good. Similar predictions have also been indicated by Eatock-Taylor and Zietsman (17) using the boundary integral method (BIM).

2) For a structure floating in deep water or infinite water, a fictitious bottom is constructed in the diffraction and radiation functionals. In numerical experiments on different choices of the distance of this fictitious bottom below the structure, it was found that its effects on the numerical solutions are very small, except in the range of very long waves. In this range, the solution accuracy is more dominated by the extent of fluid domain in the radial directions.

3) Two different meshes (one with cylindrical dampers and the

other with plane dampers) have been used in the study of vertical circular cylinder diffraction and radiation problems. The meshes with plane dampers gave better resonance comparisons with the integral equation prediction, probably due to the larger extent of fluid domain discretized in this formulation. In general, the selection of different dampers in the three-dimensional problems has less effect on the solution accuracy than it has in the two-dimensional horizontal plane problems of surface-piercing structures (discussed in Chapter 2). The water waves are allowed to flow beneath, and to diffract around, the three-dimensional structures; in contrast to the surface-piercing cases where the waves are forced to scatter around the structures only.

4) Numerical results of disc buoy responses compare fairly well with the axisymmetric Green's function results. Both techniques gave larger pitch resonance predictions than the experimental results, due to the fact that viscous damping is neglected in the numerical analyses.

5) The end effects and interference phenomena of a three-dimensional catamaran are clearly demonstrated; i.e., an increase of heave resonance frequency and sharp decrease of standing wave system between the two hulls. Again, the water waves are allowed to flow around the ends of catamaran. Similar predictions have been reported recently by Eatock-Taylor and Zietsman (17) using the Boundary Integral Method. Good agreement is obtained between the present finite element algorithm and the Boundary Integral Method where extensive

use of explicit integration on the boundary is performed to achieve computational efficiency. No irregular frequencies are experienced using the present algorithm and, therefore, the same meshes can be used for a wide range of frequencies to be studied.

6) A design example of floating vessels loading/unloading facilities has been studied, where the interference effects between multiple floating vessels and an adjacent wharf, part impermeable and part permeable, were considered. The effects of impermeable and permeable wharfs are easily incorporated with the present finite element formulation. It is seen that the heave resonance between the two vessels (corresponding to the heave resonance frequency when no wall is present) is suppressed, while the sway resonance is strongly excited at a higher frequency. This finding is essential in future design of moorings and assessment of the supporting pile structures to avoid collisions of vessels.

5.0 CONCLUSIONS

A numerical calculation procedure for the hydrodynamic interference effects between large multiple structures interacting with linear ocean waves has been presented in this study. Viscous effects were neglected and the hydrodynamic pressure forces assumed to be inertially dominated. A finite element method which incorporates radiation boundary dampers was adopted to calculate the wave forces and other field variables in the direct interference model. Numerical solutions in the frequency domain were calculated for three categories of the boundary-value formulations: two-dimensional horizontal plane, two-dimensional vertical plane and three-dimensional problems.

The two-dimensional horizontal plane interference problems were formulated by incorporating explicit integration in the vertical direction, and applied to fixed, surface-piercing structures only. Two types of radiation dampers, cylindrical and plane dampers, were investigated. The cylindrical damper formulation gives better prediction of the scattered wave field variables. The two-dimensional vertical plane interference problems in finite water depth were formulated with a flexural waves approximation to treat diffraction and radiation of oblique waves. Plane dampers were used to model the radiation condition and permeable boundaries. Both floating-floating and fixed-floating structures systems were investigated. The effects of structural permeability, moorings and inter-structural constraints were also investigated. In general, good predictions of the wave

interference effects were obtained in both the horizontal- and the vertical-plane problems. Structural permeability is seen to have a strong effect in suppressing wave resonance phenomena.

The three-dimensional interference problems have been formulated by incorporating a fictitious bottom boundary and radiation dampers in the finite element functionals. The fluid domain discretization was minimized by using this technique. Both cylindrical and plane dampers were used in a variety of single structure wave diffraction and radiation problems. In general, the selections of different radiation dampers and a fictitious bottom do not have a very strong effect on first-order structural responses. This is due to the fact the water waves are allowed to flow beneath, and to scatter around, the structures. Interference effects are shown to be strongly suppressed and shifted to shorter waves region in three-dimensional multiple structures where end effects are considered. The versatility of the present three-dimensional finite element algorithm was clearly demonstrated in the analysis of a loading/unloading facilities, where important interference phenomena were identified.

Isoparametric curved elements with quadratic shape functions were used in this study to represent the structural geometries and the inner fluid domain variables. Regular finite elements (i.e., same sizes) were used whenever possible to replicate the element matrices and, therefore, to reduce the computing effort. A Gauss elimination technique was used to solve the symmetric, banded matrix equations

derived from the wave diffraction and radiation functionals. In the three-dimensional algorithm, a blockform Gauss elimination technique was employed to increase the solution capacity in treating complicated systems.

In summary, this study provides an alternative frequency domain solution technique for the study of steady hydrodynamic interference effects between large multiple structures. The validity of the present finite element algorithms, both in two-dimensional and in three-dimensional formulations, were studied extensively.

Extensions of the present finite element algorithm are suggested for the following areas:

1) Incorporation of a ship hydrostatic calculation pre-processor (such as Bonjean's curves) into the present computer program to treat vessel interference problems;

2) Incorporation of linearized viscous damping into the present computer program to treat interference problems where the structures are very close to each other;

3) Experimental verification of the effect of permeable structures on interference phenomena, and quantitative determination of the permeability parameter;

4) Development of a nonlinear time domain solution method to treat large structural displacements and nonlinear inter-structural restoring forces;

5) Development of a nonlinear second-order diffraction algorithm

using a perturbation procedure and the present finite element formulation to treat nonlinear interference problems for steep waves;

6) Development of a wave-structure-foundation-soil interaction model wherein coarse aggregate foundation may be simulated by permeable boundary dampers, a fictitious bottom may be used to model the wave-soil interface, and the infinite elements may be used to model the homogeneous, isotropic soil half space; and

7) The present finite element formulation may be easily combined with the existing boundary element (integral equation) computer algorithms to improve their representation of the structural geometry.

BIBLIOGRAPHY

1. Adee, B.H., Richey, E.P. and Christensen, D.R., "Floating Breakwater Field Assessment Program, Friday Harbor, Washington," U.S. Army Corps of Engineers, Coastal Engineering Research Center, Technical Paper 76-17, 1976.

2. Bai, K.J., "The Added Mass of Two-Dimensional Cylinders Heaving in Water of Finite Depth," Journal of Fluid Mechanics, Vol. 81, Pt. 1, 1977, pp. 85-105.

3. Bai, K.J., "Diffraction of Oblique Waves by an Infinite Cylinder," Journal of Fluid Mechanics, Vol. 68, Pt. 3, 1975, pp. 513-535.

4. Bathe, K.J. and Wilson, E.L., Numerical Methods in Finite Element Analysis, Prentice-Hall, 1976.

5. Berkhoff, J.C.W., "Mathematical Models for Simple Harmonic Linear Water Waves, Wave Diffraction and Refraction," Delft Hydraulics Laboratory Publication, No. 163, Delft, 1976.

6. Bettess, P., "More on Infinite Elements," International Journal for Numerical Methods in Engineering, Vol. 15, 1980, pp. 1613-1626.

7. Bettess, P. and Zienkiewicz, O.C., "Diffraction and Refraction of Surface Waves Using Finite and Infinite Elements," International Journal for Numerical Methods in Engineering, Vol. 11, 1977, pp. 1271-1290.

8. Bettess, P., "Infinite Elements," International Journal for Numerical Methods in Engineering, Vol. 11, 1977, pp. 53-64.

9. Bird, H.W.K. and Shepherd, R., "Wave Interaction with Large Submerged Structures," Journal of Waterway, Port, Coastal and Ocean Div., ASCE, Vol. 108, No. WW2, 1982, pp. 146-162.

10. Bolton, W.E. and Ursell, F., "The Wave Force on an Infinitely Long Circular Cylinder in an Oblique Sea," Journal of Fluid Mechanics, Vol. 57, Pt. 2, 1973, pp. 241-256.

11. Bruun, P., Port Engineering, 2nd edition, Gulf Publication Co., Houston, 1976, pp. 157-167.

12. Chakrabarti, S.K., Discussion of "Vertical Cylinders of Arbitrary Section in Waves," by M. Isaacson, Journal of Waterway, Port, Coastal and Ocean Div., ASCE, Vol. 105, No. WW2, 1979, pp. 208-210.

13. Chakrabarti, S.K., "Wave Forces on Multiple Vertical Cylinders," Journal of Waterway, Port, Coastal and Ocean Div., ASCE, Vol. 104, No. WW2, 1978, pp. 147-161.

14. Chung, Y.K. and Coleman, M.I., "Hydrodynamic Forces and Moments for Oscillating Cylinders," Proceedings Civil Engineering in the Ocean III, ASCE, Univ. of Delaware, Vol. 3, 1975, pp. 899-913.

15. Cummings, W.E., "The Impulse Response Function and Ship Motions, " David Taylor Model Basin Report, No. 1661, Washington, D.C., 1962.

16. Deruntz, J.A. and Geres, T.L., "Added Mass Computation by the Boundary Integral Method," International Journal for Numerical Methods in Engineering, Vol. 12, 1978, pp. 531-549.

17. Eatock-Taylor, R. and Zietsman, J., "Hydrodynamic Loading on Multi-Component Bodies," Proceedings International Conference on the Behavior of Offshore Structures, BOSS' 82, 1982, pp. 424-443.

18. Eatock-Taylor, R. and Zietsman, J., "A Comparison of Localized Finite Element Formulations for Two-Dimensional Wave Diffraction and Radiation Problems," International Journal for Numerical Methods in Engineering, Vol. 17, 1981, pp. 1355-1384.

19. Frank, W., "On the Oscillation of Cylinders in or Below the Free Surface of Deep Fluids," Naval Ship Research and Development Center, Report No. 2375, 1967.

20. Fenton, J.D., "Wave Forces on Vertical Bodies of Revolution," Journal of Fluid Mechanics, Vol. 85, Pt. 2, 1978, pp. 241-255.

21. Garrett, C.J.R., "Wave Forces on a Circular Dock," Journal of Fluid Mechanics, Vol. 46, Pt. 1, 1971, pp. 129-139.

22. Garrison, C.J., "Hydrodynamic Loading of Large Offshore Structures. Three-Dimensional Source Distribution Methods," in Numerical Methods in Offshore Engineering, ed. O.C. Zienkiewicz, et. al., Wiley, Chichester, England, 1978, pp. 87-140.

23. Garrison, C.J. and Stacey, R., "Wave Loads on North Sea Gravity Platforms: A Comparison of Theory and Experiments," Proceedings Offshore Technology Conference, Houston, Paper No. OTC 2794, Vol. I, 1977, pp. 513-524.

24. Garrison, C.J., "Hydrodynamics of Large Objects in the Sea: Part I - Hydrodynamic Analysis," Journal of Hydronautics, Vol. 8, 1974, pp. 5-63.

25. Garrison, C.J., "Hydrodynamics of Large Objects in the Sea: Part II - Motions of Free-Floating Bodies," Journal of Hydronautics, Vol. 9, 1975, pp. 58-63.

26. Garrison, C.J., "On the Interaction of an Infinite Shallow Draft Cylinder Oscillating at the Free Surface with a Train of Oblique Waves," Journal of Fluid Mechanics, Vol. 39, Pt. 2, 1969, pp. 227-255.

27. Harlow, E.H., "Offshore Floating Terminals," Journal of Waterways, Harbors and Coastal Engineering Div., ASCE, Vol. 97, No. WW3, 1971, pp. 531-548.

28. Harris, R.J.S., "Platforms - Concrete Structures," in A Guide to North Sea Oil and Gas Technology, Proceedings of the Institute of Petroleum 1977 Annual Conference, London, England, 1977, pp. 66-78.

29. Hartley, G., "Moorings Method Aids Early Production," Offshore, January 1980, pp. 58-60.

30. Ho, R.T. and Harten, A., "Green's Function Techniques for Solutions of Floating Body Problems," Proceedings Civil Engineering in the Ocean III, ASCE, Univ. of Delaware, Vol. 3, 1975, pp. 939-958.

31. Hoffman, D., Geller, E.S. and Niederman, C.S., "Mathematical Simulation and Model Tests in the Design of Data Buoy," The Society of Naval Architects and Marine Engineers, presented at the Annual Meeting of SNAME, 1973.

32. Hogben, N., Miller, B.L., Searle, J.W. and Ward, G., "Estimation of Fluid Loading on Offshore Structures," Proceedings of the Institution of Civil Engineers, Vol. 63, 1977, pp. 515-562.

33. Hogben, N. and Standing, R.G., "Experience in Computing Wave Loads on Large Bodies," Proceedings of the Offshore Technology Conference, Paper No. OTC 2189, Vol. II, Houston, 1975, pp. 413-431.

34. Hogben, N. and Standing, R.G., "Wave Loads on Large Bodies," Proceedings International Symposium on the Dynamics of Marine Vehicles and Structures in Waves, Univ. College, London, 1974, pp. 258-277.

35. Hudspeth, R.T., Nakamura, T. and Leonard, J.W., "Floating Vessel Response Simulator (FVRS) by an Axisymmetric Green's Function, " Marathon Oil Company Report, 1980.

36. Hudspeth, R.T., Private Communication, 1982.

37. Isaacson, M., "Interference Effects Between Large Cylinders in Waves," Journal of Petroleum Technology, Vol. 31, No. 4, 1979, pp. 505-512.

38. Isaacson, M., "Wave Forces on Large Square Cylinders," in Mechanics of Wave-Induced Forces on Cylinders, ed. T.L. Shaw, Pitman, London, 1979, pp. 609-622.

39. Isaacson, M., "Vertical Cylinders of Arbitrary Section in Waves, " Journal of Waterway, Port, Coastal and Ocean Div., ASCE, Vol. 104, No. WW4, 1978, pp. 309-324.

40. John, F., "On the Motion of Floating Bodies II," Communications in Pure and Applied Mathematics, Vol. 3, 1950, pp. 45-101.

41. Kim, C.H., "Hydrodynamic Forces and Moments for Heaving, Swaying , and Rolling Cylinders on Water of Finite Depth," Journal of Ship Research, Vol. 13, 1969, pp. 137-154.

42. Koman, B. and Seidl, L.H., "Mooring and Berthing Forces at an Offshore Berth," Proceedings Civil Engineering in the Ocean IV, ASCE, San Francisco, Vol. 2, 1979, pp. 932-947.

43. Lebreton, J.C. and Cormault, P., "Wave Action on Slightly Immersed Structures, Some Theoretical and Experimental Considerations," Proceedings of the Symposium Research on Wave Action, Delft, Netherlands, 1969.

44. Lee, C.M., "Motion Characteristics of Floating Bodies," Journal of Ship Research, Vol. 20, No. 4, 1976, pp. 181-189.

45. Løken, A.E., "Hydrodynamic Interaction Between Several Floating Bodies of Arbitrary Form in Waves," International Symposium on Hydrodynamics in Ocean Engineering, The Norwegian Institute of Technology, Trondheim, Norway, 1981, pp. 745-779.

46. Macagno, M., "A Comparison of Three Methods for Computing the Added Mass of Ship Sections," Journal of Ship Research, Vol. 12, 1968, pp. 279-285.

47. MacCamy, R.C. and Fuchs, R.A., "Wave Forces on Piles: A Diffraction Theory," U.S. Army Corps of Engineers, Beach Erosion Board, Technical Memo, No. 69, 1954.

48. Maeda, H., "Hydrodynamical Forces on a Cross-Section of a Stationary Structure," Proceedings International Symposium on the Dynamics of Marine Vehicles and Structures, Univ. College, London, 1974, pp. 80-90.

49. Matsui, T. and Tamaki, T., "Hydrodynamic Interaction Between Groups of Vertical Axisymmetric Bodies Floating in Waves," International Symposium on Hydrodynamics in Ocean Engineering, The Norwegian Institute of Technology, Trondheim, Norway, 1981 , pp. 817-836.

50. Mei, C.C., "Numerical Methods in Water-Wave Diffraction and Radiation," Annual Review Fluid Mechanics, Vol. 10, 1978, pp. 393-416.

51. Morison, S.R., O'Brien, M.D., Johnson, J.W. and Schaaf, S.A., "The Force Exerted by Surface Waves on Piles," Petroleum Transactions, AIME, Vol. 189, 1950, pp. 149-154.

52. Naftzger, R.A. and Chakrabarti, S.K., "Scattering of Waves by Two-Dimensional Circular Obstacles in Finite Water Depth," Journal of Ship Research, Vol. 23, No. 1, 1979, pp. 32-42.

53. Newman, J.N., Marine Hydrodynamics, The MIT Press, 1978.

54. Newton, R.E., "Finite Element Analysis of Two-Dimensional Added Mass and Damping," in Finite Elements in Fluids, Vol. 1, ed. R.H. Gallagher, et al., 1975, pp. 219-232.

55. Ohkusu, M., "Ship Motions in Vicinity of a Structure," Proceedings of the First Conference on the Behavior of Offshore Structures, BOSS' 76, Trondheim, Norway, Vol. I, 1976, pp. 284-306.

56. Ohkusu, M., "Hydrodynamic Forces on Multiple Cylinders in Waves, " Proceedings International Symposium on the Dynamics of Marine Vehicles and Structures, Univ. College, London, 1974, pp. 107-112.

57. Pinkster, J.A., "Mean and Low Frequency Wave Drifting Forces on Floating Structures," Ocean Engineering, Vol. 6, 1979, pp. 593-615.

58. Sarpkaya, T. and Isaacson, M., "Interference Effects," in Mechanics of Wave Forces on Offshore Structures, Van Nostrand Reinhold Co., 1981, pp. 331-343, 445-449.

59. Sayer, P. and Spencer, R., "The Wave-Induced Motions of Adjacent Vessels," Proceedings International Symposium in Hydrodynamics on Ocean Engineering, The Norwegian Institute of Technology, Trondheim, Norway, 1981, pp. 781-798.

60. Sayer, P. and Ursell, F., "Integral-Equation Methods for Calculating the Virtual Mass in Water of Finite Depth," Proceedings of the 2nd International Conference on Numerical Ship Hydrodynamics, U.C. Berkeley, 1977, pp. 176-184.

61. Shen, S.F., "Finite-Element Methods in Fluid Mechanics," Annual Review Fluid Mechanics, Vol. 9, 1977, pp. 421-445.

62. Smith, D.A., "Finite Element Analysis of the Forced Oscillation of Ship Hull Forms," M.S. Thesis, Naval Postgraduate School, Monterey, California, 1974.

63. Spring, B.H. and Monkmeyer, P.L., "Interaction of Plane Waves with a Row of Cylinders," Proceedings Civil Engineering in the Oceans III, ASCE, Univ. of Delaware, Vol. III, 1975, pp. 979-998.

64. Spring, B.H. and Monkmeyer, P.L., "Interaction of Plane Waves with Vertical Cylinders," Proceedings of the 14th Coastal Engineering Conference, Copenhagen, Denmark, Vol. III, 1974, pp. 1828-1847.

65. Stoker, J.J., Water Waves, Wiley Interscience Publication, 1957.

66. Twersky, V., "Multiple Scattering of Radiation by an Arbitrary Configuration of Parallel Cylinders," Journal of the Acoustical Society of America, Vol. 24, 1952, pp. 42-46.

67. Ursell, F., "Irregular Frequencies and the Motion of Floating Bodies," Journal of Fluid Mechanics, Vol. 105, 1981, pp. 143-156.

68. Ursell, F., "The Refraction of Head Seas by a Long Ship," Journal of Fluid Mechanics, Vol. 67, Pt. 4, 1975, pp. 689-703.

69. Ursell, F., "The Refraction of Head Seas by a Long Ship, Part II. Waves of Long Wavelength," Journal of Fluid Mechanics, Vol. 82, Pt. 4, 1977, pp. 643-657.

70. Van Oortmerssen, G., "Some Hydrodynamic Aspects of Multi-Body Systems," Proceedings International Symposium in Hydrodynamics on Ocean Engineering, The Norwegian Institute of Technology, Trondheim, Norway, 1981, pp. 725-744.

71. Van Oortmerssen, G., "Hydrodynamic Interaction Between Two Structures, Floating in Waves," Proceedings of the 2nd Conference on the Behavior of Offshore Structures, BOSS' 79, London, Vol. I, 1979, pp. 339-356.

72. Wang, S., "Wave Radiation Due to Oscillations of Two Parallel Spaced Cylinders," Ocean Engineering, Vol. 8, No. 6, 1981, pp. 599-621.

73. Wang, S. and Wahab, R., "Heaving Oscillations of Twin Cylinders in a Free Surface," Journal of Ship Research, Vol. 15, No. 1, 1971, pp. 33-48.

74. Wehausen, J.V., "The Motion of Floating Bodies," Annual Review Fluid Mechanics, Vol. 3, 1971, pp. 237-268.

75. Wehausen, J.V. and Laitone, E.V., "Surface Waves," in Handbuch der Physik, Springer, Berlin, Vol. 9, 1960, pp. 446-778.

76. Wilson, E.L., Bathe, K.J. and Doherty, W.P., "Direct Solution of Large Systems of Linear Equations," Computer and Structures, Vol. 4, 1974, pp. 363-372.

77. Wilson, B.W., "Elastic Characteristics of Moorings," Journal of Waterways and Harbors Div., ASCE, Vol. 93, No. WW4, 1967, pp. 27-56.

78. Yamamoto, T., Yoshida, A. and Ijima, T., "Dynamics of Elastically Moored Floating Objects," Applied Ocean Research, Vol. 2, No. 2, 1980, pp. 85-92.

79. Yue, D.K.P., Chen, H.S. and Mei, C.C., "A Hybrid Element Method for Diffraction of Water Waves by Three-Dimensional Bodies," International Journal for Numerical Methods in Engineering, Vol. 12, 1978, pp. 245-266.

80. Yue, D.K.P., Chen, H.S. and Mei, C.C., "A Hybrid Element Method for Calculating Three-Dimensional Water Wave Scattering," MIT Sea Grant Report, No. 76-10, 1976.

81. Yeung, R.W., "Numerical Methods in Free-Surface Flows," Annual Review Fluid Mechanics, Vol. 14, 1982, pp. 395-442.

82. Zienkiewicz, O.C., Kelly, D.W. and Bettess, P., "The Coupling of the Finite Element Method and Boundary Solution Procedures," International Journal for Numerical Methods in Engineering, Vol. 11, 1977, pp. 355-375.

83. Zienkiewicz, O.C., The Finite Element Method, 3rd edition, McGraw-Hill Book Co., London, England, 1977.

84. Zienkiewicz, O.C., Kelly, D.W. and Bettess, P., "The Sommerfeld (Radiation) Condition on Infinite Domain and its Modelling in Numerical Procedures," Proceedings of the 3rd International Symposium on Computing Methods in Applied Science and Engineering, Versailles, France, 1977, pp. 169-203.

85. Zienkiewicz, O.C., Bettess, P. and Kelly, D.W., "The Finite Element Method for Determining Fluid Loading on Rigid Structures, Two- and Three-Dimensional Formulations," in Numerical Methods in Offshore Engineering, ed. O.C. Zienkiewicz, et al., Wiley, Chichester, England, 1978, pp. 141-183.

86. Zienkiewicz, O.C. and Bettess, P., "Infinite Elements in the Study of Fluid-Structure Interaction Problem," Proceedings of the 2nd International Symposium on Computing Methods in Applied Science and Engineering, Versailles, France, 1975, pp. 133-172.

87. "Floating Production System for the Rough Sicily Channel," Ocean Industry, December 1980, pp. 9-11.

APPENDIX

APPENDIX -- INFINITE ELEMENT

The following details the infinite element shape functions and Newton-Coates integration scheme which originated from Ref. (7).

For a two-dimensional infinite element shown in the parent shape in Fig. A.1, a long but finite strip is constructed to approximate the infinite element. This finite strip has 3 reference points in both the η and ξ directions. Therefore, a total of 9 reference points is given for which the global x, y coordinates can be specified and Lagrangian interpolations in both η and ξ directions can be used in the quadratic isoparametric representation. The coordinates in the ξ direction can be arbitrary; they are chosen as shown in Fig. A.1 to be consistent with those chosen in Ref. (7).

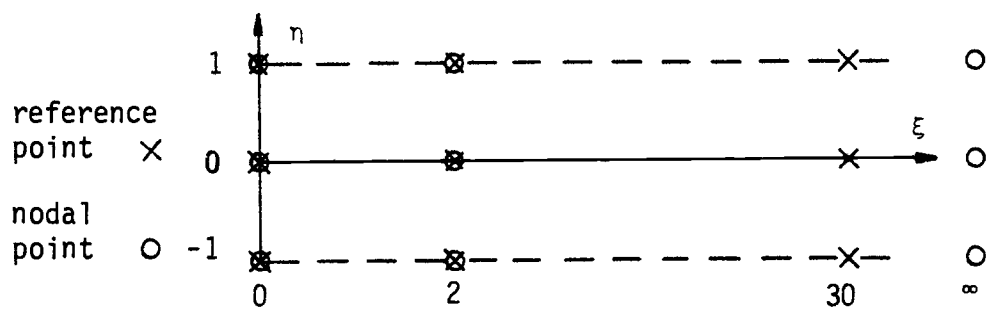

(Fig. A.1)

For each η integration coordinate, the Jacobian matrix is calculated at the three ξ coordinates to define a new infinite direction, s, as $s = \xi s'$ where

$$s' = \left(\frac{ds}{d\xi}\right)_{mean} = \frac{1}{3} \sum_{i=1}^{3} \left\{\left(\frac{dx}{d\xi}\right)^2 + \left(\frac{dy}{d\xi}\right)^2\right\}_i^{1/2} \qquad (A.1)$$

The s coordinates of the reference points are therefore 0, 2s' and 3Os'. This representation allows shape variation in the η-ξ plane but restricts the element to be stretched or telescoped in the ξ direction.

The shape function in the η direction, M_j, can be expressed by a real Lagrangian polynomial. In the s direction, the shape function of the i^{th} nodal point is expressed as

$$L_i = \exp\left(\frac{s_i - s}{L_D}\right) \exp(iKs) \prod_{\substack{k=1 \\ k\neq i}}^{n-1} \left(\frac{s_k - s}{s_k - s_i}\right) \quad ; i = 1,\ldots n-1 \tag{A.2}$$

in which n = number of nodal points in the s direction, L_D = decay length and K = wave number. The shape function for the nodal point at infinity is calculated by

$$L_n = \exp(iKs) - \sum_{i=1}^{n-1} L_i \tag{A.3}$$

These complex-valued shape functions in the s direction have the property that they have absolute values of 1 or 0 at nodal points (except at the n^{th} nodal point, where they have absolute values, approximately, of 1 and 0). They also approximate the Sommerfeld radiation condition of outgoing waves with radial decay.

The shape functions, N_{ij}, for the 9-noded infinite element are expressed explicitly by the following equations:

$$N_{ij} = L_i M_j \quad ; \quad i,j = 1,2,3$$

$$L_1 = \left(\frac{2s'-s}{2s'}\right) \exp\left(-s/L_D\right) \exp\left(iKs\right) \; ; \; M_1 = (\eta^2-\eta)/2 \tag{A.4}$$

$$L_2 = \left(\frac{s}{2s'}\right) \exp\left(\frac{2s'-s}{L_D}\right) \exp\left(iKs\right) \; ; \; M_2 = 1 - \eta^2$$

$$L_3 = \exp\left(iKs\right) - L_1 - L_2 \; ; \; M_3 = 1 - M_1 - M_2$$

When minimized with respect to the nodal unknowns, the functional integral in Eq. (2.28), Section 2.5, has two parts which are proportional to the quadratic terms of the shape functions and their derivatives, respectively. At each integration point within the infinite element, the derivatives can be found by transforming them from the η, s coordinates to the x, y coordinates, using the Jacobian matrix based on the finite-strip Lagrangian interpolation. The Gauss-Legendre integration formulas can be used in the η direction. In the s direction, a Newton-Coates integration scheme is necessary because of the harmonic terms in these shape functions.

The Newton-Coates formula evaluates integrals of the form $\int_0^\infty p(s)\exp(-\alpha s)\exp(i\beta s)ds$ by choosing the integration points to be at $(2n+1)/8$ multiples of the harmonic wavelength $(=2\pi/\beta)$, such that the zeros of real and imaginary parts of the $\exp(i\beta s)$ term can be avoided. It should be pointed out that $\beta = 2K$ (K is the wave number) because of the quadratic terms in the functional integral. The term p(s) is

further expressed as Lagrangian polynomials of these integral points such that for a n-points integration scheme, the integral can be evaluated by

$$\int_0^\infty p(s)\exp(-\alpha s)\exp(i\beta s)ds = \sum_{j=1}^{n} p(s_j) \int_0^\infty q_j(s)\exp(-\alpha s)\exp(i\beta s)ds$$

$$= \sum_{j=1}^{n} p(s_j)\, W_j \qquad (A.5)$$

For example, the first Lagrangian polynomial in a 4-points formula would be given by

$$q_1(s) = \frac{(\frac{3\pi}{4\beta} - s)(\frac{5\pi}{4\beta} - s)(\frac{7\pi}{4\beta} - s)}{(\frac{3\pi}{4\beta} - s_1)(\frac{5\pi}{4\beta} - s_1)(\frac{7\pi}{4\beta} - s_1)} \qquad (A.6)$$

in which $s_1 = \pi/4\beta$. The equality

$$\int_0^\infty s^{m-1} \exp(-\alpha s) \exp(i\beta s)\, ds = \gamma^m (m-1)! \qquad (A.7)$$

in which $\gamma = (\alpha+i\beta)/(\alpha^2+\beta^2)$ is now used to evaluate the integral weight W_1 as

$$W_1 = \int_0^\infty q_1(s) \exp(-\alpha s) \exp(i\beta s)\, ds$$

$$= \frac{35}{16}\chi - \frac{71}{12}\chi\gamma^2 + 10\,\chi^2\gamma^3 - 8\,\chi^3\gamma^4 \qquad (A.8)$$

in which $\chi = \beta/\pi$. A series of Newton-Coates integration weights from 3- to 6-points scheme is listed in Table A.1.

The assemblage of the functional derivatives may now be performed in the usual manner. In the formulation in Ref. (7), a decay length L_D was chosen by ensuring that in the region close to the area of diffraction, the decay of $\exp(-s/L_D)$ matched roughly the decay of $H_0(ks)$, the first term of the analytical series solution. The zeroeth Hankel function of the first kind is defined as $H_0(Ks) = J_0(Ks) + i\, Y_0(Ks)$ and is shown in Fig. A.2.

Numerical results of the present study are based on using $L_D = L$, the wave length. This gives approximately the same decay rate of $J_0(0)/J_0(Ks_1=7) = \exp(0)/\exp(-s_2/L_D) = 10/3$ with $s_1 = 1.114L$ and $s_2 = 1.204L$. The decay rate of the $Y_0(Ks)$ term is about the same order as the $J_0(Ks)$ term.

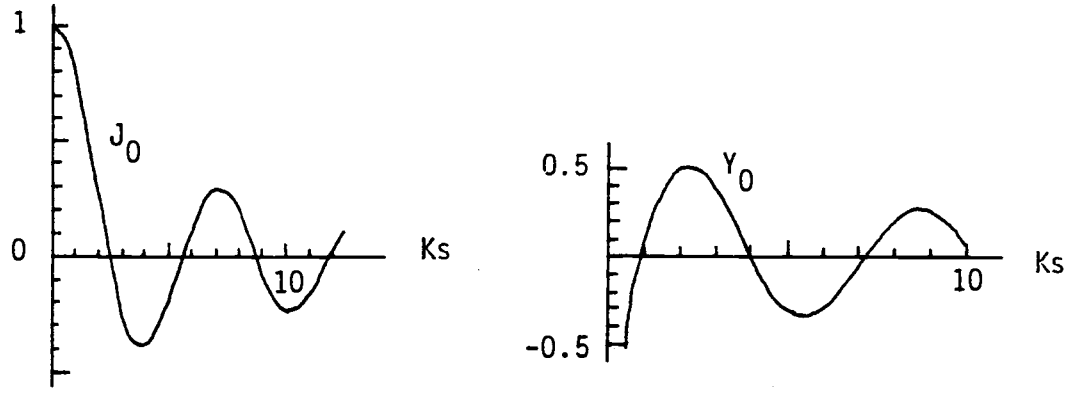

(Fig. A.2)

TABLE A.1. ABSCISSAS AND WEIGHTS FOR NEWTON-COATES INTEGRATION FORMULA

$$\int_0^\infty p(s)\exp(-\alpha s)\exp(i\beta s)ds = \sum_{j=1}^{n} p(s_j)W_j \text{; with}$$

$\gamma = (\alpha+i\beta)/(\alpha^2+\beta^2)$ and $\chi = \beta/\pi$

	3-points formula	4-points formula
s_j	W_j	W_j
$\frac{1}{4\chi}$	$\frac{15}{8}\gamma - 4\chi\gamma^2 + 4\chi^2\gamma^3$	$\frac{35}{16}\gamma - \frac{71}{12}\chi\gamma^2 + 10\chi^2\gamma^3 - 8\chi^3\gamma^4$
$\frac{3}{4\chi}$	$-\frac{5}{4}\gamma + 6\chi\gamma^2 - 8\chi^2\gamma^3$	$-\frac{35}{16}\gamma + \frac{47}{4}\chi\gamma^2 - 26\chi^2\gamma^3 + 24\chi^3\gamma^4$
$\frac{5}{4\chi}$	$\frac{3}{8}\gamma - 2\chi\gamma^2 + 4\chi^2\gamma^3$	$\frac{21}{16}\gamma - \frac{31}{4}\chi\gamma^2 + 22\chi^2\gamma^3 - 24\chi^3\gamma^4$
$\frac{7}{4\chi}$	----------	$-\frac{5}{16}\gamma + \frac{23}{12}\chi\gamma^2 - 6\chi^2\gamma^3 + 8\chi^3\gamma^4$

TABLE A.1. (Continued)

	5-points formula
s_j	W_j
$\frac{1}{4\chi}$	$\frac{315}{128}\gamma - \frac{93}{12}\chi\gamma^2 + \frac{103}{6}\chi^2\gamma^3 - 24\chi^3\gamma^4 + 16\chi^4\gamma^5$
$\frac{3}{4\chi}$	$-\frac{315}{96}\gamma + \frac{229}{12}\chi\gamma^2 - \frac{164}{3}\chi^2\gamma^3 + 88\chi^3\gamma^4 - 64\chi^4\gamma^5$
$\frac{5}{4\chi}$	$\frac{189}{64}\gamma - \frac{75}{4}\chi\gamma^2 + 65\chi^2\gamma^3 - 120\chi^3\gamma^4 + 96\chi^4\gamma^5$
$\frac{7}{4\chi}$	$-\frac{135}{96}\gamma + \frac{111}{12}\chi\gamma^2 - \frac{104}{3}\chi^2\gamma^3 + 72\chi^3\gamma^4 - 64\chi^4\gamma^5$
$\frac{9}{4\chi}$	$\frac{35}{128}\gamma - \frac{11}{6}\chi\gamma^2 + \frac{43}{6}\chi^2\gamma^3 - 16\chi^3\gamma^4 + 16\chi^4\gamma^5$

TABLE A.1. (Continued)

	6-points formula
s_j	W_j
$\frac{1}{4\chi}$	$\frac{693}{256}\gamma - \frac{3043}{320}\chi\gamma^2 + \frac{301}{24}\chi^2\gamma^3 - 47\chi^3\gamma^4 + 56\chi^4\gamma^5 - 32\chi^5\gamma^6$
$\frac{3}{4\chi}$	$-\frac{1155}{256}\gamma + \frac{5353}{192}\chi\gamma^2 - \frac{377}{8}\chi^2\gamma^3 + 203\chi^3\gamma^4 - 264\chi^4\gamma^5 + 160\chi^5\gamma^6$
$\frac{5}{4\chi}$	$\frac{693}{128}\gamma - \frac{1163}{32}\chi\gamma^2 + \frac{865}{12}\chi^2\gamma^3 - 350\chi^3\gamma^4 + 496\chi^4\gamma^5 - 320\chi^5\gamma^6$
$\frac{7}{4\chi}$	$-\frac{495}{128}\gamma + \frac{859}{32}\chi\gamma^2 - \frac{683}{12}\chi^2\gamma^3 + 302\chi^3\gamma^4 - 464\chi^4\gamma^5 + 320\chi^5\gamma^6$
$\frac{9}{4\chi}$	$\frac{385}{256}\gamma - \frac{2041}{192}\chi\gamma^2 + \frac{561}{24}\chi^2\gamma^3 - 131\chi^3\gamma^4 + 216\chi^4\gamma^5 - 160\chi^5\gamma^6$
$\frac{11}{4\chi}$	$-\frac{63}{256}\gamma + \frac{563}{320}\chi\gamma^2 - \frac{95}{24}\chi^2\gamma^3 + 23\chi^3\gamma^4 - 40\chi^4\gamma^5 + 32\chi^5\gamma^6$